

12-6-2022

Larval Ecology of Atlantic Bluefin Tuna (*Thunnus Thynnus*): New Insights from Otolith Microstructure, Biotic, and Abiotic Analyses from the Gulf of Mexico and Mediterranean Sea

Estrella Malca
Nova Southeastern University

Follow this and additional works at: https://nsuworks.nova.edu/hcas_etd_all



Part of the [Biogeochemistry Commons](#), [Biostatistics Commons](#), [Design of Experiments and Sample Surveys Commons](#), [Longitudinal Data Analysis and Time Series Commons](#), [Marine Biology Commons](#), [Natural Resources and Conservation Commons](#), [Oceanography Commons](#), [Other Oceanography and Atmospheric Sciences and Meteorology Commons](#), [Statistical Models Commons](#), and the [Systems Biology Commons](#)

Share Feedback About This Item

NSUWorks Citation

Estrella Malca. 2022. *Larval Ecology of Atlantic Bluefin Tuna (*Thunnus Thynnus*): New Insights from Otolith Microstructure, Biotic, and Abiotic Analyses from the Gulf of Mexico and Mediterranean Sea*. Doctoral dissertation. Nova Southeastern University. Retrieved from NSUWorks, . (110) https://nsuworks.nova.edu/hcas_etd_all/110.

This Dissertation is brought to you by the HCAS Student Theses and Dissertations at NSUWorks. It has been accepted for inclusion in All HCAS Student Capstones, Theses, and Dissertations by an authorized administrator of NSUWorks. For more information, please contact nsuworks@nova.edu.

Dissertation of Estrella Malca

Submitted in Partial Fulfillment of the Requirements for the Degree of

Doctor of Philosophy Oceanography/Marine Biology

Nova Southeastern University
Halmos College of Arts and Sciences

December 2022

Approved:
Dissertation Committee

Committee Chair: Tracey Sutton, Ph.D.

Committee Member: David Kerstetter, Ph.D.

Committee Member: Trika Gerard, Ph.D.

Committee Member: Raul Laiz-Carrion, Ph.D.

Committee Member: John T. Lamkin, Ph.D.

HALMOS COLLEGE OF NATURAL SCIENCES AND OCEANOGRAPHY

LARVAL ECOLOGY OF ATLANTIC BLUEFIN TUNA (*THUNNUS THYNNUS*): NEW INSIGHTS FROM OTOLITH MICROSTRUCTURE, BIOTIC, AND ABIOTIC ANALYSES FROM THE GULF OF MEXICO AND MEDITERRANEAN SEA

By

Estrella Malca

Submitted to the Faculty of
Halmos College of Natural Sciences and Oceanography
in partial fulfillment of the requirements for
the degree of Doctorate of Philosophy

Nova Southeastern University

December 2022

ABSTRACT

Atlantic bluefin tuna (ABT), *Thunnus thynnus*, spawn in the Gulf of Mexico (GoM) and the Mediterranean Sea (MED). Spawning occurs within narrow temporal and environmental parameters. Efforts to characterize growth of ABT in wild conditions revealed a wide range of growth variability during the early life stages. This series of studies examined potential biotic and abiotic influences of larval growth from seven ABT cohorts, and identified several key drivers of growth for this commercially valuable species. A detailed investigation of larval dynamics using otolith microstructure was conducted as follows. First, companion growth curves and stable isotope analysis from the same spawning season (2014) in the GoM and MED revealed distinct growth strategies. GoM larvae grew faster, had larger otoliths, and had wider increments associated with lower $\delta^{15}\text{N}$ than the MED. Second, food limitation and feeding preferences explained the most variance of recent growth between two larval patches in the GoM. While mean growth rates were similar, one nursery habitat appeared better suited for faster preflexion growth, while the other had faster flexion to postflexion growth likely attributed to abundant of preferred prey (copepod-nauplii, cladocerans). Lastly, inter-annual growth from historical SEAMAP collections (2015-2017) in the GoM revealed similar growth rates between years and that among the mesoscale oceanographic features sampled, Common Water was highly suitable habitat for ABT growth. Fisheries-independent surveys targeting ABT provide larval abundances for assessments of adult spawning stock biomass. Ecological studies such as these, that incorporate environmental parameters, and integrate standardized abundance estimates, will improve current models utilized in ABT management.

KEYWORDS: Otolith microstructure, larval fish ecology, highly migratory species, trophodynamics, stable isotopes, mesoscale oceanographic features, tuna, General Additive Models.

ACKNOWLEDGEMENTS

First, I am indebted to the crew, scientific field parties, and officers of the NOAA Ships *Gordon Gunter*, *Oregon II*, *Nancy Foster*, *R/V F.G. Walton Smith*, and *R/V SOCIB* for conducting fisheries oceanographic surveys and collecting valuable plankton and environmental datasets. Next, I want to thank my committee members Dr. Tracey Sutton, Dr. David Kerstetter, Dr. Trika L. Gerard, especially Dr. Raúl Laiz-Carrión, and my “Tuna-mentor,” Dr. John Lamkin.

I will be eternally grateful to my dearest mother, Cristal Luza, for her countless sacrifices over my lifetime. To my remarkable husband, for always revitalizing me and for stimulating my education. To mi Tia Py, my Stephan, and Tio Vico for your enduring care and support. In particular, I want to acknowledge my friends for their warmth and support. Most of all, I am thankful for my Gael’s patience during these four years. It is very likely that I learned more about the world as your parent, than from being a Ph.D. student.

Funding for collections, analyses, and lab work was provided through a collaborative framework between multiple partners. These partners include Nova Southeastern University (NSU), the National Oceanic and Atmospheric Administration (NOAA), the Spanish Institute of Oceanography (“ECOLATUN” Project CTM2015-68473-R to R. Laiz-Carrión). This research was carried out in part under the auspices of the Cooperative Institute for Marine and Atmospheric Studies (CIMAS), a Cooperative Institute of the University of Miami and NOAA under cooperative agreement NA20OAR4320472. Partial funding was also provided by the NOAA RESTORE Science Program grant (NOAA-NOS-NCCOS-2017-2004875 to J. Lamkin and T. Gerard). Funding was also provided by the NOAA Fisheries and the Environment grant to K. Shulzitski. In addition, a NSU Ph.D. Graduate Fellowship partially funded tuition along with two scholarships from the Fish Florida Scholarship Program. Finally, the NOAA Bluefin Tuna Research Program (BTRP) to W. Golet and T. Sutton supported partial tuition and analysis of samples.

I also want to recognize the database and archive staff (J. Fletcher and K. Hollihan) at the Southeast Area Monitoring and Assessment Program (SEAMAP). I acknowledge Dr. Jose Quintanilla as reader-2 (in chapter 2) and for assisting to develop ageing protocols and methods. I also acknowledge Akihiro Shiroza for larval gut content analyses, Jason Mostowy for support with code troubleshooting and for his data science contributions. I also thank Dr. Katie Shulzitski for otolith ageing, Dr. Rasmus Swalethorp for support with linear mixed modeling and dietary guidance, Dr. Mike Landry for zooplankton datasets & microzooplankton guidance, and Dr. Taylor Shropshire for providing zooplankton modeling outputs and feature type designations (in chapter 4).

I am grateful for the support of the Sutton Lab members, particularly April Cook and Nina Pruzinsky. I am thankful to the former members of the FORCES Lab, the Early Life History Lab, the Pascagoula NOAA Lab, and the Malaga Lab of the Spanish Institute of Oceanography. In particular, and in alphabetical order, I thank Dr. Alberto García, Dr. Caroline Johnstone, Amelia Martinez, Andy Millet, Alanna Mnich, Dr. Barbara A. Muhling, Sarah Privoznik, Dr. Bill Richards, Dr. Eloy Felipe Sosa Cordero, M. en C. Lourdes Vásquez Yeomans, and Ph.D. Candidate Glenn Zapfe.

TABLE OF CONTENTS

| | |
|-----------------------|-----|
| ABSTRACT | ii |
| ACKNOWLEDGMENTS | iii |
| LIST OF TABLES | vii |
| LIST OF FIGURES | x |

CHAPTER 1:

| | |
|---|----|
| LARVAL ATLANTIC BLUEFIN TUNA ECOLOGY | 1 |
| 1.1 INTRODUCTION | 1 |
| Atlantic bluefin tuna biology | 1 |
| Management of Atlantic bluefin tuna | 2 |
| Larval bluefin tuna ageing | 4 |
| Larval growth and trophodynamics | 6 |
| Study areas | 8 |
| 1.1.1 Statement of the problem and approach | 11 |
| REFERENCES | 13 |

CHAPTER 2:

COMPARATIVE EXAMINATION OF LARVAL GROWTH, STABLE ISOTOPES, AND TROPHIC POSITION OF ATLANTIC BLUEFIN TUNA FROM TWO DISCRETE SPAWNING GROUNDS 20 |

| | |
|---|----|
| 2.1 INTRODUCTION..... | 20 |
| Larval ecology: growth and trophodynamics | 21 |
| 2.2 METHODS..... | 23 |
| Larval collections | 23 |
| Physical variables | 25 |
| Larval ageing: otolith extraction and calibration | 25 |
| Larval ageing: Otolith measurement and interpretation | 26 |
| Zooplankton collection for SIA | 28 |
| Larval bluefin tuna SIA | 28 |
| Isotopic niche widths and overlap | 29 |
| Model estimates | 30 |
| 2.3 RESULTS..... | 30 |

| | |
|---|----|
| Larval collections | 30 |
| Physical variables | 34 |
| Larval ageing | 35 |
| Zooplankton SIA | 37 |
| Larval bluefin tuna SIA | 38 |
| Isotopic niche width and overlap | 38 |
| Model estimates | 38 |
| 2.4 DISCUSSION..... | 41 |
| Life history dynamics | 42 |
| Larval ageing comparisons | 43 |
| Trophic characterization | 46 |
| Isotopic niche widths and overlap | 48 |
| Modeling larval growth and trophodynamics | 50 |
| 2.5 CONCLUSION..... | 51 |
| REFERENCES..... | 53 |

**CHAPTER 3:
INFLUENCE OF FOOD QUALITY ON LARVAL GROWTH OF ATLANTIC
BLUEFIN TUNA IN THE GULF OF MEXICO** 60

| | |
|---|----|
| 3.1 INTRODUCTION | 60 |
| 3.2 METHODS | 63 |
| Larval sampling and processing | 63 |
| Otolith analyses | 65 |
| Larval gut contents and prey availability | 66 |
| Data analysis and modeling approach | 69 |
| 3.3 RESULTS | 70 |
| Biometrics and growth | 73 |
| Explained growth | 75 |
| Environmental cycle differences | 75 |
| 3.4 DISCUSSION | 77 |
| ABT larval growth | 77 |

| | |
|--|-----------|
| Environmental drivers of growth | 81 |
| 3.5 CONCLUSION | 84 |
| REFERENCES | 85 |
| | |
| CHAPTER 4: | |
| LARVAL GROWTH OF ATLANTIC BLUEFIN TUNA IN TRANSIENT | |
| MESOSCALE OCEANOGRAPHIC FEATURES OF THE GULF OF | |
| MEXICO | 93 |
| 4.1 INTRODUCTION | 93 |
| 4.2 METHODS | 95 |
| Multi-year survey and larval collections | 95 |
| Mesoscale feature types and ageing | 97 |
| Otolith analyses | 98 |
| Larval ABT diet | 99 |
| Statistical analysis | 100 |
| 4.3 RESULTS | 100 |
| Survey and larval collections | 100 |
| Abiotic conditions | 101 |
| Mesoscale feature types and ageing | 103 |
| Otolith microstructure trajectories | 105 |
| Larval ABT diet | 107 |
| 4.4 DISCUSSION | 109 |
| Larval abundances in the GoM | 109 |
| Recruitment and larval dynamics | 110 |
| Otolith microstructure trajectories | 112 |
| Mesoscale feature types and ageing | 113 |
| Larval ABT diet | 114 |
| 4.5 CONCLUSION | 117 |
| REFERENCES | 118 |

LIST OF TABLES

| | |
|--|----|
| CHAPTER 2 | |
| Table 2.1. Survey dates, number of net tows, gear types and positive <i>Thunnus thynnus</i> (ABT) stations during each sampling effort in the Gulf of Mexico (GoM) and the Mediterranean Sea (MED, Balearic Sea) during the 2014 spawning season | 24 |
| Table 2.2. Criteria for otolith ageing for <i>Thunnus thynnus</i> between 3 – 25 days post hatch (dph). The three age groups and their corresponding allowed error for left vs. right otolith comparisons, and between otolith reads are specified. The coefficient of variation (CV) was set at 10% however, for the youngest larvae (3 - 6 dph), a larger CV was permitted only if the difference between reads was one day. The two older age groups could satisfy the specified CV or the indicated difference between reads | 28 |
| Table 2.3. Summary of ANCOVA for age comparisons derived from Atlantic bluefin tuna larval otoliths from the 2014 spawning season in the Gulf of Mexico and Mediterranean Sea. The F statistic and p-values are shown for within-otolith reads for either left or right otoliths (read one and read two). Inter-reader comparisons are shown for 72 fish whose left and right otoliths were read twice, but only one read was selected randomly from reader-1 and reader-2 for analysis | 36 |
| Table 2.4. Summary of somatic, otolith metrics, and mean larval abundance (1000^{-1} m^{-3}) for Gulf of Mexico (GoM) and Mediterranean Sea (MED) during the 2014 spawning season. Values shown are for the stations selected for ageing analyses. An asterisk (*) indicates significant results at the 0.05 level for t-test between spawning regions. A double asterisk (***) indicates Wilcoxon test | 37 |
| Table 2.5. Trophic and environmental variable summary for Gulf of Mexico (GoM) and Mediterranean Sea (MED) during the 2014 spawning season. Larval <i>Thunnus thynnus</i> (ABT) trophic position (TP), $\delta^{15}\text{N}$, and $\delta^{13}\text{C}$ are shown. Parenthesis indicate the number of larvae analyzed. Mean values \pm SD are reported. An asterisk (*) indicates significant results at the 0.05 level for t-test between spawning sites. A double asterisk (***) indicates Wilcoxon test ... | 39 |
| Table 2.6. Akaike information criterion (AIC) for the best-performing generalized additive models (GAMs). The ΔAIC is the difference from the lowest AIC and the percent variance (%) explained for each selected model is indicated. The residuals of recent growth at-age (Rg) for postflexion larval <i>Thunnus thynnus</i> (ABT). The s() denote the smoothing function applied to a variable. Variables are otolith radius (μm , OR), $\delta^{15}\text{N}_{\text{ABT}}$, $\delta^{15}\text{N}_{\text{mesozoo}}$, trophic | 45 |

position (TP), larval fish abundance (1000^{-1} m^{-3}), ABT abundance (1000^{-1} m^{-3}), and sea surface temperature (SST). The SST, and abundance are from the corresponding collection location from Gulf of Mexico (GoM) and/or Mediterranean Sea (MED) during the 2014 spawning season

CHAPTER 3

Table 3.1. ANCOVA summary (upper panel) for larval *Thunnus thynnus* biometrics. Linear mixed model (lower panel) considering full otolith increment width history from all larvae. Asterisk indicates significant results at the 0.05 level. For the linear mixed model, early growth is 1-7 days post hatch (dph), and late growth is 8-15 dph. Number inside parenthesis indicates number of ABT considered for cycle 1 and cycle 5 (C1, C5 respectively) 65

Table 3.2. Names and descriptions of variables included in the generalized additive model selection process and corresponding data sources 67

Table 3.3. Generalized additive model statistics summary for recent increment width (IW, μm). The effect of the parametric coefficients on recent IW (top panel). The estimated significance levels of the smooth functions (lower panel); ΔDE is the loss in percent deviance explained caused by dropping the variable, “edf” is the estimated degrees of freedom for smoothing terms shown on lower panel. An asterisk (*) denotes statistical significance ($\alpha = 0.001$) 74

Table 3.4. Daytime prey group biomass from cycles C1 and C5 collected using 0.055- and 0.2-mm mesh size plankton nets. Ring nets sampled 0-100 m during C1 and from 0-133 m during C5. Bongo-20 sampled from 0-25m. Bottom panel indicates mean values for temperature, salinity and relative fluorescence (volts) for the upper 25 m determined from CTD casts. Asterisk (*) indicates significant results at the 0.05 level for t-test; double asterisk (**) indicates Wilcoxon test..... 76

CHAPTER 4

Table 4.1. Summary of plankton gear sampled in 2015, 2016, and 2017. Stations with positive catches / total tows are shown. Larval *Thunnus thynnus* (ABT) aged and the gear that it was collected from is shown. Mean Scombridae densities ($\text{ind. } 1000^{-3} \text{ m}^{-3}$) \pm SD for ABT, *Thunnus* spp., and *Katsuwonus pelamis* for each year. Mean temperature, salinity, and fluorescence is shown .. 98

Table 4.2. Summary of stations in five oceanographic feature types: anticyclonic boundary (AB), anticyclonic region (AR), cyclonic boundary (CB), cyclonic region (CR), and Common Water (CW). The number of aged *Thunnus thynnus* (ABT) are shown in (). Mean \pm SD for somatic (age, body 104

size), and otolith metrics for recent growth (last two completed increments as a proxy for recent growth). The range of the otolith radius (μm) is also shown

Table 4.3. Gut content analysis for *Thunnus thynnus* prey from the 2016 survey in the northern Gulf of Mexico. Prey counts indicate the mesoscale feature type they were collected from. The three features types: cyclonic boundary (CB), cyclonic region (CR), and Common Water (CW) are shown

111

LIST OF FIGURES

| | |
|---|----|
| CHAPTER 1 | |
| Figure 1.1. Spawning grounds for Atlantic bluefin tuna (<i>Thunnus thynnus</i>) in the Atlantic Ocean. Population ranges are indicated in red for western stock and in green for eastern stock. Orange indicates where their ranges overlap. This image was modified from the International Commission for the Conservation of Tunas (www.iccat.int) | 1 |
| Figure 1.2. Atlantic bluefin tuna (<i>Thunnus thynnus</i>) postflexion larvae before preservation. Image courtesy of A. Shiroza, University of Miami, CIMAS | 2 |
| Figure 1.3. Larval bluefin tuna otolith at 1000×. Daily growth units (increments ●) originate at the primordium (P) and are enumerated along the otolith radius (OR) towards the otolith margin (OM). Scale indicates 0.020-mm | 5 |
| Figure 1.4. Schematic representation of the mesoscale features in the Gulf of Mexico during summer 2010: Common Water (CW), cyclonic region (CR), cyclonic boundary (CB), anticyclonic region (AR), and anticyclonic boundary (AB). The black contour lines indicate the prevailing direction of the current, thicker lines indicate stronger flow. The red contour line indicates the Loop Current. The red and blue solid contours indicate the location of the anticyclonic (red) and cyclonic eddies (blue) | 9 |
| Figure 1.5. The western Mediterranean Sea showing the main study area for Atlantic bluefin tuna larval collections (+) during survey BF0614 in 2014 aboard the R/V <i>SOCIB</i> | 10 |
| CHAPTER 2 | |
| Figure 2.1. a) Station locations, presence/absence, and location of aged larval bluefin tuna (<i>Thunnus thynnus</i>) from a) western Mediterranean (MED) and b) Gulf of Mexico (GoM) during the 2014 spawning season at each corresponding spawning areas | 31 |
| Figure 2.2. Histograms of body size (mm) for aged larval <i>Thunnus thynnus</i> (ABT) otoliths from the Gulf of Mexico (GoM, n = 111) and the western Mediterranean Sea (MED, n = 118). Preflexion and postflexion larval stages are also specified. Numbers above bars indicate the number of larvae grouped at 1-mm intervals (mm) | 33 |
| Figure 2.3. Age at length (a), body weight (b) and otolith radius, μm (c) for 228 larval bluefin tuna (<i>Thunnus thynnus</i>) aged from the Mediterranean Sea (MED) and Gulf of Mexico (GoM) during the 2014 spawning season. Developmental | 34 |

stages (preflexion and postflexion) are indicated in panel (a) with an open symbol (blue and red, respectively). (d) Mean daily increment size at-age for the corresponding larvae, with standard error bars. Open symbols indicate less than three observations at each given age

Figure 2.4. Biplot of $\delta^{15}\text{N}$ and $\delta^{13}\text{C}$ and standard deviation for the (a) Gulf of Mexico (GoM) and (b) Mediterranean Sea (MED) during the 2014 spawning season. Postflexion larval bluefin tuna (*Thunnus thynnus*, ABT) are shown in blue symbols, microzooplankton (0.05 – 0.2 mm) in red symbols, while mesozooplankton (0.2 – 0.5 mm) are in green. Corresponding distributions for ABT, microzooplankton, and mesozooplankton are shown for each variable along the corresponding axes

40

Figure 2.5. Trophic results for postflexion larval *Thunnus thynnus* (ABT) from the Gulf of Mexico (GoM, red symbols) and the Mediterranean Sea (MED, blue symbols) during the 2014 spawning season: The a) estimated trophic position (TP_{ABT}) and b) $\delta^{13}\text{C}_{\text{ABT}}$ vs. observed recent otolith growth (μm , log-transformed). c) Scatter biplot of $\delta^{15}\text{N}$ and $\delta^{13}\text{C}$ with ellipses that represent the isotopic niche width for each region. d) Boxplot of the standard ellipse area (SEA_{B}) for the trophic niche of each region. Boxplot shows the confidence intervals of the SEA_{B} corresponding to 95%, 75% and 50%. The (x) symbols indicate the mean value for each population analyzed

47

Figure 2.6. Selected model results of the partial effect of (a) otolith radius, μm , (b) $\delta^{15}\text{N}_{\text{ABT}}$, and c) $\delta^{15}\text{N}_{\text{mesozooplankton}}$ on the average width of the last three daily increments (μm) (recent growth at-age residuals) of postflexion ABT. The model's AIC = 110.64, while the deviance explained was 57.2%. The dashed lines indicate 95% confidence intervals. The whiskers on x-axis indicate observations for that covariate. All covariates have statistical significance at the 0.05 level

51

Figure 2.7. Selected model results of the partial effect of (a, e) otolith radius, μm , (b, e) trophic position and (c, f) larval fish abundance (1000^{-1}m^{-3}) for the Gulf of Mexico (GoM, $n = 27$) spawning region (a-c) and the western Mediterranean Sea (MED, $n = 44$) (d-f). The response variable is the average width of the last three daily increments (μm), recent growth at-age residuals, for postflexion *Thunnus thynnus*. The dashed lines indicate 95% confidence intervals. The whiskers on x-axis indicate observations for that covariate. All covariates have statistical significance at the 0.05 level

52

CHAPTER 3

Figure 3.1. General study area in the northeastern Gulf of Mexico. Areas for net tow sampling during cycle experiment are indicated for survey NF1704, cycle 1 (C1, \circ) and NF1802, cycle 5 (C5, \bullet)

61

Figure 3.2. Histogram for bluefin tuna (*Thunnus thynnus*) larvae measured (mm) from a) cycle 1 (C1) and b) cycle 5 (C5) in the Gulf of Mexico. The boxplot indicates larval developmental stages preflexion, flexion and postflexion with corresponding larval length (SL, mm) from ethanol-preserved specimens (gray). Daytime-aged ABT larvae with gut contents examined are also indicated 64

Figure 3.3. Least squares regressions for aged *Thunnus thynnus* larvae examined for a) body size (SL, mm) at-age, (days post hatch, dph), b) otolith radius (μm) at-age for cycle 1 (C1, \circ), and cycle 5 (C5, \bullet). Linear regressions are shown for C1 (\cdots) and C5 (\cdots) for length at-age $y_{C1} = 0.39x + 1.43$, $R^2 = 0.78$; $y_{C5} = 0.37x + 1.74$, $R^2 = 0.86$ and the exponential regression for OR at-age $y_{C1} = 7.19e^{0.14x}$, $R^2 = 0.83$, $y_{C5} = 6.52e^{0.15x}$, $R^2 = 0.91$, respectively 71

Figure 3.4. a) Mean increment width trajectories (μm) at increment number (days post hatch, dph) for *Thunnus thynnus* from cycles C1 (\circ) and C5 (\bullet). Error bars indicate standard error and are plotted when at least five larvae were included. The dashed vertical (---) line placed between 7 and 8 dph indicates a significant observed change in increment width (μm) between C1 and C5 larvae and roughly corresponds with onset of flexion 72

Figure 3.5. Least squares regressions for aged *Thunnus thynnus* larvae from cycles C1 (\circ) and C5 (\bullet) examined for standardized residuals of recent otolith growth at-age (y-axis) and standardized a) small prey biomass, b) food limitation index (FLI), c) residual of ingested preferred prey carbon at-age, and d) temperature $^{\circ}\text{C}$ from 0 - 25 m 73

Figure 3.6. Least squares regressions for aged *Thunnus thynnus* larvae for a) body depth (mm) at-age and b) dry weight (mg) at-age and c) residuals of age-at-length vs residuals otolith radius at-age for C1 (\circ) and C5 (\bullet) from NF1704 and NF1802. Weights were converted from length at weight relationships from Equation 2a and 2b. Exponential curves for C1 (\cdots) and C5 (---) for age and depth were $y_{C1} = 0.26e^{0.12x}$, $R^2 = 0.66$, $y_{C5} = 0.21e^{0.14x}$, $R^2 = 0.85$ and for age at weight $y_{C1} = 0.04e^{0.22x}$, $R^2 = 0.77$, $y_{C5} = 0.04e^{0.23x}$, $R^2 = 0.86$. Linear regression for age-at-length residuals vs age-at-otolith residual $y_{C1} = 9.24x - 0.34$, $R^2 = 0.40$ and $y_{C5} = 9.17x + 0.34$, $R^2 = 0.45$ 78

Figure 3.7. Least squares regressions for aged *Thunnus thynnus* larvae for recent increment width (μm) at-age residuals (x-axis) and a) body length at-age residuals, b) body depth at-age residuals 80

Figure 3.8. General additive model results for the individual additive effects of four smoothing terms on the standardized residual of otolith growth (3-day mean of recent otolith increment width, μm) (y-axis) for 139 *Thunnus thynnus* larvae from the Gulf of Mexico: a) small prey biomass b) food limitation index 81

c) ingested preferred prey C representing biomass of copepod nauplii and cladocerans, and d) temperature °C (0- 25 m). All variables were standardized to zero mean and unit variance. Model AIC = 308.58 with 44.3 % of deviance explained. The grey-shaded areas indicate 95% confidence intervals

CHAPTER 4

Figure 4.1. Schematic representation of the mesoscale features types in the Gulf of Mexico from Lindo-Atichati et al. (2012). a) Mean sea surface height (SSH, cm) values for mesoscale features and b) corresponding SSH (cm) for longitudes (~91°- 85°W). c) Collection location for one *Thunnus thynnus* larva (●) from CR on 20 May 2017. Feature types are shown for (1) anticyclonic region (AR), (2) anticyclonic boundary (AB), (3) cyclonic boundary (CB), (4) cyclonic region (CR), and (5) Common Water (CW). The majority of the open GoM > 200 m depth was classified as CW (grey). Image from panel b provided by Taylor Shropshire, and is used with permission

96

Figure 4.2. Abundances of larval *Thunnus thynnus* (ABT) during 2015, 2016, and 2017 along with bathymetry (m) contours in the open Gulf of Mexico. Panel (a) shows abundances $1000^{-1} m^{-3}$ for ABT-positive stations. Panels (b-g) indicate ABT catches from aged individuals. The mesoscale feature types are indicated: anticyclonic boundary (AB, orange), cyclonic boundary (CB, light blue), cyclonic region (CR, blue), and Common Water (CW, yellow)

102

Figure 4.3. Sea surface temperature (SST, °C) for 2015, 2016, and 2017 (a-c) and for mean \pm SD in the five oceanographic mesoscale feature types: anticyclonic boundary (AB), anticyclonic region (AR), cyclonic boundary (CB), cyclonic region (CR), and Common Water (CW. Positive symbols (+) indicate stations with *Thunnus thynnus* aged in this chapter and SST are from CTD vertical casts at ~5 m depth

103

Figure 4.4. Growth curves for *Thunnus thynnus* (a) SL (mm) vs. age (days post hatch, dph), b) otolith radius (μ m) vs. age (dph), and c) otolith radius-at-age residuals vs. SL-at-age residuals for years 2015, 2016, 2017

105

Figure 4.5. Growth curves for *Thunnus thynnus* for SL (mm) vs. age (days post hatch, dph) for cyclonic region, CR (blue) vs Common Water, CW (yellow) for a) 2015 ○ (CR= 18, CW=84) and b) 2016 Δ (CR = 37, CW=98). Recent increment (μ m) vs. SL (mm) are shown for c) 2015 (CR= 18, CW=84) and d) 2016 (CR = 37, CW=98)

106

Figure 4.6. a) Growth rates ($mm d^{-1}$) in each oceanographic feature type AB, CB, CR, and CW for anticyclonic boundary, cyclonic boundary, cyclonic region, and Common Water, respectively for aged larval *Thunnus thynnus* otolith microstructure. b) Recent growth, μ m shown for each feature type

108

CHAPTER 1: Larval Atlantic bluefin tuna ecology

1.1 INTRODUCTION

Atlantic bluefin tuna biology

The highly migratory Atlantic bluefin tuna (ABT, *Thunnus thynnus*) is the largest species in the tuna family (Scombridae), reaching up to 650 kg (Block et al., 2005). ABT are exploited for their highly prized meat, which has resulted in overfishing (Rooker et al., 2007, Restrepo et al., 2010, Collette et al., 2014). Despite continued declines in population size and due to its high vulnerability given its long-lived ecology, attempts to conserve ABT have not been effective considering the resources and global interest. Ecological studies have informed the management decisions for the ABT stocks and filled multiple data gaps in a concerted effort to prevent the further decline of the species (Neilson & Campana 2008, Secor et al., 2008, Restrepo et al., 2010, Laiz-Carrión et al., 2015).

Spawning occurs mainly in two locations (Figure 1.1), with nearly all of the western stock spawning in the Gulf of Mexico (GoM) and the eastern stock spawning in the

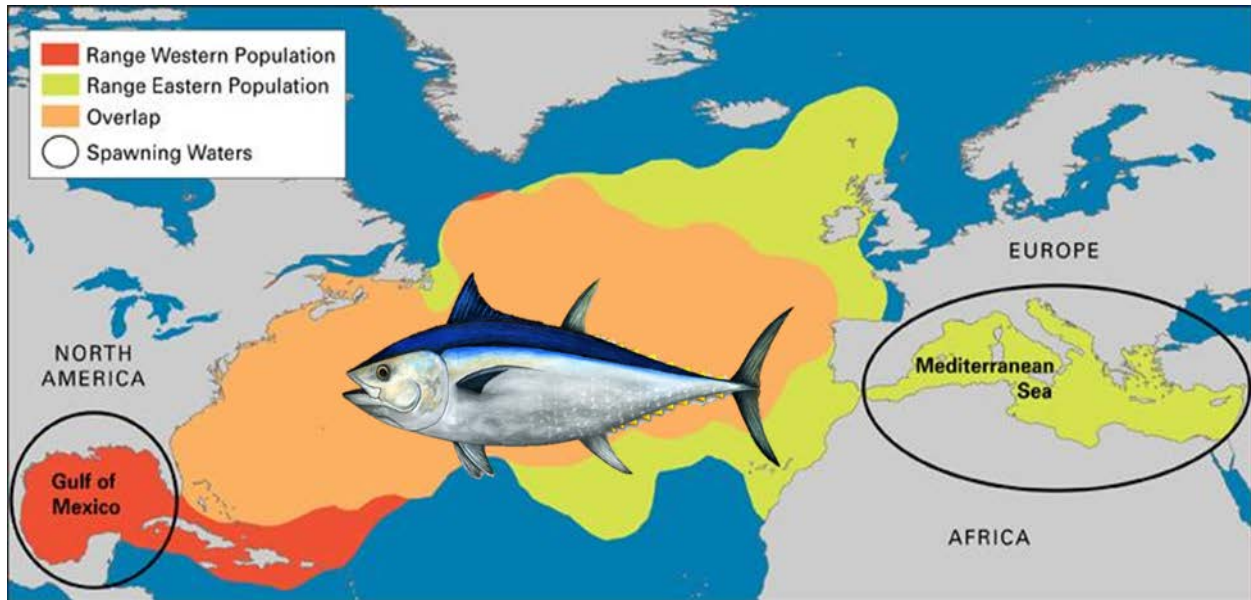


Figure 1.1. Spawning grounds for Atlantic bluefin tuna (*Thunnus thynnus*) in the Atlantic Ocean. Population ranges are indicated in red for western stock and in green for eastern stock. Orange indicates ranges overlap between adult populations. This image was modified from the International Commission for the Conservation of Tunas (www.iccat.int).

Mediterranean Sea (MED) (Fromentin & Powers, 2005, Muhling et al., 2013). These epipelagic tunas migrate large distances to comparatively oligotrophic regions (seaward beyond the 200-m isobath), ostensibly to place their larvae (Figure 1.2) in optimal habitat for survival (Bakun 2014). Spawning appears to be mediated by sea surface temperature warming above approximately 23 °C (Alemany et al., 2010, Muhling et al., 2010) and occurs in the GoM between April and June and in the MED between June to July (Muhling et al., 2013, Block et al., 2019).



Figure 1.2. Atlantic bluefin tuna (*Thunnus thynnus*) postflexion larvae before preservation. Image courtesy of A. Shiroza, University of Miami, CIMAS.

Management of Atlantic bluefin tuna

ABT are epipelagic and oceanic fish that spend their lifetime traveling long distances that cross multiple international boundaries. ABT management requires multiagency and international collaborations to agree upon lengthy management plans, in particular for the allocations of fishing quotas. In accordance with agreements by the International Commission for the Conservation of Atlantic Tunas (ICCAT), the U.S. National Marine Fisheries Service, specifically, the Atlantic Highly Migratory Species Management Division is responsible for ABT management (NOAA 2022). Within U.S. waters (Atlantic Ocean, GoM, and U.S. Caribbean),

ABT are subject to the Magnuson-Stevens Fishery Conservation and Management Act (Magnuson-Stevens Act 1996) and the Atlantic Tunas Convention Act (ATCA 1975). ATCA authorizes the Department of Commerce to implement the binding recommendations from the National Oceanic and Atmospheric Administration (NOAA) to ICCAT in the U.S.

Furthermore, ABT are highly prized which has resulted in considerable fishing pressure and complex conservation actions (Collette & Graves, 2019). Severe ABT overharvesting and underreporting of catch led to conservation efforts in the early 2010s that would increase regional and global protections, but these efforts were unsuccessful. First, a status review was conducted that considered the listing of ABT under the U.S. Endangered Species Act however, this status was not determined to be necessary because of the already numerous management regulations in place in U.S. waters (NMFS 2011). Second, an international trade ban for ABT was proposed in 2010, but was not supported by CITES¹ members (55%), with 10% abstaining to vote (Nayar 2010).

Foraging grounds for ABT are located in the North Atlantic Ocean (Figure 1.1) with management separated at the 45° meridian into two stocks: an eastern and a western stock. Eastern and western ABT stocks are managed separately (Anonymous 2019) and international assessments are carried out to ascertain the yearly biomass for both stocks (Ingram et al., 2010). While the eastern stock has been exploited for thousands of years (Di Natale 2014) and is currently at least one order of magnitude larger than the western stock, targeted harvest of the western stock started in the 1950s (Scott et al., 1994). Subsequent overfishing in the GoM spawning grounds during 1950 - 1960s may have seriously depleted existing stocks (NMFS 2011). Spawning stock biomass has remained relatively stable at ~ 15% of estimated pre-exploitation biomass (Collette et al., 2014), yet the status of the western ABT population has fluctuated from overfished in 2014, to currently not being subject to overfishing however, the population level is currently “unknown in the western Atlantic” (NMFS 2014, NMFS 2022).

Arguably, the management of this species requires integrative policies, such as ecosystem-based management, which aims to integrate multiple factors into the study and management of

¹ Convention on International Trade in Endangered Species of Wild Fauna and Flora

fishery resources instead of focusing on a single species. In addition to reduced fishing pressure, management strategies for ABT would benefit from including environmental drivers that influence their entire life history (not only the adult habitat). Total allowable catches, gear restrictions, and harvest protections during the spawning season in the GoM have likely relieved further declines however, multiple questions remain regarding the stock-recruit relationship that introduces uncertainty in the scientific assessments utilized in sustainable fishing practices in the ecosystem.

The Southeast Area Monitoring and Assessment Program (SEAMAP) is a multi-partnered program for the collection, management and dissemination of fishery-independent data and information in the southeastern United States. The Spring SEAMAP annually samples a systematic grid (0.5°) during the peak of spawning (May) in the northern GoM and is the only fishery-independent metric utilized in annual population assessments for the western ABT stock (Habtes et al., 2014). Using SEAMAP larval abundances, Scott et al. (1994) developed an ABT spawning biomass index to back-calculate observed abundances to equivalent abundances (ind. 100 m^{-2}) of one-day old larvae collected from historical bongo net tows (Scott et al., 1994; Ingram et al., 2010). This fishery-independent metric has a critical gap for measuring larval growth. The index does not take into account inter-annual and geographical variability in larval growth. In contrast, recent research indicates that growth and survival of ABT larvae for the Mediterranean (García et al., 2013, Malca et al., 2017) as well as for the Pacific bluefin tuna is highly variable, both inter-annually and spatially (Tanaka et al., 2014).

Larval bluefin tuna ageing

Otoliths are calcium carbonate structures that in addition to regulating sound and balance in teleost fishes, store the chronology of individual fishes (Campana & Neilson, 1985). Otolith increments form because of the circadian rhythm and seasonal patterns in the environment. A banding pattern can be observed on whole otoliths when examined at greater than $10\times$ magnifications (Figure 1.3). Daily increments can also be distinguished on whole otoliths of larval scombrids as they form with daily frequency that can be observed using $> 40\times$ magnifications ((Panella 1971, Campana & Jones 1992, Sponaugle 2009). Repeated

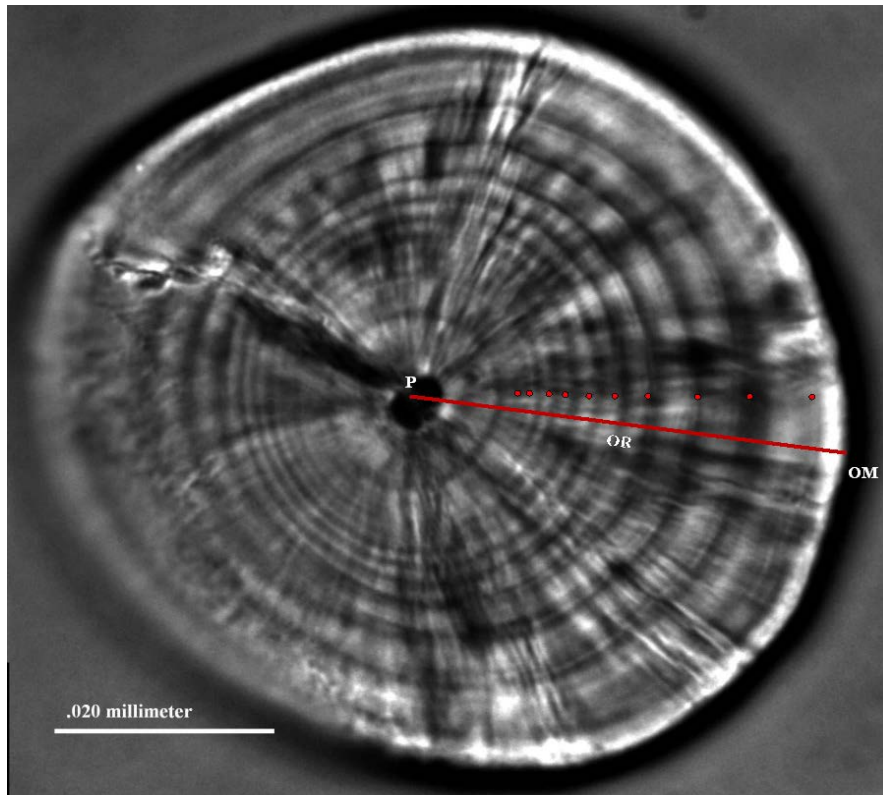


Figure 1.3. Larval bluefin tuna otolith at 1000 \times . Daily growth units (increments ●) originate at the primordium (P) and are enumerated along the otolith radius (OR) towards the otolith margin (OM). Scale indicates 0.020 mm. Image modified from Malca et al. (2017).

measurements (e.g., increment width and otolith radius) of sufficient sample sizes can reveal patterns in otolith growth (e.g., fast or slow) and reflect spatial and temporal variability.

Larval ABT otoliths have recognizable patterns that reflect continuous somatic growth as daily increments (Secor et al., 1995). Daily increment formation was validated in the closely related Pacific bluefin tuna between 5-71 days after fertilization and likely begins with the onset of exogenous feeding ~ 4 d (Brother et al., 1983, Itoh et al., 2000). A difficulty in ageing ABT otoliths (Figure 1.3) occurs because the primordium is encircled by one or more diffuse zones followed by alternating bands (one daily increment = one translucent and one opaque band) (Brothers et al., 1984, García et al., 2013). Daily increments are not consistently discernible inside this region and given the use of larval ages in stock assessments, age-adjustments have been conducted. Previous age estimates for larval ABT added between two to four days to daily increment counts to calculate days post hatch from increments counted along the otolith radius (Brothers et al., 1983, Malca et al. 2017). However, a systematic approach to adjust larval ABT

age is lacking that may reduce error into already variable abundance estimates (Ingram et al., 2017).

Larval ABT otoliths have been aged from the GoM (Malca et al., 2017) and from the Straits of Florida (Brothers et al., 1984). Malca et al., (2017) found significant differences in growth patterns between the otoliths of GoM and MED (García et al., 2013). However, these comparisons were from different annual cohorts completed independently without standardized methods. Despite the need to improve our understanding of larval ABT life history and the unidentified links to recruitment, larval growth comparisons between the two main spawning grounds have not been carried out simultaneously.

Given the highly migratory nature of bluefin tuna, larval otolith research has been an active field to examine these pelagic species during the critical first weeks of life that heavily determine future population sizes. In the last 40 years, extensive larval work on Pacific bluefin tuna *T. orientalis* (Tanaka et al., 2014, and references herein), and southern bluefin tuna *T. maccoyii* (Jenkins & Davis, 1990, Jenkins et al., 1991). Other aged *Thunnus* species include yellowfin tuna *T. albacares*, collected near the Mississippi River plume (Lang et al., 1994), and *Thunnus* spp. in the Straits of Florida (Gleiber et al., 2020b). In addition, Hernández et al. (2021) aged larvae from the Slope Sea and found similarities between growth rates in the GoM. Finally, García et al. (2013) aged larval ABT from the western MED and showed that warm anomalies resulted in increased growth rates, which may translate into stronger recruitment and larger year classes. Tanaka et al. (2006, 2014) also reported environmental influences for Pacific bluefin tuna. However, the environmental drivers of ABT larval growth in the GoM have not been explored directly to date.

Larval growth and trophodynamics

Prior to recruiting into adulthood, larval fish must find food, avoid predation, and avoid advection to unsuitable habitats. Several studies have begun to investigate these processes in larval fishes by examining trophodynamics, including diets, feeding success, and isotopic signatures (Llopiz et al., 2014, Quintanilla et al., 2020, Gleiber et al., 2020a, 2020b). Pepin et al. (2014) showed that faster growth in larval fishes resulted in more variable growth rates. Feeding ecology of larval tunas using diet contents analysis has been described (Uotani et al., 1981,

Llopiz & Hobday 2015, Kodama et al., 2017), including in the GoM (Llopiz et al. 2010, Tilley et al., 2016, Shiroza et al., 2021) and MED (Catalán et al., 2007, 2011, Morote et al., 2008, Uriarte et al., 2019). Larval ABT feed predominantly on copepods, copepod nauplii, appendicularians, and cladocerans. Whereas other tuna larvae such as *T. atlanticus* prefer calanoid copepods, *Auxis* spp. and *Katsuwonus pelamis* show a preference for appendicularians (Llopiz & Hobday 2015, Gleiber et al., 2020a).

When coupled, the known age-at-length, location of capture, and trophodynamic characteristics can provide key information for assessing the survivorship of larval ABT in their nursery grounds. To understand the observed variability of larval ABT growth, a logical next step would entail evaluating the feeding success of individual larvae concurrently with observed somatic growth using otolith microstructure analysis. Prey preferences as well as incidences of piscivory should also be considered, along with the zooplankton community within the larval ABT habitat (Gleiber et al., 2020a, 2020b). Finally, ABT larval stable isotope signatures of nitrogen ($\delta^{15}\text{N}$) and carbon ($\delta^{13}\text{C}$) combined with larval growth can characterize population-wide differences (if any) within spawning grounds and between spawning grounds (Quintanilla et al., 2020). In addition, $\delta^{15}\text{N}$ can provide relative measures of feeding niches and track changes through ontogenic development as preflexion larvae shift from exogenous feeding to piscivory during flexion and postflexion stages (Laiz-Carrión et al., 2015, 2019, Uriarte et al., 2016, 2019).

The stock-recruit relationship

One of the central questions to improving ABT stock assessments relates to drivers of recruitment. Stock-recruitment relationships are tools that enable fishing quotas and guide management plans (Camp et al., 2021). Multiple uncertainties have resulted in limited resolution of the stock-recruit relationship for ABT stocks (Collette & Graves, 2019). In addition, if less than 1% of larvae typically survive to become juveniles, then changes in larval mortality can cause large fluctuations in recruitment (Houde 2008, Bakun 2014). Events during the ABT early life history prior to reaching reproductive maturity may result in a decoupling of recruitment from established spawning stock predictions (depending on the factors and the life stage). For example, year-0 ABT (including larval populations) survival may be influenced by small-scale events such as food-availability or by large-scale events (e.g., *Deepwater Horizon* spill in 2010).

Predictions of future warming of the GoM will likely alter the spawning habitat for ABT (Muhling et al., 2011). These events highlight the importance of understanding both the broad ocean circulation on a larger scale, as well as mesoscale, and additional small-scale processes.

Stock assessments can influence decisions made by regional and international managers (e.g., ICCAT), which can in turn have an impact on the fishing quotas and other conservation strategies to manage the stock. Examination of otoliths of surviving bluefin tuna juveniles suggests fast growth as indicative of favorable conditions and higher survival rates (Brothers et al., 1984, Tanaka et al., 2006, Watai et al., 2017). Inter-annual ecological data at a finer scale may improve the accuracy of the existing tools used in ecosystem-based fisheries management. Specifically, enhancing knowledge of ABT growth dynamics can improve the ecological understanding of year-to-year variability, and could lead to better stock-specific growth estimates for ABT. In addition, stock assessments track temporal variation that can reveal trends (increases vs decreases) and can highlight strong recruitment year classes to be harvested (or protected) as needed. Ages derived from otoliths are critical to interpret the factors affecting ABT recruitment, which are essential for supporting stock assessment models, and thus effective ecosystem based management for ABT.

Study areas

Gulf of Mexico

The GoM biophysical environment is strongly influenced by oceanographic circulation patterns and seasonal temperature fluctuations (Figure 1.4). The main mesoscale feature in the GoM is the Loop Current, a northward extension of the Yucatan Current, which exits the Gulf through the Straits of Florida to become the Gulf Stream (McGillicuddy et al., 1998, Lindo-Atichati et al., 2012). The Loop Current forms an intense anticyclonic flow in the eastern Gulf, and may extend northwards as far as 28°N (Hurlburt & Thompson, 1982). These northward extensions may last for several months, until the current becomes unstable and sheds a large anticyclonic ring (Maul & Vukovich, 1994). These warm-core rings, drift westward, where they spin up smaller cyclonic eddies along the shelf, resulting in complex and dynamic oceanographic conditions in the northern GoM (Lindo-Atichati et al., 2012). Along the northern shelf of the

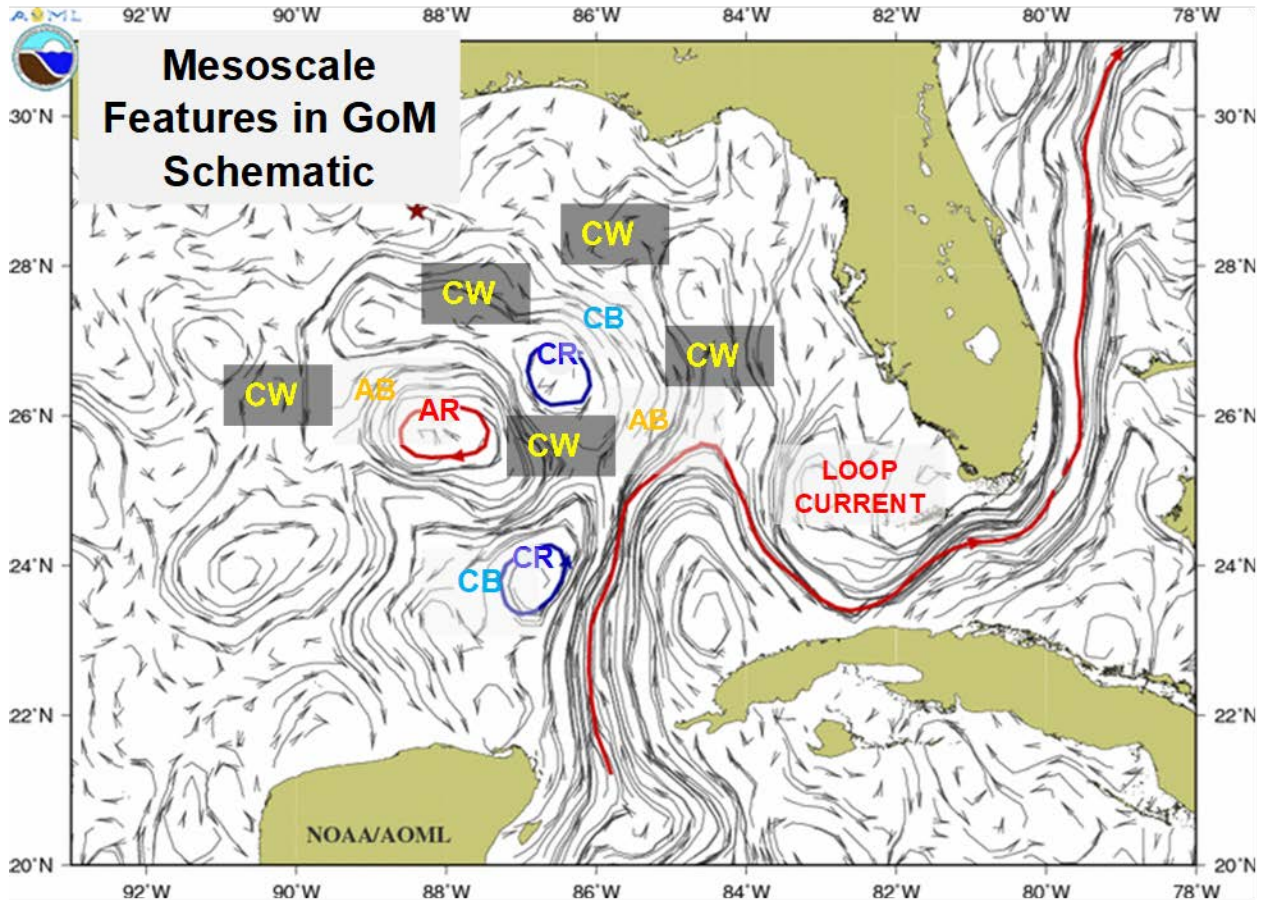


Figure 1.4. Schematic representation of the mesoscale features in the Gulf of Mexico during summer 2010: Common Water (CW), cyclonic region (CR), cyclonic boundary (CB), anticyclonic region (AR), and anticyclonic boundary (AB). The black contour lines indicate the prevailing direction of the current, thicker lines indicate stronger flow. The red contour line indicates the Loop Current. The red and blue solid contours indicate the location of the anticyclonic (red) and cyclonic eddies (blue). Image modified from NOAA AOML.

GoM, most of the year, cyclonic circulation is driven by the along-coast wind stress component. The circulation occurs as a strong coastal current located along the inner shelf that interacts with a weak broad current over the outer shelf (Zavala-Hidalgo et al., 2003). In this way, the low-salinity water from the Mississippi and Atchafalaya rivers are advected westward along the shelf developing along-shelf fronts. Moreover, this water mass is richer in nutrients and sediments and enhances productivity resulting in higher concentrations of chlorophyll-a (Biggs & Muller-Karger, 1994, Nababan et al., 2011).

These oceanographic features structure the Gulf into habitats with different physical and biological characteristics, with associated surface fronts delineating boundaries between different surface water characteristics (Domingues et al., 2016, Johnston et al., 2019). Eddies and fronts may act as mechanisms of enrichment, concentration and retention, which could in turn benefit larval growth and survival (Bakun, 2006, Shulzitski et al., 2016). ABT larvae are distributed across these features in the GoM during the April-June spawning season and larvae spawned are likely exposed to several different hydrodynamic and ecological regimes over the several weeks before they begin schooling and develop into juveniles.

Mediterranean Sea

There are three main spawning areas for the eastern ABT stock in the MED region: the Balearic spawning grounds in the west, the Tunisia-Malta spawning grounds in the central region, and the Cyprus spawning grounds in the eastern MED (Alvarez-Berastegui et al., 2018). Among them, the most studied spawning area is located in the Balearic Sea (Figure 1.5). The Spanish Institute of Oceanography along with multiple partners have examined larval tuna

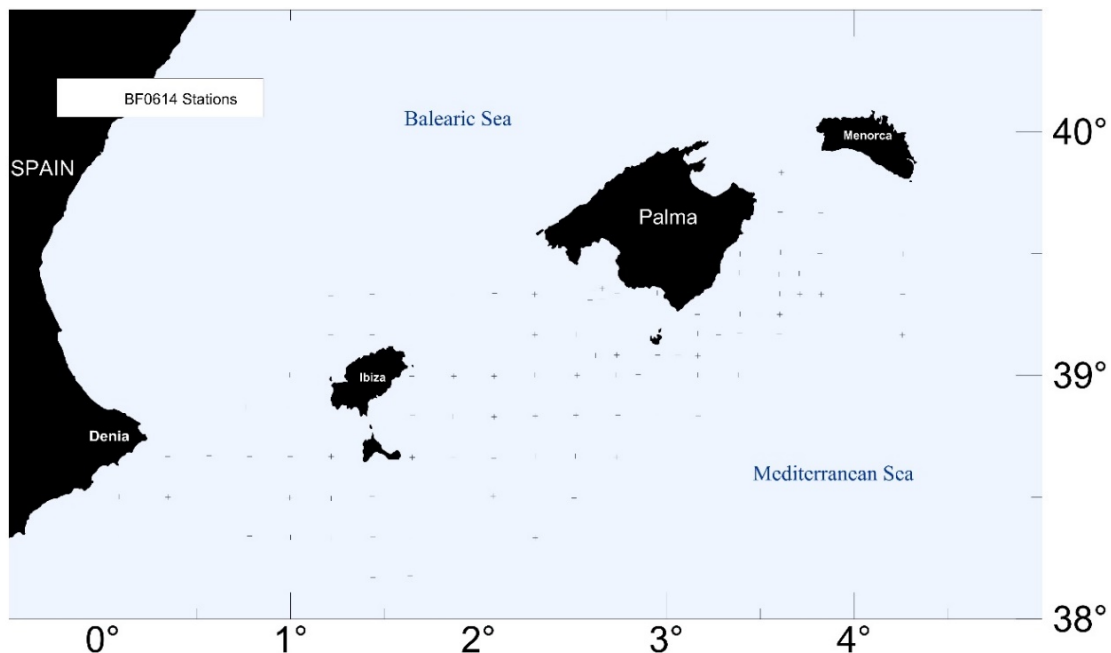


Figure 1.5: The western Mediterranean Sea showing the main study area for Atlantic bluefin tuna larval collections (+) during survey BF0614 in 2014.

dynamics in the region in various projects (e.g., TUNIBAL², ECOLATUN³, GBYP⁴) for several years (2001- 2005, and 2012-present) (Alemany et al., 2010, Alvarez-Beristegui et al., 2016, García et al., 2017, Alvarez et al., 2021). Similar to the index developed for the GoM's western stock, fishery independent indices were developed for the eastern stock using larval catches from ichthyoplankton surveys (Ingram et al., 2017, Alvarez-Berastegui et al., 2018). The index includes 2001 through 2005, and 2012-present day. In the western MED, larval ABT abundances are significantly greater than larval abundances from the GoM (Muhling et al., 2013). Beginning in late May and early June, adults begin to arrive into the Balearic Sea with incoming Atlantic surface waters and spawn mostly in the fronts associated with the lee created by the Mallorcan Islands. These fronts result in a trophic cascade when the cooler resident waters mix with the warmer Atlantic water masses (Balbín et al., 2014, Laiz-Carrión et al., 2015). Several larval studies have examined trophodynamics, diet analyses, and reared-larvae born in the MED, however larval growth has not been integrated into recent ecological studies after the early 2000s when García et al. (2013) aged larvae from 2003, 2004, and 2005.

1.1.1 Statement of the problem and approach

Otolith biometrics can improve our understanding of biotic and abiotic drivers that play a key role in the development of credible predictive recruitment models for ABT that ultimately contribute to stock assessment models. Isolating the drivers of larval growth individually is unrealistic due to the interwoven influences that the environment and individual variability exert on each other. In the subsequent chapters, three approaches are utilized that attempt to untangle some of the variability and focus on larval growth strategies of larval ABT through ontogeny as they interact with their nursery grounds in their quest for survival.

Chapter 2:

Despite the need to improve the understanding of larval ABT life history and the unidentified links to recruitment, larval growth comparisons between the two main spawning

² Tunidos Baleares Project (2001-2005, Mini TUNIBAL 2006-2007)

³ Comparative trophic ECOlogy of LArvae of Atlantic bluefin TUNa from NW Mediterranean and Gulf of Mexico spawning areas, CTM2015-68473-R.

⁴ Atlantic-Wide Research Programme for Bluefin Tuna (Managed by ICCAT)

grounds have yet to be calibrated for the same spawning season to examine temporal and spatial variability. First, this chapter generated companion growth curves for the 2014 ABT spawning season in the GoM and MED by ageing otoliths from larvae collected from the respective spawning grounds, and compared age-at-length estimates. Second, potential density-dependence and trophodynamics using bulk $\delta^{15}\text{N}$ and $\delta^{13}\text{C}$ were compared using recent otolith growth for postflexion larvae using general additive models to examine the variability of larval growth in conjunction with trophic variables for each corresponding spawning ground.

Chapter 3:

The mechanisms that link variability in nitrogen sources and food-web fluxes in the GoM has not been examined in relation to habitat quality, feeding, growth, and survival for ABT larvae. This chapter is part of a larger collaborative project that aimed to define the mechanisms that link these processes to larval growth and survival. First, larval patches of ABT were tracked and followed the using Lagrangian-based drogued buoys across 2-4 days in the northern GoM in May 2017 and 2018. Second, age-at-length estimates for larvae were incorporated in a generalized additive model to examine the variability of observed recent larval growth with a suite of environmental variables that included trophic position of larvae, diet, prey field, and *in situ* abiotic conditions.

Chapter 4:

Mesoscale eddies are hypothesized to provide important habitat for larval fishes particularly in the open ocean. Otolith microstructure patterns have revealed that mesoscale oceanographic features influence larval growth (e.g., faster growth). Mesoscale oceanography heavily influences larval ABT nurseries in particular, habitat quality. In this study, ABT growth curves were developed and inter-annual variability between three cohorts was assessed. Second, feature-specific growth curves were compared for inter-feature growth, and size-specific growth between the youngest vs. oldest larvae were analyzed. The goal was to ascertain whether these entrained larvae experience the benefit of increased growth in specific mesoscale features. Lastly, gut contents were examined from the 2016 aged ABT larvae to explore feeding dynamics within mesoscale features.

REFERENCES

- Aleman, F., Quintanilla, L., Velez-Belchí, P., García, A., Cortés, D., Rodríguez, J.M., et al. (2010). Characterization of the spawning habitat of Atlantic bluefin tuna and related species Balearic Sea (western Mediterranean). *Prog. Oceanogr.* 86:21–48.
- Anonymous, (2019). Report of the standing committee on research and statistics (SCRS). ICCAT, Madrid, Spain.
https://www.iccat.int/Documents/Meetings/Docs/2019/REPORTS/2019_SCRS_ENG.pdf
- Alvarez, I., Rasmuson, L. K., Gerard, T., Laiz-Carrión, R., Hidalgo, M., Lamkin, J. T., Malca, E., Ferra, C. et al. (2021) Influence of the seasonal thermocline on the vertical distribution of larval fish assemblages associated with Atlantic bluefin tuna spawning grounds. *Oceans*, 2, 64–83.
- Alvarez-Berastegui, D., Hidalgo, M., Tugores, M., Reglero, P., Aparicio-González, A., Ciannelli, L., Juza, M., Mourre, B. et al. (2016) Pelagic seascape ecology for operational fisheries oceanography: modelling and predicting spawning distribution of Atlantic bluefin tuna in Western Mediterranean. *ICES J. Mar. Sci.*, 73, 1851–1862.
- Alvarez-Berastegui, D., Mourre, B., Saber, S., Juza, M., Ortiz de Urbina, J., Macias, D., Reglero, P. (2018). Environmental variability in three major Mediterranean tuna spawning grounds. *Col. Vol. Sci. Pap. ICCAT*, 75(2): 337-344.
- Bakun, A. (2014) Ocean eddies, predator pits and bluefin tuna: implications of an inferred ‘low risk–limited payoff’ reproductive scheme of a (former) archetypical top predator. *Fish Fish.*, 14, 424-448.
- Balbín, R., López-Jurado, J.L., Flexas, M.M., Reglero, P., Vélez-Velchí, P., et al. (2014) Interannual variability of the early summer circulation around the Balearic Islands: Driving factors and potential effects on the marine ecosystem. *J. Mar. Syst.*, 138:70-81.
- Biggs, D.C., Müller-Karger, F. (1994) Ship and satellite observations of chlorophyll stocks in interacting cyclone-anticyclone eddy pairs in the western Gulf of Mexico. *J. Geophys. Res.*, 99(C4):7371-7384.
- Block, B. A., Teo, S.L.H., Walli, A., Boustany, A., Stokesbury, M. J. W., Farwell, C. J., et al. (2005) Electronic tagging and population structure of Atlantic bluefin tuna. *Nature*, 434(7037): 1121-1127, doi: 10.1038/nature03463.
- Block, B. A. (2019) *The future of bluefin tunas: ecology, fisheries management, and conservation*. John Hopkins University Press, Baltimore, MD, USA, 346 pp.

- Brothers, E.B., Prince, E.D., Lee, D.W. (1984). Age and growth of young-of-the-year bluefin tuna, *Thunnus thynnus*, from otolith microstructure. In: Prince, E.D. and Pulos, L.M., eds. Procedures of the international workshop on age determination of oceanic pelagic fishes: tunas, billfishes, and sharks. NOAA Tech. Repos. N. M. F. S., 8, 49–60.
- Camp, E.V., Ahrens, R.N.M, Collings, A.B., Lorezen, K. (2021) Fish population recruitment: what recruitment means and why it matters. Downloaded on 20 November 2022, doi.org/10.32473/edis-fa222-2020.
- Campana, S. E., and Jones, C. (1992) Measurement and interpretation of the microstructure of fish otoliths. In: Stevenson, D. K. and Campana, S. E. (eds) Otolith microstructure examination and analysis. Can. Spec. Publ. Fish. Aquat. Sci., 117, 59-71.
- Campana, S.E., and Neilson., J.D. (1985). Microstructure of fish otoliths. Can. J. Fish. Aquat. Sci. 42:1014-1042.
- Catalán, I. A., Alemany, F., Morillas, A. & Morales-Nin, B. (2007). Diet of larval albacore *Thunnus alalunga* (Bonnaterre, 1788) off Mallorca Island (NW Mediterranean). Sci. Mar., 71, 447– 454.
- Catalán I.A., Tejedor, A., Alemany, F., Reglero, P. (2011) Trophic ecology of Atlantic bluefin tuna *Thunnus thynnus* larvae. J. Fish. Biol., 78: 1545–1560.
- Collette, B.B. and Graves, J. 2019. Tunas and Billfishes of the World. Johns Hopkins University Press, Baltimore, Maryland.
- Collette, B., Amorim, A.F., Boustany, A., Carpenter, K.E., de Oliveira Leite Jr., N., Di Natale, et al. (2014) *Thunnus thynnus*. The IUCN Red List of Threatened Species. Version 2014.2. <www.iucnredlist.org>. Accessed on September 16, 2014.
- Di Natale, A. (2014). The ancient distribution of bluefin tuna fishery: how coins can improve our knowledge. Collect. Vol. Sci. Pap. ICCAT, 70(6):2828-2844.
- Domingues, R., Goni, G., Bringas, F., Muhling, B., Lindo-Atichati, D. and Walter, J. (2016) Variability of preferred environmental conditions for Atlantic bluefin tuna (*Thunnus thynnus*) larvae in the Gulf of Mexico during 1994–2011. Fish. Oceanogr., 25, 420–446.
- Fromentin, J. M. and Powers, J. E. (2005) Atlantic bluefin tuna: population dynamics, ecology, fisheries and management. Fish and Fish., 6, 281–406.
- García, A., Cortés, D., Quintanilla, J., Ramirez, T., Quintanilla, L., Rodríguez, J. M. and Alemany, F. (2013) Climate-induced environmental conditions influencing interannual variability of Mediterranean bluefin (*T. thynnus*) larval growth. Fish. Oceanogr., 22: 274–287.

- García, A., Laiz-Carrión, R., Uriarte, A., Quintanilla, J., Morote, E., Rodriguez, J., Alemany, F. (2017). Differentiated stable isotopes signatures between pre- and post-flexion larvae of Atlantic bluefin tuna (*T. thynnus*) and of its associated tuna species of the Balearic Sea (NW Mediterranean). *Deep. Sea. Res., Part II*, 140: 18-24.
- Gleiber, M. R., Sponaugle, S., Robinson, K. and Cowen, R. (2020a) Food web constraints on larval growth in subtropical coral reef and pelagic fishes. *Mar. Ecol. Prog. Ser.*, 650, 19–46.
- Gleiber, M.R., Sponaugle, S., Cowen, R. K. (2020b) Some like it hot, hungry tunas do not! Implications of temperature and plankton food web dynamics on growth and diet of tropical tuna larvae. *ICES J. Mar. Sci.*, 77 (7-8):4058–4074, <https://doi.org/10.1094/icesjms/fsaa201>.
- Habtes, S., Muller-Karger, F., Roffer, M., Lamkin, J.T., Muhling, B.A. (2014). A comparison of sampling methods for larvae of medium and large epipelagic fish species during spring SEAMAP ichthyoplankton surveys in the Gulf of Mexico. *Limnol. Oceanog. Meth.*, 12, 86–101.
- Hernández, C. H., Richardson, D. E., Rypina, I. I., Chen, K., et al. (2021) Support for the Slope Sea as a major spawning ground for Atlantic bluefin tuna: evidence from larval abundance, growth rates, and particle-tracking simulations. *Can. J. Fish. Aquat. Sci.* 79: 814-824.
- Houde, E. D. (2008) Emerging from Hjort’s Shadow. *J. Northw. Atl. Fish. Sci.*, **41**: 53–70, [doi:10.2960/J.v41.m634](https://doi.org/10.2960/J.v41.m634).
- Hurlburt, H.E., Thompson, J.D. (1982) The dynamics of the Loop Current and shed eddies in a numerical model of the Gulf of Mexico. Elsevier Oceanography Series. Elsevier. pp. 244-297.
- Ingram Jr., G. W., Richards, W. J., Lamkin, J. T. and Muhling, B. A. (2010) Annual indices of Atlantic bluefin tuna (*Thunnus thynnus*) larvae in the Gulf of Mexico developed using delta-lognormal and multivariate models. *Aquat. Living Resour.*, 24, 45-47.
- Ingram Jr., G.W., Alvarez-Berastegui, D., Reglero, P., Balbín, R., García, A. (2017) Incorporation of habitat information in the development of indices of larval bluefin tuna (*Thunnus thynnus*) in the Western Mediterranean Sea (2001–2005 and 2012–2014). *Deep Sea Res., Part II*, 140, 204-211. <https://doi.org/10.1016/j.dsr2.2017.04.012>.
- Itoh, T., Shiina, Y., Tsuji, S., Endo, F., Tezuka, N. (2000). Otolith daily increment formation in laboratory reared larval and juvenile bluefin tuna *Thunnus thynnus*. *Fish. Sci.*, 66(5):834-839.

- Johnston, M., Milligan, R.J., Easson, C.G., Penta, B., DeRada, S., Sutton, T. (2019) An empirically-validated method for characterizing pelagic habitats in the Gulf of Mexico using ocean model data. *Limnol. & Oceanogr. Method.*, 17(6): 363-375, doi.org/10.1002/Iom3.10319.
- Kodama, T., Hirai, J., Tamura, S., Takahashi, T., Tanaka, Y., et al. (2017). Diet composition and feeding habits of larval Pacific bluefin tuna *Thunnus orientalis* in the Sea of Japan: integrated morphological and metagenetic analysis. *Mar. Ecol. Prog. Ser.*, 583, 211–226.
- Laiz-Carrión, R., Gerard, T., Uriarte, A., Malca, E., Quintanilla, J.M., Muhling, B.A., Alemany, F., Privoznik, S. L. et al. (2015) Trophic ecology of Atlantic bluefin tuna (*Thunnus thynnus*) larvae from the Gulf of Mexico and NW Mediterranean spawning grounds: a comparative stable isotope study. *PLoS One*, 10(9):122, e0144406, doi:10.1471/journal.pone.0144406.
- Laiz-Carrión, R., Gerard, T., Suca, J.J., Malca, E., Uriarte, A., Quintanilla, J.M., Privoznik, S.L., Llopiz, J.K., et al. (2019) Stable isotope analysis indicates resource partitioning and trophic niche overlap in larvae of four tuna species in the Gulf of Mexico. *Mar. Ecol. Prog. Ser.*, 619:54-68. <https://doi.org/10.4454/meps12958>.
- Lang, K.L., Grimes, C.B., Shaw, R.F. (1994) Variations in the age and growth of yellowfin tuna larvae, *Thunnus albacares*, collected about the Mississippi River plume. *Environ. Biol. Fish.*, 39, 259–270.
- Llopiz, J. K., Richardson, D. E., Shiroza, A., Smith, S. L. and Cowen, R. K. (2010) Distinctions in the diets and distributions of larval tunas and the important role of appendicularians. *Limnol. Oceanogr.*, 55, 984–996.
- Llopiz, J.K, Cowen, R.K., Hauff, M.J., Ji, R., Munday, P.L., Muhling, B.A., Peck, M.A. (2014). Early Life History and Fisheries Oceanography: New Questions in a Changing World *Oceanogr.*, 27 (4), 26-41.
- Llopiz, J. K., and Hobday, A. J. (2015) A global comparative analysis of the feeding dynamics and environmental conditions of larval tunas, mackerels, and billfishes. *Deep Sea Res. Part II: Top. Stud. Oceanogr.*, 114, 114 - 124.
- Malca, E., Muhling, B. A., Franks, J., García, A., Tilley, J., Gerard, T., et al (2017) The first larval age and growth curve for (*Thunnus thynnus*) from the Gulf of Mexico: comparisons to the Straits of Florida, and the Balearic Sea (Mediterranean). *Fish. Res.*, 190, 24 - 44.
- Maul, G.A. and Vukovich, F.M. (1994) The relationship between variations in the GOM Loop Current and straits of Florida volume and transport. *J. Phys. Oceanogr.*, 24: 785 - 796.

- McGillicuddy, D.J., Jr, Robinson, A.R., Siegel, D.A., Jannasch, H.W., Johnson, R., Dickey, T.D., McNeil, J., Michaels, A.F., and Knap, A.H. (1998). Influence of mesoscale eddies on new production in the Sargasso Sea. *Nature* 394: 263-266.
- Morote, E., Olivar, M. P., Pankhurst, P. M., Villate, F. and Uriarte, I. (2008) Trophic ecology of bullet tuna *Auxis rochei* larvae and ontogeny of feeding-related organs. *Mar. Ecol. Prog. Ser.*, 454, 244 - 254.
- Muhling, B. A., Lamkin, J. T. and Roffer, M. A. (2010) Predicting the occurrence of Atlantic bluefin tuna (*Thunnus thynnus*) larvae in the northern Gulf of Mexico: building a classification model from archival data. *Fish. Oceanogr.*, 19, 526 – 549.
- Muhling, B. A. *et al.* (2011) Predicting the effects of climate change on bluefin tuna (*Thunnus thynnus*) spawning habitat in the Gulf of Mexico. *ICES J. Mar. Sci.*, **68**, 1051–1062.
- Muhling, B.A., Reglero, P., Ciannelli, L., Alvarez-Berastegui, D., Alemany, F., Lamkin, J.T., Roffer, M.A. (2013). Comparison between environmental characteristics of larval bluefin tuna *Thunnus thynnus* habitat in the GOM and western Mediterranean Sea. *Mar. Ecol. Prog. Ser.* 486, 257–276.
- Muhling, B.A., Lamkin, J.T., Alemany, F., García, A., Farley, J.H., Ingram, G.W. Jr., Berastegui, D.A., Reglero, P., et al. (2017) Reproduction and larval biology in tunas, and the importance of restricted area spawning grounds. *Rev. Fish. Biol. Fish.*, 27,697–732. <https://doi.org/10.1007/s11160-017-9471-4>.
- Nababan, B., Muller-Karger, F., Hu, C., Biggs, D. (2011). Chlorophyll variability in the Northeastern Gulf of Mexico. *Int. J. Remote Sens.*, 32, 8373-8391.
- National Marine Fisheries Service. (2011) Status review report of Atlantic Bluefin Tuna (*Thunnus thynnus*). Report to National Marine Fisheries Service, Northeast Regional Office.
- National Marine Fisheries Service. (2014) FishWatch NOAA. Western Atlantic bluefin tuna (*Thunnus thynnus*). Downloaded 30 October 2014, www.nmfs.noaa.gov/seafood_profiles/species/tuna/species_pages/atl_bluefin_tuna.htm.
- National Marine Fisheries Service. (2022) FishWatch NOAA. U.S. Seafood Facts: Western Atlantic bluefin tuna. Downloaded 20 April 2020, <https://www.fishwatch.gov>.
- Nayar, A. (2010) Bad news for tuna is bad news for CITES. *Nature*. Downloaded on 20 November 2022, <https://doi.org/10.1038/news.2010.139>.
- Neilson, J.D., Campana, S.E. (2008). A validated description of age and growth of western Atlantic bluefin tuna (*Thunnus thynnus*). *Can. J. Fish. Aquat. Sci.* 65(8):1524 - 1527.

- Pannella, G. (1971) Fish otoliths: daily growth layers and periodical patterns. *Science*, 173, 1124–1127.
- Pepin, P., Robert, D., Bouchard, C., Dower, J.F., Falardeau, M., Fortier, L., Jenkins, G.P., et al. (2014). Once upon a larva: revisiting the relationship between feeding success and growth in fish larvae. *ICES J. Mar. Sci.*, doi: 10.1094/icesjms/fsu201.
- Quintanilla, J.M., Laiz-Carrión, R., García, A., Quintanilla, L.F., Cortés, D., Gómez-Jakobsen et al. (2020) Early life trophodynamic influence on daily growth patterns of the Alboran Sea sardine (*Sardina pilchardus*) from two distinct nursery habitats (bays of Málaga and Almería) in the Western Mediterranean Sea. *Mar. Env. Res.*, 162: 105195.
- Restrepo, V.R., Diaz, G.A., Walter, J.F., Neilson, J.D., Campana, S.E., Secor, D., Wingate, R.L., (2010). Updated estimate of the growth curve of Western Atlantic bluefin tuna. *Aquat. Livi. Res.*, 24:445-442.
- Rooker, J.R., Alvarado-Bremer, J.R., Block, B.A., Dewar, H., DeMetrio, G., et al. (2007). Life history & stock structure of Atlantic bluefin tuna (*Thunnus thynnus*). *Rev. Fish. Sci.*, 15:265-410.
- Scott, G.P., Turner, S.C., Grimes, C.B., Richards, W.J., Brothers, E.B. (1994) Indices of larval bluefin tuna, *Thunnus thynnus*, abundance in the GOM: Modeling variability in growth, mortality, and gear selectivity: Ichthyoplankton methods for estimating fish biomass. *Bull. Mar. Sci.*, 54: 912-929.
- Secor, D.H., Wingate R.L., Neilson J.D., Rooker J.R., Campana S.E., (2008). Growth of Atlantic bluefin tuna: direct age estimates. *Col. Vol. Sci. Pap. ICCAT 2008/84*.
- Secor, D.H., Dean, J.M., Campana, S.E. (1995). Recent developments in fish otolith research. Univ. of South Carolina Press. Columbia, S.C. 740 pp.
- Shiroza, A., Malca, E., Lamkin, J. T., Gerard, T., Landry, M. R., Stukel, et al. (2021) Diet and prey selection of Atlantic Bluefin Tuna (*Thunnus thynnus*) larvae in spawning grounds of the Gulf of Mexico. *J. Plankton Res.*, 44(5):728-746. Doi:10.1094/plankt/fbab020.
- Shulzitski, K, Sponaugle, S, Hauff, M, Walter, KD, Cowen, RK. (2016) Encounter with mesoscale eddies enhances survival to settlement in larval coral reef fishes. *Proc. Natl. Acad. Sci.* 114(25):6928-44. doi: 10.1074/pnas.1601606114.
- Sponaugle, S. 2009. Daily otolith increments in the early stages of tropical fish. Pages 93-132, In B. S. Green, B. D. Mapstone, G. Carlos, and G. A. Begg, (eds). *Tropical Fish Otoliths: Information for Assessment, Management and Ecology*. Springer, New York, NY.

- Tanaka, Y., Satoh, K., Iwahashi, M., Yamada, H. (2006) Growth-dependent recruitment of Pacific bluefin tuna *Thunnus orientalis* in the northwestern Pacific Ocean. Mar. Ecol. Prog. Ser. 319, 225–235.
- Tanaka, Y., Minami, H., Ishihi, Y., Kumon, K., Higuchi, K., Eba, T., et al. (2014) Differential growth rates related to initiation of piscivory by hatchery-reared larval Pacific bluefin tuna *Thunnus orientalis*. Fish. Sci., DOI 10.1007/s12562-014-0798-7.
- Tilley, J. D., Butler, C. M., Suárez-Morales, E., Franks, J. S., Hoffmayer, E. R., Gibson, D., Comyns, B. H., Ingram, Jr., G. W., et al. (2016) Feeding ecology of larval Atlantic bluefin tuna, *Thunnus thynnus*, from the central Gulf of Mexico. Bull. Mar. Sci., 92, 421–444.
- Uotani, K. Matsuzaki, Y. Makino, K. Noda, O. Inamura, M. Horikawa (1981). Food habits of larvae of tunas and their related species in the area northwest of Australia Nippon Suisan Gakk, 47: 1165-1172, 10.2441/suisan.47.1165.
- Uriarte, A., García, A., Ortega, A., De La Gándara, F., Quintanilla, J., Laiz-Carrión, R. (2016). Isotopic discrimination factors and nitrogen turnover rates in reared Atlantic bluefin tuna larvae (*Thunnus thynnus*): effects of maternal transmission. Sci. Mar., 80: 447 - 456.
- Uriarte, A., Johnstone, C., Laiz-Carrión, R., García, A., Llopiz, J. K., Shiroza, A., et al. (2019) Evidence of density-dependent cannibalism in the diet of wild Atlantic bluefin tuna larvae (*Thunnus thynnus*) of the Balearic Sea (NW-Mediterranean). Fish. Res., 212, 64-71.
- Watai, M., Ishihara, T., Abe, O., Ohshimo, S., Strussmann, C. A. (2017) Evaluation of growth-dependent survival during early stages of Pacific bluefin tuna using otolith microstructure analysis. Mar. Freshwater Res., 68, 2008-2017.
- Zavala-Hidalgo, J., Morey, S.L., O'Brien, J.J. (2003) Seasonal circulation on the western shelf of the Gulf of Mexico using a high-resolution numerical model. J. Geophys. Res., 108(C12):3389 DOI:10.1029/2003JC001879.

CHAPTER 2: Comparative examination of larval growth, stable isotope analysis, and trophic position of Atlantic bluefin tuna from two discrete spawning grounds

INTRODUCTION

The highly migratory Atlantic bluefin tuna (*Thunnus thynnus* Linnaeus, 1758, hereafter referred to as ABT) is the largest scombrid, reaching up to 650 kg (Block et al., 2005). The ABT's highly prized meat has led to substantial overfishing (Rooker et al., 2007, Collette et al., 2011). Subsequently, multiple ecological studies have sought to inform ABT management decisions aiming to mitigate the species' further decline (Fromentin & Powers 2005, Secor et al., 2008, Restrepo et al., 2010, Laiz-Carrión et al., 2019, Gerard et al., 2022).

ABTs spawn in two locations, with nearly all of the western stock spawning in the Gulf of Mexico (GoM), while the eastern stock spawns in various regions of the Mediterranean Sea (MED) (Fromentin & Powers 2005, Muhling et al., 2013, Gordo et al., 2021). These oceanic (seaward of the 200-m isobath) tuna migrate large distances from nutrient-rich feeding areas to highly oligotrophic regions and position their larvae in an arguably optimal habitat for survival (Bakun 2012). Furthermore, ABT spawning appears to be mediated by sea surface temperatures (SSTs) above approximately 23 °C (Muhling et al., 2010, Alemany et al., 2010), and occurs in the GoM between April and June and in the MED between June to July (Laiz-Carrión et al., 2015, Muhling et al., 2017).

Although ABT's two spawning areas are both oligotrophic environments that experience a noticeable increase in SST prior to spawning, they diverge in environmental characteristics during the spawning periods. The GoM is influenced by eddies that are shed by the Loop Current year-round and propagate westward (Domingues et al., 2016, Lindo-Atichati et al., 2012). These features enrich the circulatory dynamics by introducing fast-moving, warmer Caribbean water into the region. In the MED, the summer hydrodynamics are influenced by the incoming North Atlantic Sea entering the region via the Strait of Gibraltar. This warmer and less saline water mass interacts with the local bathymetry, the topography of various islands, and the cooler and more saline Mediterranean Sea. When the Atlantic water mass propagates eastward, local productivity is enhanced in this area (Vélez-Belchí & Tintoré 2001, Sabatés, et al., 2007, Balbín et al., 2014).

Larval ageing is particularly relevant in ABT fisheries management because abundances from annual fisheries surveys provide yearly estimates of adult spawning biomass by using observed larval length distributions (Scott et al., 1993, Ingram et al., 2010, 2017). Previous studies have aged larval ABT otoliths from both spawning areas (García et al., 2006, 2013, Malca et al., 2017). For instance, otolith growth has been used to examine larval development, nutritional changes, and environmental gradients that influence larval growth. Daily otolith increments are visible as bipartite structures composed of a transparent layer (L-zone) and a darker but often-wider layer (D-zone) under transmitted light (Campana & Jones, 1992, Secor et al., 1995). Moreover, daily increments widen with ontogeny for several larval tuna species (*Katsuwonus pelamis*, Zygis et al., 2015, *T. atlanticus* Gleiber et al., 2020b, *Auxis* spp. (Laiz-Carrión et al., 2013), for bluefin tunas, *T. thynnus* (Malca et al., 2017, García et al., 2013), for *T. orientalis* (Watai et al., 2017), and for *T. maccoyii* (Jenkins & Davis, 1990).

In the MED, García et al. (2013) aged multiple cohorts from the early 2000's and reported a positive association between growth rates, SST and microzooplankton quality. Subsequently, Malca et al. (2017) compared GoM larval growth from the 2012 spawning season to the MED larval growth from the 2003-2005 spawning seasons in García et al. (2013). Malca et al. (2017) found significant differences in growth patterns between the two nursery grounds, with comparatively faster growth in the GoM. However, the inferences in the latter study relied on larvae that were aged using somewhat inconsistent methodologies and collected in different years from the GoM and the MED. Ageing estimates during the first weeks of life can vary significantly between seasons and locations (García et al., 2013, Long & Porta, 2019), and these differences can yield different growth rates. Subsequently, these variations in measurements can introduce error into larval abundance estimates (Ingram et al., 2010, 2017). Despite the need to improve the understanding of larval ABT life history and the unidentified links to recruitment, larval growth comparisons between the two main spawning grounds have yet to be calibrated by the same readers for the same spawning season to examine temporal and spatial variability.

Larval ecology: growth and trophodynamics

Previous trophodynamic studies of larval Scombridae have focused on stomach contents analysis (SCA) to characterize the larval diet after yolk absorption is completed and exogenous feeding begins. Larval ABT in the GoM predominantly feed on copepods, copepod nauplii,

appendicularians, and cladocerans (Llopiz et al., 2015, Tilley et al., 2016, Shiroza et al., 2021). Interestingly, active selection of cladocerans (podonids) over copepods was reported for ABT (Shiroza et al., 2021), and other tuna larvae (e.g., *Auxis* spp., *Katsuwonus pelamis*), show a preference for appendicularians (Llopiz et al., 2010, Llopiz & Hobday, 2015). ABT in the MED have a similar diet to the GoM, though selectivity has not been examined in depth yet with respect to respective prey field (Catalán et al., 2007, 2011, Uriarte et al., 2019). Despite the utility of SCA, it represents a “last meal” perspective of diet composition, with some rapidly digested prey potentially underestimated (Polis & Strong, 1996, Pinnegar & Polunin, 1999). Moreover, diet composition at geographic and temporal scales requires large numbers of samples across space, time, and requires extensive taxonomic expertise to accomplish.

In order to augment SCA, a biogeochemical approach utilizing natural abundances of stable isotopes of nitrogen ($^{15}\text{N}/^{14}\text{N}$, represented as $1\delta^{15}\text{N}$) and carbon ($^{13}\text{C}/^{12}\text{C}$ or $\delta^{13}\text{C}$) from consumers' tissues has proven useful in ecosystem studies (Fry 2006, Montoya 2007, Varela et al., 2019, Hildebrand 2022) including the GoM (Woodstock et al., 2021). Isotopic ratios reflect feeding pathways (Bodin et al., 2021). In general, higher $\delta^{15}\text{N}$ values specify higher trophic levels (Post 2002), and $\delta^{13}\text{C}$ reflects food web dynamics (Bodin et al., 2021). In pelagic environments, phytoplankton are the base of the feeding pathway. The primary producers have low $\delta^{15}\text{N}$ with variable $\delta^{13}\text{C}$ values reflecting primary producers. Moving upwards in the food web, small zooplankton will in turn have larger (i.e., more enriched) isotopic values and larval fishes that consume a copepod-rich diet will have even more enriched values.

For larval ABT, the $\delta^{15}\text{N}$ values are linked to the corresponding $\delta^{15}\text{N}$ zooplankton prey baseline that allows the estimation of trophic position (TP) as well as the corresponding trophic niche width (Laiz-Carrión et al., 2015, 2019). Nitrogen and carbon stable isotope signatures help to characterize the complex ecosystem of migratory species (Laiz-Carrión et al., 2013, 2015, 2019, García et al., 2017). Stable isotope analysis (SIA) of nitrogen from adult muscle tissues reflects the signature of the combined prey ingested for several months; however, for larval fishes the SIA signatures reflect only a few days of larval life (Peterson & Fry, 1987, Logan et al., 2006, Montoya 2007). SIA is a suitable method for testing hypotheses on developmental changes in sources of nutrition as it provides information on assimilated food (Laiz-Carrión et al., 2011, 2019). The analysis of nitrogen stable isotopes from prey to predators can be used as a proxy for estimating trophic position (TP) which reflects the efficiency of nitrogen transfer

through a food web (Montoya 2007, Caut et al., 2009). SIA provides time-integrated information about assimilated diet over longer timeframes than SCA (Peterson & Fry, 1987). TP indicates the ecological role of species in the ecosystem (Post 2002, Quezada-Romegialli et al., 2018).

Therefore, estimating the TP of organisms is crucial for understanding trophodynamics and the influence of trophic interactions on larval growth variability throughout ontogenetic development (Pepin & Dower, 2007, Laiz-Carrión et al., 2019, Quintanilla et al., 2020).

Differences between isotopic signatures between preflexion and postflexion ontogenetic stages reflect transgenerational maternal transmission of the nitrogen isotopic signature (Uriarte et al., 2016, Laiz-Carrión et al., 2019). Preflexion ABT larvae have higher nitrogen values, reflecting the maternal ABT adult signature. Consequently, the trophic information based on SIA (TP, isotopic niche width, and overlap analyses) should only include postflexion tuna larvae. Laiz-Carrión et al. (2013, 2015) observed trophic ecology disparities for ABT larvae between MED and GoM. These studies called for further research to investigate and evaluate the implications of these trophic differences on daily growth variability. In this way, a direct relationship between isotopic signature and growth strategies in larval stages can be determined, providing a useful method to analyze the trophic influence of trophic pathways on growth variability (Laiz-Carrión et al., 2011, Pepin et al., 2014, Quintanilla et al., 2015, 2020).

This study generated companion growth curves for the 2014 ABT spawning season in the GoM and MED by ageing larval otoliths collected from the respective spawning grounds and developing rigorous protocols for age-at-length estimates for larval ABT in the Atlantic Basin. In addition, a detailed comparison of otolith measurements between readers and among otoliths were tested to standardize ageing of larval tunas in general. Finally, potential density-dependence and trophodynamics using bulk $\delta^{15}\text{N}$ and $\delta^{13}\text{C}$ were compared using recent otolith growth for postflexion larvae using a General Additive Model (GAM) to examine the variability of larval growth in conjunction with trophic variables for each corresponding spawning ground.

METHODS

Larval collections

Two surveys collected larval ABT in the GoM and the MED during the peak spawning seasons in 2014 (Table 2.1). In the GoM, the *in situ* SST from CTD vertical profiling and surface flow-through thermosalinograph measurements guided sampling to target suitable larval ABT

habitat at approximately 15 to 25 n.m. intervals. The GoM survey avoided both warm temperatures (> 28 °C) indicative of Loop Current water and cooler temperatures (< 22° C) (Muhling et al., 2010). In the MED, a historical grid of stations were located at approximately 15 n.m. intervals in the Balearic archipelago region. The transient gradients created by the mixing between resident Mediterranean waters and warmer incoming Atlantic Ocean waters has been indicative of positive larval ABT habitat (Muhling et al., 2013).

These surveys were part of a collaborative project (ECOLATUN¹) that intended to standardize sampling techniques and examine the larval ecology at each corresponding study area. In the first effort, 76 stations were sampled aboard the R/V *F.G. Walton Smith* from 28 April to 25 May 2014 in the northern GoM using an “S-10” net (1 × 2 m frame fitted with 0.5-mm mesh net) towed the upper 10 m of the water column for ~10 minutes (Habtes et al., 2014). During the second effort, 98 stations were sampled aboard the R/V *SOCIB* from 17 June to 3 July in the Balearic Sea in the western Mediterranean (MED dataset henceforth). In the MED, a squared-mouth Bongo net (90-cm diameter) fitted with 0.5-mm mesh

Table 2.1. Survey dates, number of net tows, gear types and positive *Thunnus thynnus* (ABT) stations during each sampling effort in the Gulf of Mexico (GoM) and the Mediterranean Sea (MED, Balearic Sea) during the 2014 spawning season.

| Spawning grounds | 2014 sampling dates | Net tows | Gear, mesh | ABT stations (% positive) |
|------------------|---------------------|----------|----------------------------|---------------------------|
| GoM | 3-30 May | 74 | 1 × 2 m S-10 net, 0.505-mm | 34 (43%) |
| MED | 13 June - 3 July | 113 | 90 cm bongo, 0.505-mm | 64 (56%) |

was towed obliquely from ~ 30 m to the surface. Both frames were fitted with a flowmeter (2030, General Oceanics) positioned at the center of the mouth of each net to measure the volume of water filtered (m³).

Larval ABT were identified following Richards et al., (2006) at sea using stereomicroscopes (0.8 – 10×). Larvae were immediately preserved in liquid nitrogen to preserve tissues for subsequent isotopic analysis. Larvae were stored in a -80 °C freezer upon return from

¹ Comparative trophic ECOlogy of LArvae of Atlantic bluefin TUNa from NW Mediterranean and Gulf of Mexico spawning areas, CTM2015-68473-R.

the respective surveys. Each larva was assigned an identifier number that did not contain any morphometric information to prevent reader bias. Body length was measured to the end of the notochord for preflexion larvae, or up to the base of caudal peduncle in postflexion larvae. Body length (BL) was measured to the nearest 0.05 mm using the image analysis software Image J (Schneider et al., 2012). The remaining larval fish collected in the surveys were identified to the lowest taxonomic level. Total larval abundances, scombrid, and ABT abundances were tabulated for each survey. Abundances were standardized by dividing the abundance collected at each station by the corresponding volume filtered during the net tow for each study area. In cases where specimens of certain body sizes were underrepresented in GoM samples, specimen sets were supplemented with 15 ABT larvae originally preserved in ethanol. For these ethanol-preserved larvae, BLs were adjusted for ethanol-induced shrinkage by the following formula from Malca et al. (2022), developed for GoM ABT:

$$SL_{\text{ethanol}} = 0.907 (SL_{\text{saltwater}}) + 0.047.$$

Physical variables

Hydrographic data including temperature and salinity were collected at each sampling station using a Seabird SBE 9/11 Plus CTD profiler deployed to a target depth of 300 m or within 10 m of the seabed at shallow stations. A handful of stations lacked water profiles, thus the shipboard flow-through measurements for temperature (SST) and salinity (SSS) were extracted from the nearest (in time) net deployment in either spawning ground.

Larval ageing: otolith extraction and calibration

Ageing calibration was conducted independently by two experienced readers at two laboratories on either side of the Atlantic Ocean. A reader at the Instituto Español de Oceanografía in Malaga, Spain, read the otoliths first, then a second reader at the NOAA SEFSC² Miami Lab, USA, read the same set of otoliths. The readers examined a subset of all larvae collected from each study area (GoM and MED) following the same protocols, including otolith selection, nomenclature, preparation, increment reads, and best practices for the interpretation of daily increments. First, sagittal and lapilli otoliths (when possible) were extracted from larval ABT using minutien pins or sharpened glass probes. Otoliths were cleaned of any debris, dried

² Southeast Fisheries Science Center

and transferred into one drop of mounting medium (nail lacquer or Flo-Texx™), with the distal side of the sagittal otolith facing up. The otoliths were placed on a microscope slide labeled with the corresponding identifier number. Sagittal otoliths were chosen for ageing because they are the largest. However, for younger and less developed larvae, the sagittae and lapilli resembled each other in shape, size and topography; therefore, the otolith with the larger otolith radius (OR) was designated to be the sagittal otolith when it was not visually apparent.

The readers analyzed previously calibrated images captured with a compound microscope at 1000× using image analysis software. Reader-1 used a Zeiss A.1 with Image Pro Plus 7 while reader-2 used a Leica DM4 P with LAS X. Sagittal otoliths were examined with a compound microscope at 400 to 1000× with immersion oil under transmitted light, and daily increments were counted twice along the OR. The OR was measured from the center of the primordium to the edge of the OR along the longest axis. Each read was conducted at least one day apart to avoid reader bias. Age estimates were compared from the left and right sagittae from the same fish to examine possible within-otolith differences for a subset of larvae from each study area. Although previous ageing studies conducted for a variety of fishes found no significant differences between age estimates derived from the left versus the right sagittae (Campana 1999, Jenkins & Davis, 1990), this comparison had not been done for ABT larval otoliths.

Larval ageing: otolith measurement and interpretation

Daily otolith increment widths (IW, μm) were measured from the center of the primordium across the “diffuse zone” (non-incremental region) as described by Itoh et al. (2000) and Brothers et al. (1983) and successively to the edge of each D-zone along the OR at 1000× magnification. An increment was determined as complete when the beginning of the subsequent L-zone was apparent. Suitable age estimations of larval tunas (*Thunnus*) should consider that the first daily increment observed (inc_{obs}) is not always equivalent to day-1 of life. This offset occurs because the primordium is surrounded by an optically “diffuse zone” that is made of a discontinuous region that is not representative of daily incremental growth (Brothers et al., 1983, Itoh et al., 2000, Watai et al., 2017). Both readers systematically corrected for the uncertainty of the diffuse zone by assuming that the otolith size at hatch was located at a distance of 7 μm from the center of the primordium. This theoretical hatch radius (7 μm) estimate was based on previous ABT otolith reads ($n = 403$, hatch = $7.005 \mu\text{m} \pm 0.58$ (mean \pm SD) from TUNIBAL

surveys conducted in the western MED (Balearic Sea during 2003, 2004, and 2005) reported by García et al. (2013). Similarly, *T. maccoyii* otoliths were also observed to have a $hatch_{rad} \sim 7 \mu m$ (Jenkins & Davis, 1990).

In the wild, the width of the first increment for larval ABT were variable, ranging from 0.9-1.5 μm and increasing in width with ontogeny (Brothers et al., 1983, Malca et al., 2017, 2022, García et al., 2006, 2013). To account for this expected variability, the protocol was adjusted to limit the size of the predicted increment to be within observed IW ranges specific to each sagittal otolith. Age corrections were conducted as follows. First, the IW of the first observed increment was subtracted from the $hatch_{rad}$ and “predicted” increments were added until reaching the first observed increment. In addition, the width of the predicted increments had to be less than or equal to the first observed IW. The last observed increment ($inc_{X_{obs}}$) is often difficult to discern, and some ageing studies may dismiss problematic otoliths, lowering sample size. Thus, in a similar manner, if the IW of the $inc_{X_{obs}}$ was greater than the distance between the OR and the last $inc_{X_{obs}} - inc_{X_{obs}-1}$, an inc_{pred} was also added. Predicted increments were age-adjusted when appropriate and final age estimates were represented as days posthatch (dph).

Measurements of precision within and between readers were calculated using the coefficient of variation (CV) for dph (Chang 1982). Next, the CV was standardized for the interpretation for age estimations following Table 2.2. Larval tunas collected in the wild are typically younger larvae (< 6 -8 days) and otolith reads can range due to difficulties interpreting the first daily increments. Thus, young larval reads often have very high CV values compared to older larvae (~10 days) and large CVs (> 15%) are often regarded as poor quality reads and some studies discard them from further analyses. Yet this approach may prevent the youngest larvae from contributing to the overall larval growth variability. This study implemented a protocol that preserves young larvae (Table 2.2), allowing a predefined set of differences between reads during the evaluation of the CV between otolith reads.

Finally, least squares regressions were calculated for best fit of age (dph) at length, OR, weight (mg), and mean IW (μm) for each study area. Recent otolith growth was calculated as the mean of the last three completed IWs. Analyses of covariance (ANCOVA) were carried out using age as a continuous covariate and log-transformed biometric variables when required to meet normality assumptions.

Table 2.2. Criteria for otolith ageing for *Thunnus thynnus* between 3 – 25 days post hatch (dph). The three age groups and their corresponding allowed error for left vs. right otolith comparisons, and between otolith reads are specified. The coefficient of variation (CV) was set at 10% however, for the youngest larvae (3 - 6 dph), a larger CV was permitted only if the difference between reads was one day. The two older age groups could satisfy the specified CV or the indicated difference between reads.

| Age | CV % | Condition | Allowed error (days) |
|------------|-------------|------------------|-----------------------------|
| 3-6 | ≥ 10 | if | ± 1 |
| 7-13 | ≤ 10 | or | ± 1 |
| 14-25 | ≤ 10 | or | ± 2 |

Zooplankton collection for SIA

Zooplankton SIA measurements are necessary to interpret larval SIA data. Small zooplankton fractions were collected using a Bongo net (20-cm diameter, hereafter, bongo-20) fitted with 0.05- and 0.2 –mm mesh nets to target small (50-200 μm) and large (>200 μm) sizes of zooplankton. These zooplankton fractions have been utilized in previous studies (Laiz-Carrión, et al., 2015, 2019, Quintanilla, et al., 2020) as a proxy of prey for larval fishes. In the MED, the bongo-20 was attached to the bongo-90 and was towed concurrently. In the GoM, a separate tow was carried out for ~5 minutes from 0 to 10 m in an undulating manner and towed at least once during local daytime and nighttime throughout the survey. In both surveys, the bongo-20 was fitted with a flowmeter to calculate volume of water filtered (m^3), consistent with the bongo-90 sampling procedures mentioned above. Both nets were fractioned through a 0.2-mm mesh sieve to exclude any larger plankton. All zooplankton was frozen at $-20\text{ }^\circ\text{C}$ at sea. Lastly, dry weights (nearest 1 μg) of small and large (microzooplankton and mesozooplankton, hereafter) were standardized to mg m^{-3} by dividing with the volume filtered by each net.

Larval bluefin tuna SIA

Postflexion larvae selected for ageing were also analyzed for SIA. After extracting otoliths, larvae were dehydrated in a freeze dryer for 24 h and then dry weighed (mg). Next, the

stomachs were removed and the remaining larval tissues were packed in tin vials (0.03 ml). Natural abundance of $\delta^{15}\text{N}$ and $\delta^{13}\text{C}$ were measured using an isotope-ratio spectrometer (Thermo-Finnigan Delta-plus) coupled to an elemental analyzer (FlashEA1112 Thermo-Finnigan) at the Instrumental Unit of Analysis of the University of Coruña. Ratios of $^{15}\text{N}/^{14}\text{N}$ and $^{12}\text{C}/^{13}\text{C}$ were expressed in conventional delta notation (δ), relative to the international standard, Atmospheric Air (N_2) and Pee-Dee Belemnite (PDB) respectively, using acetanilide as standard (Fry, 2002). A lipid content correction was applied to the $\delta^{13}\text{C}$ values used for this species following Laiz-Carrión et al., (2015) and hereafter, $\delta^{13}\text{C}$ refers to lipid-corrected values.

Trophic position (TP) estimates were calculated only for postflexion larvae to avoid artificial enrichment provided by the ABT maternal influence on the $\delta^{15}\text{N}$ values as reported by Uriarte et al. (2016):

$$TP = TP_{\text{basal}} + \frac{\delta^{15}\text{N}_{\text{larva}} - \delta^{15}\text{N}_{\text{microzoo}}}{\Delta^{15}\text{N}_{\text{larvae}}},$$

$\delta^{15}\text{N}_{\text{larva}}$ are the isotopic signatures for individual ABT larvae and $\delta^{15}\text{N}_{\text{microzoo}}$ are the isotopic values of microzooplankton of the same or closest station to larval collection. TP_{basal} is the base consumer trophic position represented by the microzooplankton (0.05 - 0.2 mm), which consisted of primary producers and primary consumers, and has a designated value of 2 (Bode et al., 2007, Coll et al., 2006, Laiz-Carrión et al., 2015, 2019). The mean value of 1.46 ‰ was used as an experimental nitrogen isotopic discrimination factor for ($\Delta^{15}\text{N}$) proposed by Varela et al. (2012) for ABT juveniles.

Isotopic niche widths and overlap

Isotopic niche analyses followed Laiz-Carrión et al. (2019). Briefly, standard ellipse areas were calculated using the variance and covariance of $\delta^{13}\text{C}$ and $\delta^{15}\text{N}$ values with a sample-size correction following Jackson et al. (2011, 2012). The overlap of these sample-size-corrected standard ellipse areas (SEA) provides an estimate of the isotopic niche overlap. In this study, this approach compared overlap between postflexion ABT larvae from the GoM and MED. Isotopic niche widths and overlap analyses were conducted using the R package SIBER (stable isotope Bayesian ellipses in R) v.3.3.0 (Jackson et al., 2011, R Development Core Team 2022).

Model estimates

This study explored the effect of several biotic and abiotic variables on recent otolith growth using generalized additive models (GAMs) with a Gaussian distribution. GAMs are non-parametric flexible models that allow researchers to fit linear and nonlinear relationships between the explanatory and response variables within the same environment (Wood 2004, 2017). All models were estimate using the mgcv library in R (R Development Core Team, 2022) and variables are listed in Table 2.5. Three GAMs were estimated, one for all postflexion ABT larvae, and two region-specific models. Recent growth was the dependent variable for the subset of larvae (n=68) with all considered metrics measured (see Table 2.5, Table 2.5). In addition, larval abundances and hydrographic variables were included in the model selection process. To account for multi-collinearity, correlations (Spearman's correlation matrix, $\rho > 0.6$) between all potential explanatory variables were identified and strongly correlated variables were modeled against the response in single-variable GAMs. The Akaike Information Criterion (AIC, Akaike 1974) of the single-variable GAMs were compared between correlated variable pairs, and the variable with the lowest AIC was included in the final model selection process. After the set of non-correlated explanatory variables was identified, overall multi-collinearity was assessed using the variance inflation factor (VIF) with three as cutoff. Smoothing functions were applied to continuous predictor variables restricted to four knots to avoid overfitting.

To select a final model, several factors were considered. First, the restricted maximum likelihood (REML) method was used as it applies a double penalty to smooth terms and allows for removal of variables with minor predictive values (Marra & Wood, 2011). Second, model diagnostics and residuals were checked for potential deviations from normality and homogeneity of variance, and finally, smooth plots were examined for ecological context prior to final model selections.

RESULTS

Larval collections

In the GoM, 74 S-10 net tows collected 454 ABT larvae from 34 stations (Figure 2.1, Table 2.1). Given the span of the stations occupied by the GoM survey, the collection sought to include larvae throughout the study area. Sporadic but positive catches began on 3 May up until

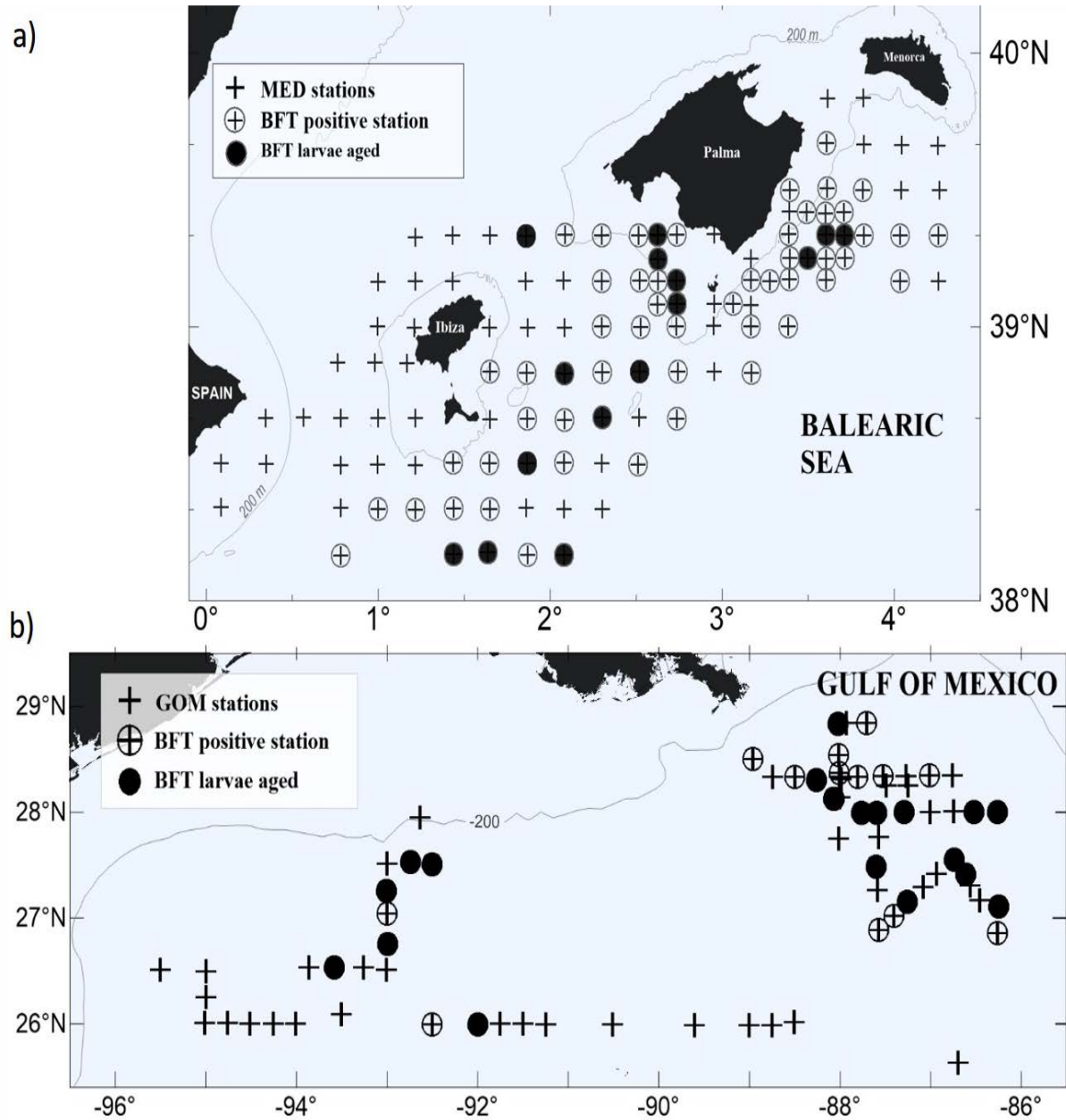


Figure 2.1. a) Station locations, presence/absence, and location of aged larval bluefin tuna (*Thunnus thynnus*) from a) western Mediterranean (MED) and b) Gulf of Mexico (GoM) during the 2014 spawning season at each corresponding spawning areas.

30 May 2014 as sampling advanced from east to west and then towards the northeast, with 50 stations completed in the east and 27 stations completed in the west (using 90° W to divide the GoM), see Figure 2.1. The positive ABT catches occurred when SST exceeded 22.24 °C, reaching up to 26.55 °C.

In the MED, 113 bongo-90 tows were conducted and 56% ($n = 64$) of stations were positive for ABT (Table 2.1). Although more than 5600 ABT larvae were collected, the majority were from a relatively small geographic region ($\sim 90 \text{ km}^2$) located in the south of the Balearic Islands (Figure 2.1). The MED survey collected ABT larvae for a total of 15 days beginning on 18 June 2014, when mean daily SST approached $23 \text{ }^\circ\text{C}$.

Larval ABT catches were highly variable and significantly different ($\rho < 0.05$) between spawning areas (see Table 2.4). Back-calculated spawning events calculated by subtracting observed ages from the day of collection point to daily spawning events taking place throughout the sampling timeframe in both spawning areas. ABT abundances ($\text{ind. } 1000^{-1} \text{ m}^{-3}$) were almost 1.5 orders of magnitude lower in the GoM than in the MED. There was only one station in the northern GoM with $> 100 \text{ ind. } 1000^{-1} \text{ m}^{-3}$ on the last day of the survey. Of the ten stations with the highest combined larval fish catches, only at two did ABT larvae dominate the larval assemblage ($> 75\%$); there was no correlation between scombrid abundances and ABT abundances in the GoM stations (Table 2.4). The MED abundances for ABT were $603 \text{ ind. } 1000^{-1} \text{ m}^{-3}$, with five stations having $> 1000^{-1} \text{ ind. } 1000^{-1} \text{ m}^{-3}$ (maximum $1774 \text{ ind. } 1000^{-1} \text{ m}^{-3}$ at one station near Palma de Mallorca). There was no correlation between overall larval fish abundance and ABT abundance, however there was a significant ($\rho > 0.05$) correlation between combined scombrid abundance and ABT abundance ($r = 0.99$) in the MED. For example, in the five most ABT-abundant stations, ABT comprised over 98% of the scombrid assemblage.

Larval somatic metrics were similar between spawning grounds for BL, weight, and age distribution (Figure 2.2, Table 2.4). Lengths were similar between spawning areas ($\rho > 0.05$, Figure 2.2) however, MED larvae were on average smaller ($5.20 \pm 1.23 \text{ mm}$ vs. 5.85 ± 1.08 , respectively). Larger larvae were less abundant in both spawning areas. The largest and heaviest larva was collected from the GoM (10.16 mm , 3.01 mg). Larvae measuring 9 mm were not collected in either spawning site and only six 8-mm larvae were collected (four in the GoM, and two in the MED). Larval ABT weights were also higher for the GoM (0.45 ± 0.4 vs. 0.39 ± 0.3), however the MED had more larvae ($n = 9$) at ages 17-21 dph compared to the GoM ($n = 2$) (Figure 2.3b). Conversely, otolith-derived metrics significantly differed ($\rho < 0.05$) for OR

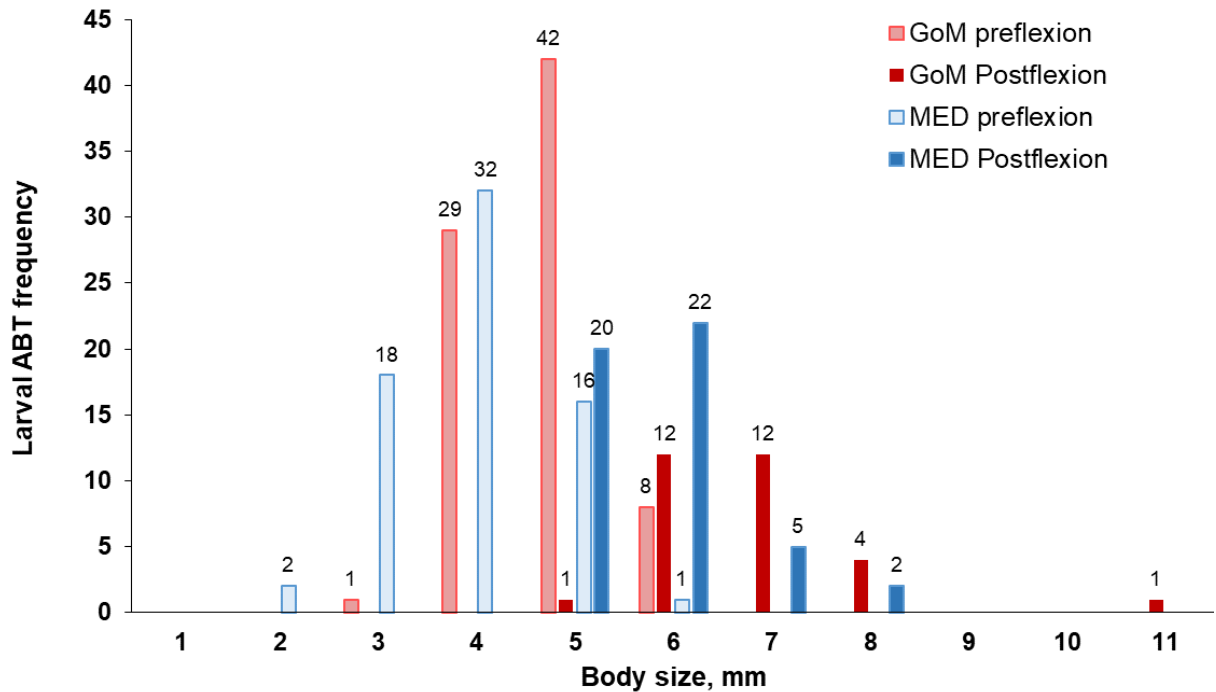


Figure 2.2. Histograms of body size (mm) for aged larval *Thunnus thynnus* (ABT) otoliths from the Gulf of Mexico (GoM, n = 111) and the western Mediterranean Sea (MED, n = 118). Preflexion and postflexion larval stages are also specified. Numbers above bars indicate the number of larvae grouped at 1-mm intervals (mm).

and mean IW, with the GoM having larger otoliths, yet the MED had larger mean IW (Figure 2.3c and 2.3d). Overall, the MED otoliths had larger mean IW values when compared to the GoM, however, GoM larvae had larger IWs at the same age throughout ontogeny. For example, a mean IW of 3 μm was reached at ~ 9 dph for GoM ABT larvae, while the MED reached the same IW at ~ 12 dph. Mean overall recent growth did not differ between spawning areas (2.55 ± 1.25 GoM, 2.16 ± 1.01 MED), however GoM larvae had larger recent growth-at-age ($> 10\%$ for larvae 6 dph up until 15 dph). Lastly, postflexion ABT's BL relative to otolith growth patterns were consistent. The least squares regressions for age-at-length residuals vs. OR-at-age residuals between spawning areas suggest that despite some differences between them, somatic growth was relative to otolith growth and can be compared.

Developmental stages were unevenly represented, with preflexion fish dominating (64%) catches in both spawning grounds. Postflexion larval stages ranged from 5.71 to 10.16 mm. In the GoM, seven flexion stage larvae ranged from 6.11 to 7.08 mm, and they overlapped in size

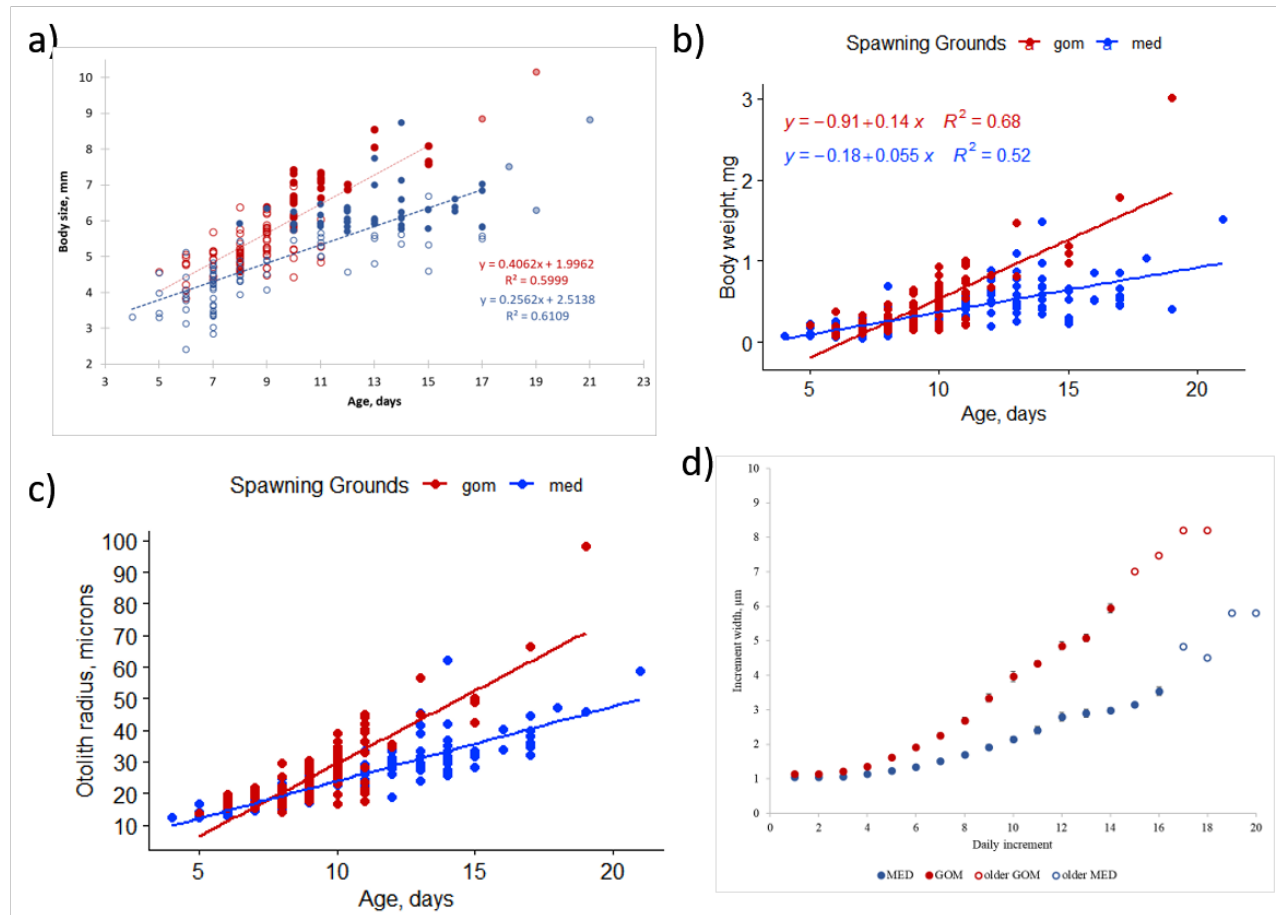


Figure 2.3. Age at length (a), body weight (b) and otolith radius, μm (c) for 228 larval bluefin tuna (*Thunnus thynnus*) aged from the Mediterranean Sea (MED) and Gulf of Mexico (GoM) during the 2014 spawning season. Developmental stages (preflexion and postflexion) are indicated in panel (a) with an open symbol (blue and red, respectively). (d) Mean daily increment size at-age for the corresponding larvae, with standard error bars. Open symbols indicate less than three observations at each given age.

with preflexion and postflexion larvae. In the GoM, larvae within the flexion stage were combined with the postflexion fish because they were > 6 mm in subsequent analyses.

Physical variables

Sea surface temperature and salinity differed between spawning grounds (Table 2.5) with the GoM being on average 0.61 $^{\circ}\text{C}$ warmer than the MED. Overall, salinity values were much higher in the MED when compared to the GoM (mean salinities: 37.81 vs. 35.67) and did not overlap at all (Table 2.5). These two variables were considered for examining growth variability in the GAM modeling approach.

Larval ageing

The within-otolith comparisons (left vs. right otolith) between reader-1 and reader-2 yielded no significant differences between daily age increments derived by either reader independently. Individual otolith reads from this subset of the full ageing dataset (~40%) were significantly and positively correlated, first between the two reads conducted by each reader, and again when comparing between readers ($p > 0.05$, $r = 0.98$ and $r = 0.99$, respectively). Reader-1 aged left and right otoliths for 77 ABT (32 from the GoM and 45 from the MED) while reader-2 aged 75 ABT (35 from the GoM and 40 from the MED). This otolith-calibration exercise concluded that reads from left and right sagittal otoliths were comparable and is reported for the first time for ABT larvae.

In total, 1,186 otolith reads were generated by both readers because each otolith was read between two to eight times. For the full dataset, no significant differences ($p > 0.05$) were found between the age-estimates derived by either reader independently. Reader-1 aged 115 and 106 otoliths from the GoM and MED respectively, while reader-2 aged 112 and 106, respectively. The precision of reads generated by both readers was ~5% CV (Table 2.3), with reader-1 having a $CV = 4.93\% \pm 4.78$ and reader-2 having a slightly higher $CV = 5.96\% \pm 4.91$. Finally, for all otolith reads that passed the ageing criteria, one randomly selected read represented the otolith for subsequent analysis. A total of 2.8% of all reads did not pass the established protocols in Table 2.2 because they were either physically damaged, had microscopy-related artifacts, and/or were simply unable to be interpreted consistently by either reader. For reader-1, seven GoM and ten MED otoliths did not pass the ageing protocol, while for reader-2, seven GoM and seven MED failed the protocol. When this was the case, those reads were not considered for random selection of the representing otolith read. However, none of the otoliths were discarded because if one of the reads passed the protocols, the otolith was allowed to remain in the dataset.

There are several reasons for which individual reads did not abide by the ageing criteria. Most often, reads had age estimates that differed by more than two days. In addition, for a handful of otoliths, the primordium was difficult to discern because additional otolith material accreted within the diffuse region and thus the starting point of the OR could have been slightly off-center. Marking the end point of the OR was also difficult for older and more robust otoliths due to artificial microscopy-induced shadows obstructing the edge of the otolith. Multiple images were evaluated to avoid misrepresenting OR length. Interestingly, otolith size did not

appear to influence the difficulty in age estimation for both readers, however older fish were more time-consuming to age due to uncertainty in marking the edge of the D-zones for wider increments.

Mean age corrections were 3.01 ± 0.95 (mean \pm SD) and include inc_{pred} from the otolith “diffuse zone” (2.8 ± 0.89) as well as terminal increments added. Terminal increments were added to larvae from all ages, but were more frequent for older larvae (> 12 dph) from the GoM. One terminal increment was added to 83 GoM reads and to 50 MED reads by reader-1, while only two instances were recorded in which two terminal increments were added to an otolith read.

Table 2.3. Summary of ANCOVA for age comparisons derived from Atlantic bluefin tuna larval otoliths from the 2014 spawning season in the Gulf of Mexico and Mediterranean Sea. The F statistic and p-values are shown for within-otolith reads for either left or right otoliths (read one and read two). Inter-reader comparisons are shown for 72 fish whose left and right otoliths were read twice, but only one read was selected randomly from reader-1 and reader-2 for analysis.

| Reader | Oto ₁ (read 1 vs. read 2) | Oto ₂ (read 1 vs. read 2) | Oto _{left} vs. Oto _{right} |
|--------------------------|--|--|--|
| Reader-1 CV = 5.48% | $F_{(1,356)} = 0.248,$ $\rho = 0.619$ | $F_{(1,232)} = 0.004,$ $\rho = 0.951$ | $F_{(1,154)} = 0.367, \rho = 0.546$ |
| Reader-2 CV = 4.17% | $F_{(1,362)} = 0.161,$ $\rho = 0.688$ | $F_{(1,216)} = 0.069,$ $\rho = 0.792$ | $F_{(1,142)} = 0.028, \rho =$ 0.867 |
| Reader-1 vs. reader-2 | | | $F_{(1,132)} = 0.055, \rho = 0.815$ |
| Reader-1 vs. reader-2 | | | $F_{(1,384)} = 0.87, \rho = 0.352$ |

Larval somatic growth rates were much larger for GoM when compared to the MED (0.41 vs. 0.26 mm SL d^{-1} , Figure 2.3a) as well as for age-at-DW (0.14 vs. 0.06, Figure 2.3b). Among the otolith biometrics, similar trends were observed between populations with greater age-at-OR and age-at-IW (Figure 2.3c, 2.3d). A linear relationship best explained the age-at-length data and the least squares regression for the growth curves were $y = mx + b$ with $m=0.41$, $b=1.99$, $r^2=0.60$ for the GoM. In the MED, the parameters were $m=0.25$, $b=2.5$ with $r^2 = 0.61$. Significant differences ($\rho < 0.001$) were found between ANCOVA analyses for the somatic and otolith metrics analyzed between the GoM and MED.

Table 2.4. Summary of somatic, otolith metrics, and mean larval abundance (1000^{-1} m^{-3}) for Gulf of Mexico (GoM) and Mediterranean Sea (MED) during the 2014 spawning season. Values shown are for the stations selected for ageing analyses. An asterisk (*) indicates significant results at the 0.05 level for t-test between spawning regions. A double asterisk (**) indicates Wilcoxon test.

| | | GoM | MED | ρ |
|--|------------------------|--------------|---------------|----------|
| Somatic metrics | Body length, mm SL | 3.59 – 10.16 | 2.41 – 8.83 | 0.746 |
| | Weight, mg | 0.07 – 3.01 | 0.04 – 1.51 | 0.906 |
| | Age, days | 5 – 19 | 4 - 21 | 0.575 |
| Otolith metrics, μm | Otolith radius | 13.75 – 98.2 | 12.32 – 62.13 | < 0.001* |
| | Increment width | 0.85 – 4.59 | 0.89 – 3.56 | < 0.05* |
| | Recent growth | 0.93 – 7.54 | 0.87 – 5.6 | 0.869 |
| Larval Abundance ind. 1000^{-1} m^{-3} | All larval fish | 207 | 945 | <0.05 ** |
| | Scombridae | 56 | 650 | <0.05* |
| | <i>Thunnus thynnus</i> | 21 | 603 | <0.001* |

Zooplankton SIA

Zooplankton were analyzed for the subset of stations with aged ABT larvae from each spawning region. For example, although the bongo-20 was towed 36 times in the GoM, only 12 stations' zooplankton parameters are represented in this study. In the MED, 10 stations are represented in this study. Microzooplankton was similar between regions for biomass, $\delta^{13}\text{C}$, and $\delta^{15}\text{N}$ values (Table 2.4). The $\delta^{15}\text{N}_{\text{micro}}$ were the most depleted values when compared to mesozooplankton and to larval ABT $\delta^{15}\text{N}$ values in both regions (Figure 2.4a, and Figure 2.4b), thus permitting to utilize microzooplankton fraction as the isotopic baseline of the food chain in each respective ecosystem. The $\delta^{13}\text{C}_{\text{micro}}$ were lower in the GoM when compared to the MED, however values overlapped with larval $\delta^{13}\text{C}_{\text{ABT}}$. Mesozooplankton biomass was significantly different between regions ($\rho < 0.001$) with the GoM having nine times more mesozooplankton biomass (mg m^{-3}). Although, $\delta^{13}\text{C}_{\text{meso}}$ was significantly different ($\rho < 0.05$), the ranges overlapped between regions. In contrast, $\delta^{15}\text{N}_{\text{meso}}$ did not differ between regions ($\rho > 0.05$).

Larval bluefin tuna SIA

The stable isotope signatures for all larvae (preflexion and postflexion ABT combined) yielded no statistically significant differences between $\delta^{15}\text{N}$ and $\delta^{13}\text{C}$ between the GoM and MED, ($\rho > 0.05$, Table 2.5). Overall, the youngest larvae had the larger $\delta^{15}\text{N}$ values, particularly for the MED larvae. In the MED, the $\delta^{15}\text{N}$ values followed a parabolic trend, with younger larvae (4 - 6 dph) starting out with high $\delta^{15}\text{N}$ ($> 7\text{‰}$) that decreased to on average $\sim 5\text{‰}$ and increased again to $\sim 5.5\text{‰}$ for the oldest larvae (17 - 21 dph). The youngest larvae in the GoM (5 - 6 dph) also started out with relatively lower $\delta^{15}\text{N}$ values ($\sim 5.8\text{‰}$) and although these values also decreased, the increase observed for the MED was not observed in the GoM cohort analyzed. When excluding preflexion larvae, postflexion stages from the GoM were significantly higher ($\rho < 0.05$) for both $\delta^{15}\text{N}$ values and TP when compared to the MED (Table 2.5). In addition, TP was significantly different ($\rho < 0.05$) and higher at-age for GoM larvae when compared to the MED, however, within the GoM, TP was highly variable. The ranges for $\delta^{13}\text{C}_{\text{ABT}}$ values were similar between regions (Table 2.5) with different trends within each spawning area. In the GoM, despite a 15% narrower range of $\delta^{13}\text{C}_{\text{ABT}}$ values when compared to the MED, $\delta^{13}\text{C}_{\text{ABT}}$ values increased with larval BL (and age) ($\rho < 0.05$). In the MED, $\delta^{13}\text{C}$ did not have an association with larval BL. However, within each of the spawning areas, $\delta^{13}\text{C}_{\text{ABT}}$ values had statistically significant associations with larval ontogeny.

Isotopic niche widths and overlap

Isotopic niche widths differed for larval ABT from the GoM when compared to the MED with wider standard ellipse areas (SEAc) in the GoM (Figure 2.5c and 2.5d). Trophic niche widths were 1.05‰ and 0.93‰ for the GoM and MED, respectively. There was a 62.3% trophic niche overlap between regions (Figure 2.5c) with the GoM's width $\sim 11\%$ larger than the MED.

Model estimates

Among the variables examined, one of the trophic variables (TP, $\delta^{15}\text{N}_{\text{ABT}}$, or $\delta^{15}\text{N}_{\text{mesozoo}}$) was consistently selected in all best-performing GAMs (Table 2.6). For the combined GoM and MED postflexion larvae, the model with the highest explanatory power (57.2% variance explained) included three variables: OR, $\delta^{15}\text{N}_{\text{ABT}}$, and $\delta^{15}\text{N}_{\text{mesozoo}}$ (Figure 2.6). The second best

model included four variables, OR, TP, $\delta^{15}\text{N}_{\text{mesozoo}}$ and abundance larval fish (Table 2.6). Between these two models, the latter had a lower AIC value (107.91) and \sim two less degrees of freedom ($df_1 = 6.87$ vs. $df_2 = 9.18$), yet it explained slightly less (45.8 %) of the recent growth variance (Table 2.6). For both models, the most important explanatory variable was OR (48% and 26.8%, respectively) which had a positive, although non-linear association with recent

Table 2.5. Trophic and environmental variable summary for Gulf of Mexico (GoM) and Mediterranean Sea (MED) during the 2014 spawning season. Larval *Thunnus thynnus* (ABT) trophic position (TP), $\delta^{15}\text{N}$, and $\delta^{13}\text{C}$ are shown. Parenthesis indicate the number of larvae analyzed. Mean values \pm SD are reported. An asterisk (*) indicates significant results at the 0.05 level for t-test between spawning sites. A double asterisk (**) indicates Wilcoxon test.

| | | GoM | MED | ρ |
|---|--------------------------------------|-------------------|-------------------|----------------|
| Trophic variables | | | | |
| Microzooplankton (0.05 - 0.2 mm) | Biomass, mg m^{-3} | 1.41 ± 0.66 | 1.42 ± 0.67 | 0.746 |
| | $\delta^{13}\text{C}_{\text{micro}}$ | -19.35 ± 0.49 | -18.56 ± 0.72 | 0.906 |
| | $\delta^{15}\text{N}_{\text{micro}}$ | 2.21 ± 0.86 | 2.57 ± 0.42 | 0.575 |
| Mesozooplankton (0.2 – 0.5 mm) | Biomass mg m^{-3} | 13.98 ± 7.66 | 1.57 ± 1.60 | $< 0.001^*$ |
| | $\delta^{13}\text{C}_{\text{meso}}$ | -20.20 ± 0.59 | -20.69 ± 0.90 | 0.032^* |
| | $\delta^{15}\text{N}_{\text{meso}}$ | 3.45 ± 0.83 | 3.51 ± 0.40 | 0.869 |
| Larval ABT (GoM n = 27, MED = 44) | TP | 3.74 ± 0.59 | 3.46 ± 0.59 | 0.025^* |
| | $\delta^{15}\text{N}$ | 5.03 ± 1.07 | 4.63 ± 0.78 | 0.048^* |
| | $\delta^{13}\text{C}$ | -19.25 ± 0.36 | -19.26 ± 0.38 | 0.511 |
| Abiotic variables | | | | |
| Temperature, $^{\circ}\text{C}$ | SST | 24.30 ± 0.67 | 23.719 ± 0.62 | 0.023^* |
| Salinity, psu | SSS | 35.72 ± 0.68 | 37.79 ± 0.29 | $< 0.001^{**}$ |

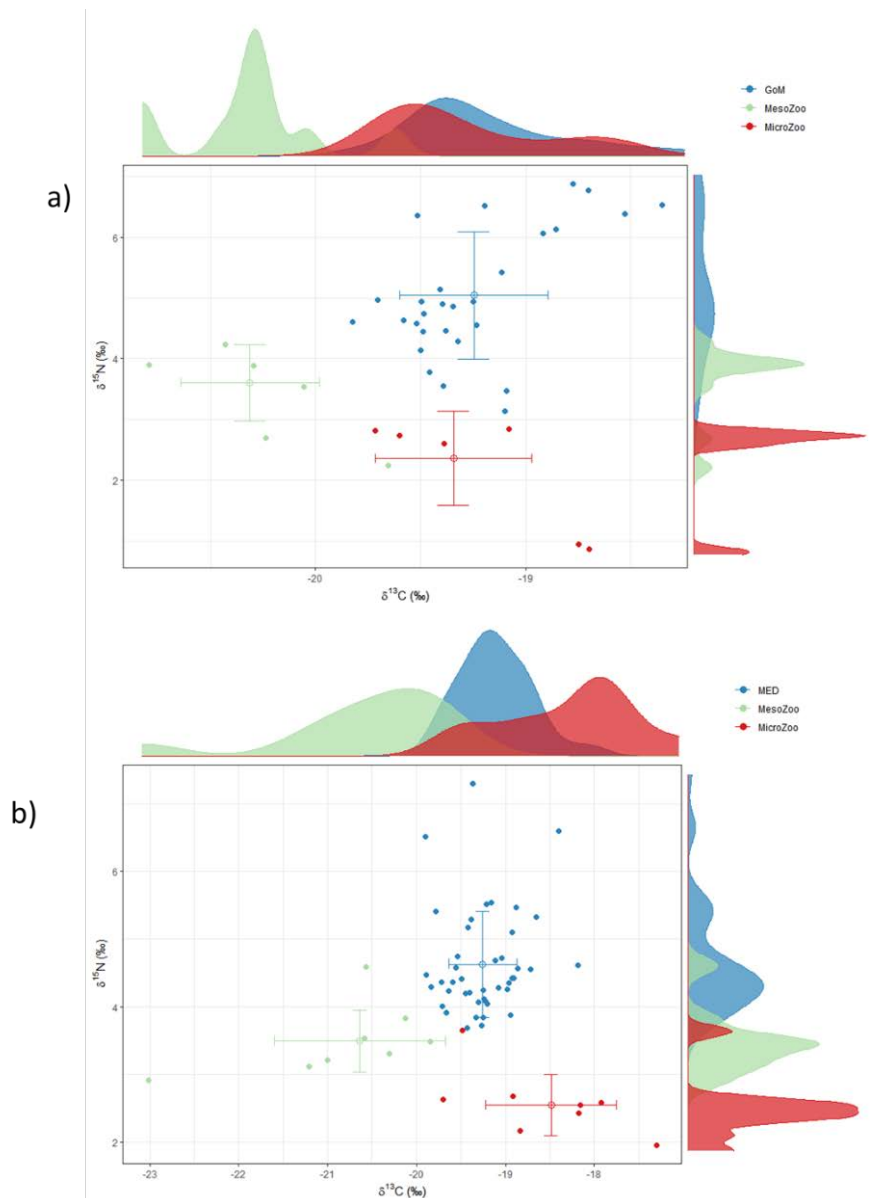


Figure 2.4. Biplot of $\delta^{15}\text{N}$ and $\delta^{13}\text{C}$ and standard deviation for the (a) Gulf of Mexico (GoM) and (b) Mediterranean Sea (MED) during the 2014 spawning season. Postflexion larval bluefin tuna (*Thunnus thynnus*, ABT) are shown in blue symbols, microzooplankton (0.05 – 0.2 mm) in red symbols, while mesozooplankton (0.2 – 0.5 mm) are in green. Corresponding distributions for ABT, microzooplankton, and mesozooplankton are shown for each variable along the corresponding axes.

growth (Figure 2.6a). In the best model, the second most important variable, $\delta^{15}\text{N}_{\text{ABT}}$ explained 36% of the variance while it had a negative association with recent growth (Figure 2.6b). Lastly, $\delta^{15}\text{N}_{\text{mesozoo}}$ explained 27.7% of the variance and it had a positive association recent growth (Figure 2.6c). In the second-best model, TP explained 23.7% of the variance and it had a negative association with recent growth. The TP pattern was similar to the $\delta^{15}\text{N}_{\text{ABT}}$ pattern in the

best-fit model. Although, $\delta^{15}\text{N}_{\text{mesozoo}}$ only explained 8.9% of the variance, its influence on recent growth was still statistically significant. Lastly, larval fish abundance only explained 2.8% of the variance.

The best-performing model for the GoM included three variables that significantly explained the majority of the recent growth variance (76.7%): $\delta^{15}\text{N}_{\text{mesozoo}}$, OR, and TP. These variables explained 33.3%, 27 %, and 14.8% of the variance, respectively (Figure 2.7a-c). In the second-best model, OR, TP and larval fish abundance explained 8%, 8%, 5.5% of the variance, respectively. Next, OR had a positive association with recent growth. The abundance of larval fish had a positive association with recent growth, and although it improved the model fit, it was not a significant influence.

The best-performing model for the MED included the same variables as for the GoM's best-performing model. However, OR, $\delta^{15}\text{N}_{\text{mesozoo}}$, and TP together only explained 28.8% of the variance (Table 2.6). In the second-best model, SST explained 10.9% of the variance, while ABT abundance did not have explanatory power. Temperature had a negative association with recent growth, however it appears that overfitting occurred as half of the larvae were sourced from the same MED station with SST at 24.4 °C, while eight larvae were from a station with 23.1 °C.

Finally, ABT abundance (1000^{-1} m^{-3}) increased with recent growth, but its influence was not statistically significant ($\rho > 0.05$). This variable should fall out of the model, however when it was removed, the overall variance explained fell to 26.6% and the model's performance decreased (AIC marginally increased ~2 points). Consequently, ABT abundance was retained in the second-best MED model.

DISCUSSION

This study is among the first to use larvae collected during the same spawning season (2014) from the GoM and MED to standardize methodologies, compare larval growth, and relate SIA with growth using GAMs in the two main ABT spawning areas. Larval growth was comparatively faster for the GoM however, there were fluctuating relationships between recent somatic growth and trophic variables. Furthermore, specific trophic characteristics ($\delta^{15}\text{N}$, TP and $\delta^{15}\text{N}_{\text{mesozoo}}$) consistently explained recent larval growth variance. Finally, evidence of density-dependent (larval fish and ABT abundances) association with larval growth is also discussed.

Life history dynamics

Adult ABT forage in North Atlantic feeding grounds during the spring bloom (Block et al., 2005). Tagging, otolith chemistry, and genomics (Block et al., 2005, Rooker et al., 2007, Rodríguez-Ezpeleta et al., 2019) indicate that after feeding, ABT begin the long distance migration to their respective spawning areas. Thermodynamics combined with the timing of ABT arrival into adequate spawning habitat limits the reproductive seasons to ~ 2 months, with tagged adults returning to feeding grounds approximately in July and August for the GoM and MED, respectively (Block et al., 2005, Wilson et al., 2015). Given this relatively short spawning window when compared to tropical tunas that spawn ~ 6 months (Muhling et al., 2017), every day of the spawning season counts towards successful fertilization and subsequent larval survival (Muhling et al., 2017). While the MED survey sampled approximately ~90 km² of the Balearic archipelago, the GoM survey sampled an extensive portion of the northern GoM (Figure 2.1a and 2.1b), and yet the catches were very different. These results are not surprising, given that only ~20-35% of the northern GoM has favorable conditions for ABT spawning to occur (Domingues et al., 2016). In addition, cooler temperatures (< 23 °C) may have influenced low ABT catches in the GoM (Muhling et al., 2010). Surface waters reached > 23.5 °C only after 7 May, where in previous years, this threshold temperature for the onset of ABT spawning (Muhling et al., 2010) was reached in late April (Zapfe, G., pers. comm.). During the 2014 spawning seasons, temperature ranges in ABT-positive stations were very narrow (2.6 °C and 2 °C in the GoM and MED, respectively), and thus any temperature-induced influences may be difficult to determine.

Larval fish distribution and abundance differed significantly in 2014 between the two spawning areas (Table 2.4). In the MED, larval ABT catches accounted for the discrepancy. In the GoM, ABT contributed only ~ 10% to the total larval assemblage (Laiz-Carrión et al., 2019). Despite these disparities, the GoM survey's ABT catches were comparable to previous years (1990-2006). During those years, 11% ± 4.9 of stations sampled were ABT-positive (ranged from 7 - 24%, Muhling et al., 2010). Larval bluefin tuna aggregate in patches (Satoh et al., 2014, Gerard et al., 2022) and in frontal regions (Alemany et al., 2010, Domingues et al., 2016). These fronts will concentrate prey, intralarval competition, and predator abundance. For example, during the MED survey, at high ABT abundances (> 35 ABT) that coincided with a large size range, cannibalism was observed (Uriarte et al., 2019). In the GoM, ABT co-occurred with at least six other scombrids (Laiz-Carrión et al., 2019). In the MED, larval ABT abundances were

almost 1.5 orders of magnitude higher and ABT dominated both the scombrid assemblage and the combined larval fish assemblage (64%). Comparable to Alemany et al. (2010), when larval ABT overlapped with other scombrids, it was most often with the congener (*T. alalunga*) and with *Auxis* spp. The trends observed in this study are very similar to previous larval assemblage comparisons for scombrids between the GoM and MED (García et al., 2017, Alvarez et al., 2021) and within the MED alone (Uriarte et al., 2019).

Larval ageing comparisons

Otolith-derived metrics inform fisheries stock assessments and are used to back-calculate spawning sites and times (Richardson et al., 2016, Russo et al., 2022), estimate survival and recruitment (Sponaugle 2010, Gleiber et al., 2020b), as well as examine spatiotemporal dynamics (Campana 1999). Understanding the early life history dynamics of bluefin tuna spawning grounds is crucial for effective and adaptive management (Sato, et al., 2008, Watai et al., 2017).

For the first time ABT larval growth comparisons are reported from the same spawning season (2014) in the two main spawning grounds. The calibration exercise between laboratories was successful and yielded good CVs. Age estimates between left and right sagittae from the same fish found no statistical differences in the estimates (between and within two readers). In addition, the ethanol-induced shrinkage equation utilized in this study allowed a comparison between growth curves derived from ethanol-preserved larvae and from freshly thawed larvae. Comparisons between growth studies are common and age-at-length estimates are obtained from larvae preserved in various preservatives. Low larval catches or size ranges often limit studies to smaller sample sizes. This was avoided in this study due to inclusion of additional larvae to supplement the GoM's ageing estimates.

Variations in estimating larval age (dph) during the first week of larval life can result in different growth rates and introduce error into already variable abundance estimates (Ingram et al., 2017). The first daily increment forms soon after the opening of the bluefin tuna mouth and coincides with the onset of exogenous feeding in ~4 d (Brother et al., 1983, Itoh et al., 2000). Previous age estimates for larval ABT concluded that adding between two to four days was a suitable correction (Brothers et al., 1983, Malca et al., 2017) to calculate days post hatch from increments counted along the OR. In this chapter, the proposed age-adjustment added ~ 3 days to observed increment counts and ranged from adding 1 day up to 5 days. This approach towards

age correction fits into the morphological development of ABT (Yúfera et al., 2014). In addition, the theoretical hatch proposed (7 μm) for ABT larvae has also been observed at a similar distance from the primordium in *T. maccoyii* otoliths (Jenkins & Davis, 1990). Utilizing observed individualized otolith-based trends could provide a more consistent and adequate estimate than simply adding x -number of days.

Larval bluefin tunas experience strong selection pressures to grow up quickly in order to survive (Bakun 2012, Pepin et al., 2015, Watai et al., 2018). Larval growth rates in the GoM were 0.40 mm d^{-1} and are smaller than reported by Malca et al. (2012) from the northern GoM (2000-2012, $0.46 \text{ mm SL increment}^{-1}$). However, those age estimates utilized raw increment counts and were not adjusted for dph (Malca et al., 2107). In contrast, the growth rates reported for the 2014 GoM cohort are similar to those reported by Malca et al. (2022) (0.39 and 0.37 mm d^{-1}), which also used the same age-adjustment protocol utilized in this study. Malca et al. (2022) aged ABT larvae from ethanol-preserved larvae collected in two contrasting habitats in the north and northeast GoM in 2017 and 2018, respectively. Adjusting for the shrinkage that occurs upon larval preservation and adjusting for the inflated growth rate ($\sim 7\%$, $n = 288$), the adjusted-growth rates from the GoM (2000-2012) were $\sim 0.43 \text{ mm d}^{-1}$. The larval growth rates from this study are comparable than those reported by Malca et al. (2022). This lack of inter-annual growth rate differences between several years in the GoM (2012, 2014, and 2022) points to a consistent early life history pattern that may imprint natal homing for the larvae born in the GoM (western ABT stock).

Larval growth rates in the MED were smaller (0.26 mm d^{-1}) than previously reported (0.35 - $0.41 \text{ mm increment}^{-1}$) for the Balearic archipelago in 2003-2005 (García et al., 2013). In this case, both the MED 2014 larvae and the 2003-2005 MED larvae were preserved similarly, however García et al. (2013) did not correct for dph. Adjusting the inflated growth rate reduces García's et al. (2013) estimates by approximately $\sim 7\%$ and despite this adjustment (0.33 - 0.38 mm d^{-1} for 2003-2005), the MED 2014 cohort appears to be growing at a slower rate. Unusually warm SST ($26 \text{ }^\circ\text{C} \pm 0.54$) during the 2003 spawning season resulted in higher relative growth rates for MED larvae (García et al., 2006, 2013), however the 2004 and 2005 spawning seasons had adequate temperatures ($23.87 \text{ }^\circ\text{C} \pm 0.31$, $24.96 \text{ }^\circ\text{C} \pm 0.83$, see Table 3 in García et al., 2013) and do not explain the slower growth observed in the MED. Temperature increases tuna larval growth (García et al., 2013, Gleiber et al., 2020a, 2020b) however, higher temperatures

Table 2.6. Akaike information criterion (AIC) for the best-performing generalized additive models (GAMs). The Δ AIC is the difference from the lowest AIC and the percent variance (%) explained for each selected model is indicated. The residuals of recent growth at-age (Rg) for postflexion larval *Thunnus thynnus* (ABT). The $s()$ denote the smoothing function applied to a variable. Variables are otolith radius (μm , OR), $\delta^{15}\text{N}_{\text{ABT}}$, $\delta^{15}\text{N}_{\text{mesozoo}}$, Trophic position (TP), larval fish abundance (1000^{-1} m^{-3}), ABT abundance (1000^{-1} m^{-3}), and sea surface temperature (SST). The SST and abundance are from the corresponding collection location from Gulf of Mexico (GoM) and/or Mediterranean Sea (MED) during the 2014 spawning season.

| Best performing GAM Models | | Δ AIC | Variance % |
|----------------------------|---|--------------|------------|
| GoM & MED | $\text{Rg} \sim s(\text{OR}) + s(\delta^{15}\text{N}_{\text{ABT}}) + s(\delta^{15}\text{N}_{\text{mesozoo}})$ | 2.69 | 57.2 |
| | $\text{Rg} \sim s(\text{OR}) + \text{TP} + \delta^{15}\text{N}_{\text{mesozoo}} + s(\text{Abundance}_{\text{larval fish}})$ | 0 | 45.8 |
| GoM | $\text{Rg} \sim s(\text{OR}) + \text{TP} + \delta^{15}\text{N}_{\text{mesozoo}}$ | 0 | 76.7 |
| | $\text{Rg} \sim s(\text{OR}) + s(\text{TP}) + s(\text{Abundance}_{\text{larval fish}})$ | 14.30 | 63.0 |
| MED | $\text{Rg} \sim s(\text{OR}) + s(\text{TP}) + s(\delta^{15}\text{N}_{\text{mesozoo}})$ | 2.04 | 28.8 |
| | $\text{Rg} \sim s(\text{OR}) + s(\text{TP}) + s(\text{SST}) + s(\text{Abundance}_{\text{ABT}})$ | 0 | 32.6 |

also requires sufficient food to support faster metabolic demands. In the GoM, temperature has been shown to be influential for recent growth when higher biomasses of preferred prey (cladocerans and copepod nauplii) were present (Shiroza et al., 2021, Malca et al., 2022). In this study, microzooplankton biomasses were similar between spawning areas, while the mesozooplankton biomass was much lower in the MED, pointing to a more food-limited habitat. Uriarte et al. (2019) reported cannibalism within the same MED cohort that was aged in this study. Perhaps the slower growing MED larvae (which include at least 40 larva from the same station that Uriarte et al. (2019) found cannibals), were experiencing food-limited conditions (slower growth) prior to collection. Larval ABT exhibit piscivorous behavior starting at > 13 dph (Malca et al., 2022), it is then plausible that cannibalism may help the overall survival of older

larvae in food-limited conditions when size- and density-dependent factors occurred (Dahl et al., 2018).

Individual instantaneous growth rates (mm d^{-1}) and increment size (μm) increased with larval ontogeny within the GoM between preflexion and postflexion larvae. In the MED preflexion larvae also had a positive trend, however, the observed acceleration in instantaneous growth (and increment size) for postflexion GoM larvae was not observed in postflexion MED otoliths (Figure 2.3a and 2.3d). These different microstructural (daily-scale) patterns mirror differences in overall growth strategies between spawning areas. For example, preflexion larvae between the ages of six to nine, had instantaneous growth rates that were 15% larger in the GoM when compared to the MED. Similarly, instantaneous growth was also higher for postflexion in the GoM vs. the MED, though slightly less pronounced (13%), probably hinting at a flattening of larval growth acceleration beginning to occur between spawning areas. Different processes can influence growth at various size classes. Unfortunately, due to the limited number of postflexion larvae collected and aged in this study, this comparison was limited, and was only possible for larvae between 10 and 11 dph. Larval GoM increments were 12.5% wider than the MED, with individual increment widths increasing at different rates in both spawning areas. In the GoM, there was a robust increase in daily growth (six to 12 dph), ranging from 2% to 24%, and even up to 42% at 15 dph. In the MED, daily increment deposition was less accelerated and some daily increment widths remained relatively similar or even decreased at times. Focusing on recent somatic growth (~3 d) prior to collection, unsurprisingly, a similar pattern emerges. Recent growth was 22% higher for preflexion GoM larvae when compared to the MED. Postflexion larvae had wider increments in both spawning areas, but these increments grew 32% wider in the GoM when compared to the MED. These findings along with previously reported otolith metrics for the GoM and MED (Malca et al., 2017) point to distinct early life histories between the two ABT spawning grounds.

Trophic characterization

Nitrogen ($\delta^{15}\text{N}$) levels increase with increasing trophic steps (Post 2002, Montoya 2007). Microzooplankton and mesozooplankton $\delta^{15}\text{N}$ values from this study followed this enrichment

pattern (Table 2.5, Figure 2.4). Similarly, larval $\delta^{15}\text{N}$ values should increase with body size. Although this enrichment pattern was observed for other tuna species in the GoM (Laiz-Carrión et al., 2019) and in the MED (García et al., 2017), larval ABT hatch with high $\delta^{15}\text{N}$ due to maternal influence (Uriarte et al., 2016). In a rearing experiment with MED ABT larvae, Uriarte et al. (2016) reported that these elevated values decrease with age until larval flexion begins and $\delta^{15}\text{N}$ increases after ~ 15 dph. The opposite trend for $\delta^{13}\text{C}$ was reported in the same study (see Figure 3 in Uriarte et al. (2016)). It takes approximately two weeks (15 dph) for the larval ABT

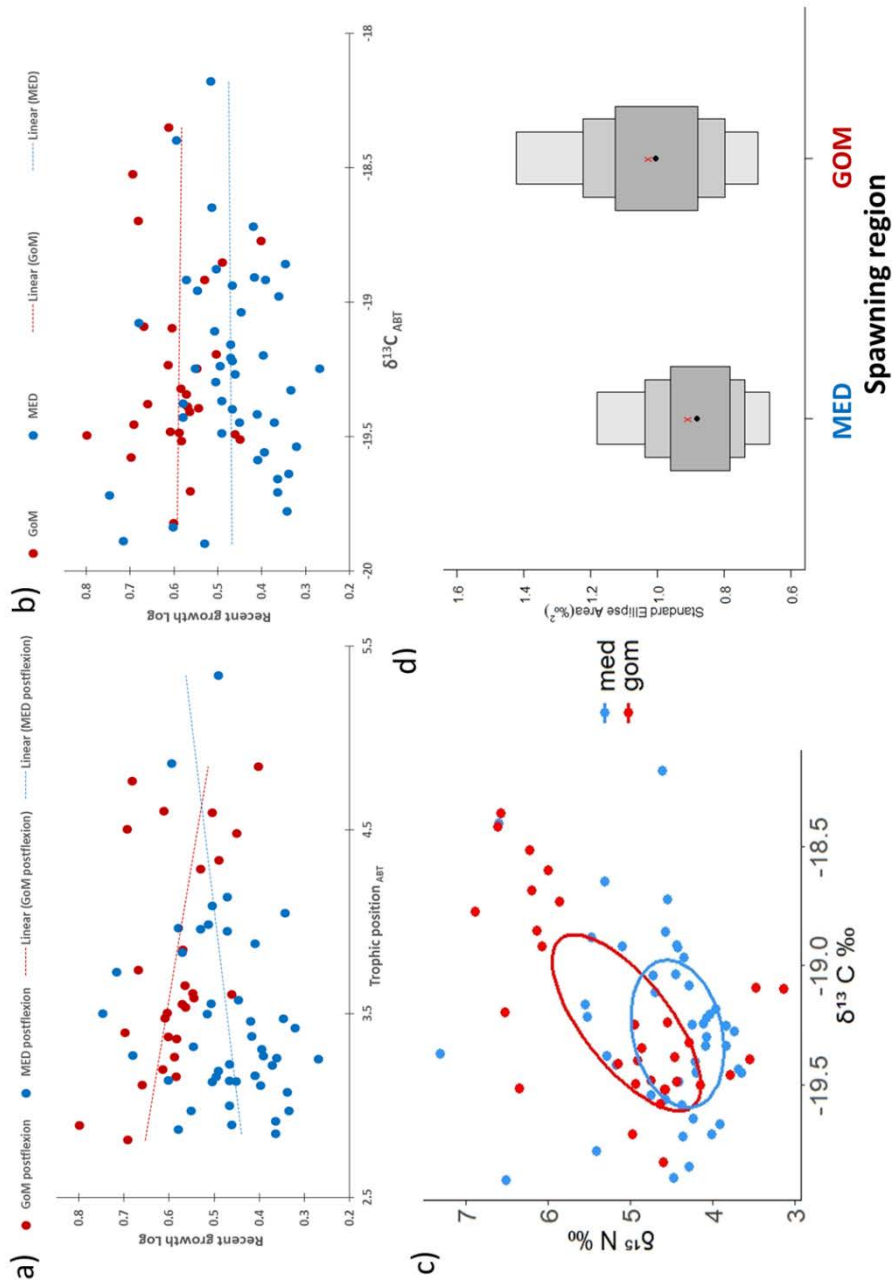


Figure 2.5. Trophic results for postflexion larval *Thunnus thynnus* (ABT) from the Gulf of Mexico (GoM, red symbols) and the Mediterranean Sea (MED, blue symbols) during the 2014 spawning season: The a) estimated trophic position (TP_{ABT}) and b) $\delta^{13}\text{C}_{\text{ABT}}$ vs. observed recent otolith growth (μm , log-transformed). c) Scatter biplot of $\delta^{15}\text{N}$ and $\delta^{13}\text{C}$ with ellipses that represent the isotopic niche width for each region. Boxplot of the standard ellipse area (SEA_B) for the trophic niche of each region. Boxplot shows the confidence intervals of the SEA_B corresponding to 95 %, 75 % and 50 %. The red symbols (x) indicate the mean value for each population analyzed.

skeletal muscles and their corresponding $\delta^{15}\text{N}$ and $\delta^{13}\text{C}$ signatures to shed the maternal influence. In the wild, isotope signatures are likely more variable and at least in the GoM, this pattern may not closely follow lab experiments conducted with MED larvae. Yet evidence of the maternal influence has been observed especially in younger larvae collected in the GoM (Laiz-Carrión et al., 2019) and in the MED (García et al., 2017). In this study, preflexion larvae were excluded from SIA, however relatively few ABT larvae ($n = 32$) were > 15 dph. In the GoM, faster growers (positive residuals of size at-age and positive residuals of otolith size at-age) had high $\delta^{15}\text{N}$ with marginally higher TP, while in the MED, faster growers had lower $\delta^{15}\text{N}$ values and lower TP. At least in the MED, the lower $\delta^{15}\text{N}$ may support the hypothesis that the 2014 cohort aged were feeding on preys with lower $\delta^{15}\text{N}$ values and were consequently growing slower.

Unlike previous larval ABT trophic position estimations, this study utilized an updated nitrogen discrimination factor ($\Delta^{15}\text{N}_{\text{muscle}} = 1.46 \text{ ‰}$) from Varela et al., (2012). Previous studies have utilized a higher value (1.64 ‰) from Varela et al. (2011). The recent value was derived from larval ABT that were reared until the juvenile stage and analyzed upon termination of the experiment and although not ideal, it is more suitable for this larval comparison. This minor discrepancy between $\Delta^{15}\text{N}$ prevents a direct comparison of the TP estimates derived in this study to previously reported TP estimates (Laiz-Carrión et al., 2015, 2019). However, when utilizing the higher discrimination factor (from Varela et al. (2011)), TP estimates were 3.55 and 3.30 for the GoM and MED, respectively. These now comparable values are higher than the TP reported from the GoM in 2012 and from the MED in 2013 (Laiz-Carrión et al., 2015). The adjusted TP estimations in this study are also higher than reported in Laiz-Carrión et al. (2019) for larvae from the same survey (2014) in the GoM, likely due to a different set of stations selected for ageing analysis.

A larger range of $\delta^{13}\text{C}$ was observed in the MED compared to the GoM ($\Delta\delta^{13}\text{C}_{\text{ABT}} = 3.02$ and 0.9, respectively). The MED survey sampled throughout the Balearic archipelago, which is influenced by continental carbon sources (Sabatés et al., 2007) and localized upwelling at fronts and eddies (Alemany et al., 2010, Muhling et al., 2013). In the GoM survey, all of the stations were offshore (> 200 nm) and away from the Loop Current. Higher $\delta^{13}\text{C}$ values for larger-at-age larvae followed opposite trends in the two spawning areas. In the GoM, larvae grew faster with higher values, whereas in the MED, the opposite was true. The $\delta^{13}\text{C}$ overlapped between spawning areas, and the range was narrow within each spawning area indicating that overall,

larval ABT consume prey within a similar range of carbon values. Coincidentally the faster growing MED larvae's $\delta^{13}\text{C}$ values overlapped the most with the slowest growing GoM larvae, again highlighting distinct larval growth strategies. Piscivorous ABT larvae would be expected to have larger $\delta^{13}\text{C}$ values and higher increment widths, however instances of piscivory are rare in wild collections (Uriarte et al., 2019). For example, Shiroza et al. (2021) observed only five larval fish prey in over 150 larval ABT guts. However, there is likely a lag between food ingestion, digestion and increment deposition. The MED otoliths examined in this study did not yet show wider increment widths.

Isotopic niche widths and overlap

Isotopic niches represented by Bayesian ellipses (Fig. 2.5c) further support that postflexion ABT larvae from both the GoM and MED were feeding on prey with similar $\delta^{13}\text{C}$ ranges but mostly differentiated by $\delta^{15}\text{N}$ values. Standard Ellipse Area (SEA) (Fig. 2.5d) specified broader isotopic niche (11% larger) for GoM larvae suggesting a more diverse diet (euryphagous) than those from MED (stenophagous). When comparing these distinct geographic areas, the large overlap (64%) reported indicates that larvae have comparable trophic niches in their respective spawning areas.

These differences in larval growth strategies and trophic positions further affirm that larvae from these environmentally dissimilar and geographically distant locations have distinct trophic characteristics. Larval growth may be faster in the GoM when compared to the MED however, this does not imply that the GoM produces higher quality (or more abundant) recruits when compared to the MED. The eastern ABT adult stock is more than one order of magnitude larger than the western ABT stock (NOAA 2009). Larval ABT shared a similar isotopic niche in each spawning area and though adult ABT position larvae in oligotrophic environments, it appears that these habitats are suitable for larval survival within each spawning area (Bakun 2012). In addition to copepods, ABT diet has been associated with cladocerans, ciliates, and appendicularians (Catalán et al., 2011, Tilley et al., 2016, Shiroza et al., 2021) that utilize the microbial food web. Thus, the length and efficiency of food webs in these oligotrophic habitats will influence trophic position estimates (Stukel et al., 2022).

Modeling larval growth and trophodynamics

The association for all models between recent growth (residual of recent growth-at-age, Rg) point to trophic characteristics significantly explaining recent growth variability. Trophic variables ($\delta^{15}\text{N}_{\text{ABT}}$, $\delta^{15}\text{N}_{\text{mesozoo}}$, TP) were among the variables that explained a larger portion of the variance. During the model selection process, most trophic variables were significantly correlated, especially microzooplankton and mesozooplankton biomass, however SIA had higher explanatory influence, therefore these two variables were not included in the model estimates. The ABT larval $\delta^{13}\text{C}$ values had no obvious trend in either region (Figure 2.5b) and as a result, $\delta^{13}\text{C}$ values were excluded as a potential explanatory variable in the model. Although temperature and salinity were significantly different between regions, salinity correlated with multiple trophic metrics and was not included in the final model selections.

In the combined model, otolith radius (OR) was the most important variable. Otolith size has not always been positively coupled with increasing increment width, particularly in food-limited conditions (Gleiber et al., 2020a) or in the deep sea. The OR largely explained variances in the combined model and in each region-specific model pointing to regular accretion of increments in both regions. Region-specific GAMs were informative because the relationship between recent larval growth and larval isotopic signatures was significantly different (ANCOVA, $\rho < 0.05$) between $\delta^{15}\text{N}$, $\delta^{13}\text{C}$, and TP between regions. Importantly, $\delta^{15}\text{N}_{\text{mesozoo}}$ consistently and significantly explained at least some of the recent growth variance (7 – 33%, Figure 2.6 and 2.7) confirming that larval growth is sensitive to the $\delta^{15}\text{N}$ values of the associated prey fields. Trophic position explained 14.8 and 6.9% of the variance in the GoM and MED, respectively. The different contribution of TP between spawning areas may indicate that the GoM cohort was more susceptible to the trophic position of their prey than in the MED. In warmer temperatures, the ABT within the GoM may have higher metabolic requirements than ABT within the MED. In the MED, faster-growing larvae were feeding on preys with lower $\delta^{15}\text{N}$ values and had lower TP. This would agree with the hypothesis that MED larvae were in a more oligotrophic habitat.

This study has shown that there are distinct growth strategies in the two main spawning regions. Combining recent growth and SIA explains some of these differences and captures habitat qualities for fast-growing larvae. In addition to larval metrics (measurements of length

and age) for each spawning area, the environmental gradients including prey quality and quantity should be factored into management efforts.

CONCLUSION

Otolith biometrics can improve the understanding of biotic and abiotic drivers that play a key role in the development of credible predictive recruitment models for ABT that contribute to stock assessment models. This study generated companion growth curves for the 2014 ABT spawning season in the GoM and MED by ageing otoliths from larvae collected from the two main spawning grounds, and identified significant population differences, with distinct growth strategies. Larvae from the GoM grew faster when compared to the MED (0.41 vs. 0.26 mm SL d⁻¹) and faster-growing larvae from the GoM had higher TP, $\delta^{15}\text{N}$, and $\delta^{13}\text{C}$ values. Although prey field biomasses are important to characterize the environment, the $\delta^{15}\text{N}_{\text{mesozoo}}$ of the prey field was a more important driver of larval growth and should be incorporated in larval modeling efforts. Combining otolith biometrics with SIA signatures from larvae and the associated prey field can play a key role in ongoing management efforts of this important fishery resource.

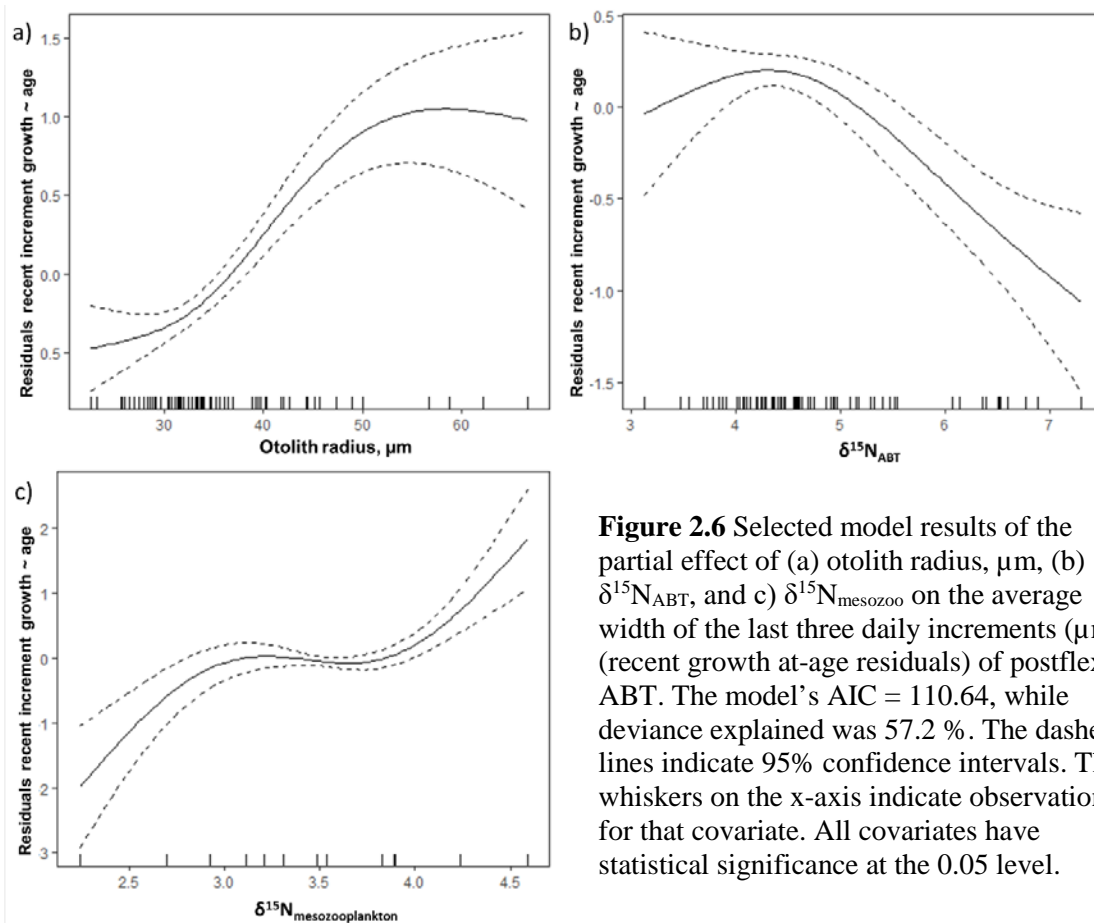


Figure 2.6 Selected model results of the partial effect of (a) otolith radius, μm , (b) $\delta^{15}\text{N}_{\text{ABT}}$, and (c) $\delta^{15}\text{N}_{\text{mesozoo}}$ on the average width of the last three daily increments (μm) (recent growth at-age residuals) of postflexion ABT. The model's AIC = 110.64, while deviance explained was 57.2%. The dashed lines indicate 95% confidence intervals. The whiskers on the x-axis indicate observations for that covariate. All covariates have statistical significance at the 0.05 level.

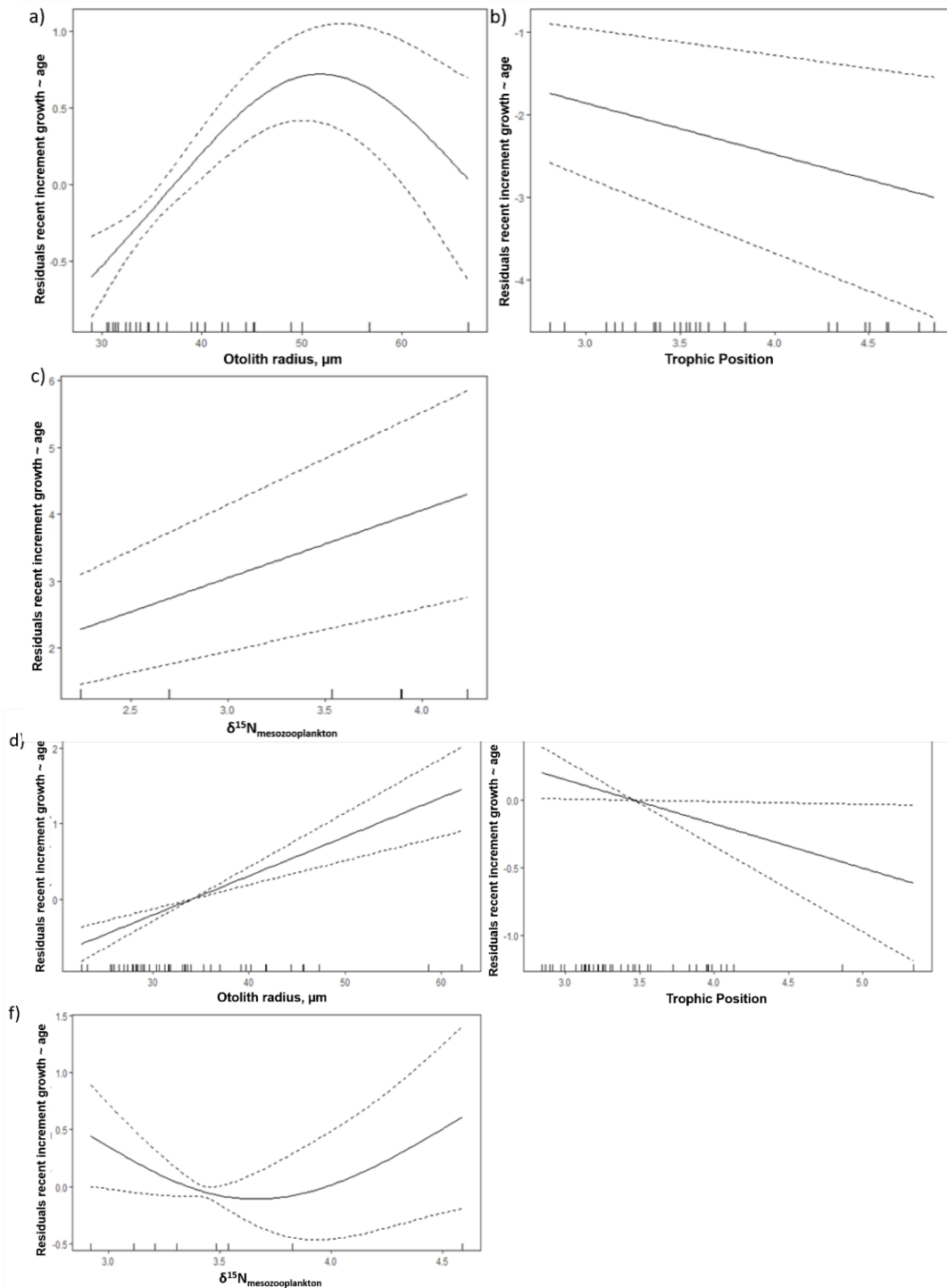


Figure 2.7. Selected model results of the partial effect of (a, e) otolith radius, μm , (b, e) trophic position and (c, f) larval fish abundance (1000^{-1}m^{-3}) for the Gulf of Mexico (GoM, $n=27$) spawning region (a-c) and the western Mediterranean Sea (MED, $n=44$) (d-f). The response variable is the average width of the last three daily increments (μm), recent growth at-age residual for postflexion *Thunnus thynnus*. The dashed lines indicate 95% confidence intervals. The whiskers on x-axis indicate observations for that covariate. All covariates have statistical significance at the 0.05 level.

REFERENCES

- Akaike (1974). A new look at the statistical model identification. *IEEE Trans. Automat. Contr.*, 19(6):716-723, doi:10.1109/TAC.1974.1100705.
- Alemaný, F., Quintanilla, L., Velez-Belchí, P., García, A., Cortés, D., Rodríguez, J.M., Fernández de Puelles, M.L., González-Pola, C., López-Jurado, J.L. (2010). Characterization of the spawning habitat of Atlantic bluefin tuna and related species Balearic Sea (western Mediterranean). *Prog. Oceanogr.*, 86:21–38.
- Alvarez, I., Rasmuson, L.K., Gerard, T., Laiz-Carrión, R., Hidalgo, M., Lamkin, J.T., Malca, E., et al. (2021) Influence of the seasonal thermocline on the vertical distribution of larval fish assemblages associated with Atlantic bluefin tuna spawning grounds. *Oceans*, 2, 64-83.
- Bakun A. (2012). Ocean eddies, predator pits and bluefin tuna: implications of an inferred ‘low risk–limited payoff’ reproductive scheme of a (former) archetypical top predator. *Fish & Fish.*, 424-438, doi: 10.1111/faf.12002.
- Balbín, R., López-Jurado, J.L., Flexas, M.M., Reglero, P., Vélez-Velchí, P., et al. (2014) Interannual variability of the early summer circulation around the Balearic Islands: Driving factors and potential effects on the marine ecosystem. *J. Mar. Syst.*, 138:70-81.
- Block, B. A., Teo, S.L.H., Walli, A., Boustany, A., Stokesbury, M. J. W., Farwell, C. J., et al. (2005) Electronic tagging and population structure of Atlantic bluefin tuna. *Nature*, 434(7037): 1121-1127, doi: 10.1038/nature03463.
- Bode, A., Álvarez-Ossorio, M.T., Cunha, M.E., Garrido, S., Benito Peleteiro, J., Porteiro, C., Valdés, L. and Varela, M. (2007). Stable nitrogen isotope studies of the pelagic food web on the Atlantic shelf of the Iberian Peninsula. *Prog. Oceanogr.*, 74: 115-131.
- Bodin, N., Pethybridge, H., Duffy, L.M., Lorrain, A., Allain, V., Logan, J.M., Ménard, F., Graham, B., Choy, C.A., Somes, C.J., Olson, R.J., Young, J.W. (2021) Global data set for nitrogen and carbon stable isotopes of tunas. *Ecology*, 102(3):e03265, doi: 10.1002/ecy.3265.
- Brothers, E.B., Prince, E.D., Lee, D.W. (1983). Age and growth of young-of-the-year blue fin tuna, *Thunnus thynnus*, from otolith microstructure. *In*: Prince, E.D. and Pulos, L.M. (eds) Procedures of the international workshop on age determination of oceanic pelagic fishes: tunas, billfishes, and sharks. NOAA Tech. Repos, N. M. F. S., 8:49-60.
- Campana, S.E., Jones, C. (1992). Analysis of otolith microstructure data. *In*: Stevenson, D.K., Campana, S.E. (eds) Otolith microstructure examination and analysis. *Can. Spec. Publ. Fish. Aqu. Sci.* 117:73-100.
- Campana, S.E., (1999). Chemistry and composition of fish otoliths: pathways, mechanisms and applications. *Mar. Ecol. Prog. Ser.*, 188, 263–297.
- Catalán, I.A., Alemany, F., Morillas, A., Morales-Nin, B. (2007) Diet of larval albacore *Thunnus alalunga* (Bonnaterre, 1788) off Mallorca Island (N.W. Mediterranean). *Sci. Mar.*, (71(2): 347-354, doi: 10.3989/scimar.2007.71n2347e.

- Catalán I.A., Tejedor, A., Alemany, F., Reglero, P. (2011) Trophic ecology of Atlantic bluefin tuna *Thunnus thynnus* larvae. *J. Fish. Biol.*, 78: 1545–1560.
- Caut, S., Angulo, E. and Courchamp, F. (2009). Variation in discriminant factors ($\Delta^{15}\text{N}$ and $\Delta^{13}\text{C}$): the effect of diet isotopic values and applications for diet reconstruction. *J. Appl. Ecol.*, 46: 443–453, doi.org/10.1111/j.1365-2664.2009.01620.x.
- Chang, W.Y.B. (1982). A statistical method for evaluating the reproducibility of age determination. *Can. J. Fish. Aquat. Sci.*, 39:1208–1210.
- Coll, M., Palomera, I., Tudela, S. and Sarda, F. (2006). Trophic flows, ecosystem structure and fishing impacts in the South Catalan Sea northwestern Mediterranean. *J. Mar. Syst.*, 59: 63–96.
- Collette, B., Amorim, A.F., Boustany, A., Carpenter, K.E., de Oliveira Leite Jr., et al. (2011). *Thunnus thynnus*. The IUCN Red List of Threatened Species 2011: e.T21860A9331546. <http://dx.doi.org/10.2305/IUCN.UK.2011-2.RLTS.T21860A9331546.en>. Downloaded 19 April 2019. Link: <https://www.iucnredlist.org/species/21860/9331546>.
- Dahl, K.A., Portnoy, D.S., Hogan, J.D., Johnson, J.E., Gold, J.R., Patterson, W.F., 2018. Genotyping confirms significant cannibalism in northern Gulf of Mexico invasive red lionfish, *Pterois volitans*. *Biol. Invasions*, 1–14.
- Domingues, R., Goni, G., Bringas, F., Muhling, B., Lindo-Atichati, D. and Walter, J. (2016) Variability of preferred environmental conditions for Atlantic bluefin tuna (*Thunnus thynnus*) larvae in the Gulf of Mexico during 1993–2011. *Fish. Oceanogr.*, 25: 320–336.
- Fromentin, J.M., Powers, J.E. (2005). Atlantic bluefin tuna: population dynamics, ecology, fisheries and management. *Fish Fish.*, 6:281–306.
- Fry, B. (2006) Stable isotope ecology. Springer, New York, NY. 308, doi.org/10.1007/0-387-33745-8.
- García, A., Cortés, D., Ramírez, T., Rifika, F., Alemany, F., Rodríguez, J. M., Carpena, A., Alvarez, J. P. (2006) First data on growth and nucleic acid and protein content of field-captured Mediterranean bluefin (*T. thynnus*) and albacore (*T. alalunga*) larvae: a comparative study. *Sci. Mar.*, 70: 67–78.
- García, A., Cortés, D., Quintanilla, J., Ramírez, T., Quintanilla, L., Rodríguez, J.M., Alemany, F. (2013). Climate-induced environmental conditions influencing interannual variability of Mediterranean bluefin (*Thunnus thynnus*) larval growth. *Fish. Oceanogr.*, 22(4):273–287.
- García, A., Laiz-Carrión, R., Uriarte, A., Quintanilla, J., Morote, E., Rodríguez, J., Alemany, F. (2017). Differentiated stable isotopes signatures between pre- and post-flexion larvae of Atlantic bluefin tuna (*Thunnus thynnus*) and of its associated tuna species of the Balearic Sea (NW Mediterranean). *Deep. Sea. Res., Part II*, 140: 18–24.
- Gerard, T., Lamkin, J. T., Kelly, T. B., Knapp, A. N., Laiz-Carrión, R., Malca, E., Selph, K. E., Shiroza, A. et al. (2022) Bluefin larvae in Oligotrophic Ocean Foodwebs, Investigations of Nutrients to Zooplankton: overview of the BLOOFINZ-Gulf of Mexico program. *J. Plankton Res.*, 44(5): 600–617.

- Gleiber, M. R., Sponaugle, S., Robinson, K., Cowen, R. (2020a) Food web constraints on larval growth in subtropical coral reef and pelagic fishes. *Mar. Ecol. Prog. Ser.*, 650, 19–36.
- Gleiber, M.R., Sponaugle, S., Cowen, R. K. (2020b) Some like it hot, hungry tunas do not! Implications of temperature and plankton food web dynamics on growth and diet of tropical tuna larvae. *ICES J. Mar. Sci.*, 77 (7-8):3058–3073, <https://doi.org/10.1093/icesjms/fsaa201>.
- Gordoa, A., Fraile, I. Arrizabalaga, H., Raventós, N. (2021). Growth of Mediterranean young-of-the-year bluefin tuna *Thunnus thynnus* (Scombridae): regional differences and hatching periods. *Scien. Mar.*, 85(2), doi.org/10.3989/scimar.05108.006.
- Habtes, S., Muller-Karger, F., Roffer, M., Lamkin, J.T., Muhling, B.A. (2014). A comparison of sampling methods for larvae of medium and large epipelagic fish species during spring SEAMAP ichthyoplankton surveys in the Gulf of Mexico. *Limnol. Oceanog. Meth.*, 12, 86–101.
- Hildebrand, R. (2022) Feeding ecology of highly migratory epipelagic offshore predators in the western North Atlantic Ocean. MS. Thesis, Nova Southeastern University, 69 pp.
- Houde, E.D. (2008) Emerging from Hjort’s Shadow Evaluation of ecosystem based reference points for Atlantic Menhaden in the Northwest Atlantic Ocean View project Emerging from Hjort’s Shadow. *J. N. W. Atl. Fish. Sci.*, 41: 53-70.
- Ingram, G.W., Richards, W.J., Lamkin, J.T., Muhling, B.A. (2010). Annual indices of Atlantic bluefin tuna (*Thunnus thynnus*) larvae in the Gulf of Mexico developed using delta-lognormal and multivariate models. *Aqua. Living. Res.*, 23:35-47.
- Ingram Jr., G.W., Alvarez-Berastegui, D., Reglero, P., Balbín, R., García, A. (2017) Incorporation of habitat information in the development of indices of larval bluefin tuna (*Thunnus thynnus*) in the Western Mediterranean Sea (2001–2005 and 2012–2013). *Deep Sea Res., Part II*, 140: 203-211. <https://doi.org/10.1016/j.dsr2.2017.03.012>.
- Itoh, T., Shiina, Y., Tsuji, S., Endo, F., Tezuka, N. (2000). Otolith daily increment formation in laboratory reared larval and juvenile bluefin tuna *Thunnus thynnus*. *Fish. Sci.*, 66(5): 834-839.
- Jackson, A. L., Inger, R., Parnell, A. C., Bearhop, S. (2011). Comparing isotopic niche widths among and within communities: SIBER – Stable Isotope Bayesian Ellipses in R. *J. Animal Ecol.*, 80: 595–602.
- Jackson, M. C., Donohue, I., Jackson, A. L., Britton, J. R., Harper, D. M., Grey, J. (2012) Population-Level Metrics of Trophic Structure Based on Stable Isotopes and Their Application to Invasion Ecology. *PLoS ONE*, 7(2): e31757.
- Jenkins, G. P. and Davis, T. L. O. (1990) Age, growth rate, and growth trajectory determined from otolith microstructure of southern bluefin tuna *Thunnus maccoyii* larvae. *Mar. Ecol. Prog. Ser.*, 63: 93-104.
- Johnstone, C., Pérez, M., Malca, E., Quintanilla, J.M., Gerard, T., Lozano-Peral, D., Alemany, F., Lamkin, J.T., et al. (2021) Genetic connectivity between Atlantic bluefin tuna larvae spawned in the Gulf of Mexico and in the Mediterranean Sea. *PeerJ*, 9, e11568. <https://doi.org/10.7717/peerj.11568>.

- Laiz-Carrión R., Quintanilla J., Mercado J. and García A. (2011). Combined Study of daily growth variability and nitrogen-carbon isotopic signature analysis of Alborán Sea schooling sardine *Sardina pilchardus* (Walbaum, 1792) larvae. *J. Fish Biol.* 79: 896–914, 10.1111/j.1095-8649.2011.03048.x.
- Laiz-Carrión, R., Quintanilla, J.M., Torres, A.P., Alemany, F., García, A. (2013) Hydrographic patterns conditioning variable trophic pathways and early life dynamics of bullet tuna *Auxis rochei* larvae in the Balearic Sea. *Mar. Ecol. Prog. Ser.*, 475: 203–212.
- Laiz-Carrión, R., Gerard, T., Uriarte, A., Malca, E., Quintanilla, J.M., Muhling, B.A., et al. (2015). Trophic ecology of Atlantic bluefin tuna (*Thunnus thynnus*) larvae from the Gulf of Mexico and NW Mediterranean spawning grounds: a comparative stable isotope study. *PLoS ONE*, doi:10.1371/journal.pone.0133406.
- Laiz-Carrión, R., Gerard, T., Suca, J.J., Malca, E., Uriarte, A., Quintanilla, J.M., Privoznik, S.L., Llopiz, J.K., et al. (2019) Stable isotope analysis indicates resource partitioning and trophic niche overlap in larvae of four tuna species in the Gulf of Mexico. *Mar. Ecol. Prog. Ser.*, 619:53-68. <https://doi.org/10.3354/meps12958>.
- Lindo-Atichati, D., Bringas, F., Goni, G., Muhling, B., Muller-Karger, F.E., Habtes, S. (2012). Varying mesoscale structures influence larval fish distribution in the northern Gulf of Mexico. *Mar. Ecol. Prog. Ser.*, 463:245-257.
- Llopiz, J.K., Richardson, D.E., Shiroza, A., Smith, S.L., Cowen, R.K. (2010) Distinctions in the diets and distributions of larval tunas and the important role of appendicularians. *Limnol. Oceanogr.*, 55: 983–996.
- Llopiz, J.K., Hobday, A.J. (2015) A global comparative analysis of the feeding dynamics and environmental conditions of larval tunas, mackerels, and billfishes. *Deep Sea Res., II* 113: 113–124.
- Logan, J., Haas, H., Deegan, L., Gaines, E. (2006) Turnover rates of nitrogen stable isotopes in the salt marsh mummichog, *Fundulus heteroclitus*, following a laboratory diet switch. *Oecologia*, 147(3):391-5, doi: 10.1007/s00442-005-0277-z.
- Long, J.M., and Porta, M.J. (2019) Age and growth of stocked juvenile Shoal Bass in a tailwater: Environmental variation and accuracy of daily age estimates. *PLoS ONE* 14(10): e0224018, <https://doi.org/10.1371/journal.pone.0224018>.
- Malca E., Muhling B.A., Franks, J., García, A., et al. (2017). Age and growth of larval bluefin tuna (*Thunnus thynnus*): comparison of the Gulf of Mexico to the Straits of Florida, and Balearic Sea (Mediterranean). *Fish. Res.*, 190: 24-33.
- Malca, E., Shropshire, T.M., Landry M.R., Quintanilla, J.M., Laíz-Carrión, Shiroza, A., Stukel, M.R., Lamkin, J.T., Gerard, T.G., Swalethorp, R. (2022). Influence of food quality on larval growth of Atlantic bluefin tuna (*Thunnus thynnus*) in the Gulf of Mexico. *J. Plankton Res.*, 44(5):474-762, doi.org/10.1093/plankt/fbac024.
- Marra, G., and Wood, S. N. (2011) Practical Variable Selection for Generalized Additive Models. *Comput. Stat. Data Anal.*, 55: 2372–2387.

- Montoya, J.P. (2007). Natural abundance of ^{15}N in marine planktonic ecosystems. In *Stable Isotopes in Ecology and Environmental Science*. Eds Michener, R. and Lajtha, K. Wiley-Blackwell, USA, 176-194.
- Muhling, B.A., Lamkin, J.T., Roffer, M.A. (2010). Predicting the occurrence of bluefin tuna (*Thunnus thynnus*) larvae in the northern GOM: Building a classification model from archival data. *Fish. Oceanogr.*, 19: 526-539.
- Muhling, B.A., Reglero, P., Ciannelli, L., Alvarez-Berastegui, D., Alemany, F., Lamkin, J.T., Roffer, M.A. (2013). Comparison between environmental characteristics of larval bluefin tuna *Thunnus thynnus* habitat in the GOM and western Mediterranean Sea. *Mar. Ecol. Prog. Ser.*, 486:257-276.
- Muhling, B.A., Lamkin, J.T., Alemany, F., García, A., Farley, J.H., Ingram, G.W. Jr., Berastegui, D.A., Reglero, P., et al. (2017) Reproduction and larval biology in tunas, and the importance of restricted area spawning grounds. *Rev. Fish. Biol. Fish.*, 27,697–732.
<https://doi.org/10.1007/s11160-017-9471-4>.
- NOAA. “Western Atlantic Bluefin Tuna.” US Department of Commerce, 18 April 2019, www.fisheries.noaa.gov/species/western-atlantic-bluefin-tuna.
- Peterson, B. J., & Fry, B. (1987). Stable isotopes in ecosystem studies. *Ann. Rev. Ecol. Syst.*, 18, 293–320.
- Pepin, P., Dower, J.F. (2007) Variability in the trophic position of larval fish in a coastal pelagic ecosystem based on stable isotope analysis. *J. Plank. Res.*, 29: 727–737.
- Pepin, P., Robert, D., Bouchard, C., Dower, J.F., Falardeau, M., Fortier, L., Jenkins, G.P., et al. (2014). Once upon a larva: revisiting the relationship between feeding success and growth in fish larvae. *ICES J. Mar. Sci.* 72 (2), 359–373.
- Pinnegar, J.K., Polunin, N.V.C. (1999) Differential fractionation of $\delta^{13}\text{C}$ and $\delta^{15}\text{N}$ among fish tissues: implications for the study of trophic interactions. *Funct. Ecol.*, 13: 225–231.
- Polis, G., Strong, D.R. (1996) Food web complexity and community dynamics. *Am. Nat.*, 147: 813–846.
- Post, D.M. (2002) Using stable isotopes to estimate trophic position: models, methods and assumptions. *Ecology*, 83: 703–718.
- Quintanilla J, Laiz-Carrión R., Uriarte A. and García A. (2015). Influence of trophic pathways on daily growth patterns of Western Mediterranean anchovy (*Engraulis encrasicolus*) larvae. *Mar. Ecol. Prog. Ser.*, 531: 263–275. DOI:10.3354/meps11312.
- Quintanilla, J. M., Laiz-Carrión, R., García, A., Quintanilla, L. F., Cortés, D., Gómez-Jakobsen, F., Yebra, L., Salles, S., Putzeys, S., León, P. and Mercado, J. M. (2020). Early life trophodynamic influence on daily growth patterns of the Alboran Sea sardine (*Sardina pilchardus*) from two distinct nursery habitats (Bays of Málaga and Almería) in the Western Mediterranean Sea. *Mar. Env. Res.*, 162: 105195, doi:10.1016/j.marenvres.2020.105195.
- R Core Team, (2022). R: A language and environment for statistical computing. R Foundation for Statistical Computing, Vienna, Austria. ISBN 3-900051-07-0, <http://www.R-project.org/>.

- Richards, W.J. (Ed). (2006). Early stages of Atlantic fishes. An identification guide for the Western Central North Atlantic. CRC, Taylor and Francis Group L.L.C. 2591 p.
- Restrepo, V.R., Diaz, G.A., Walter, J.F., Neilson, J.D., Campana, S.E., Secor, D., Wingate, R.L., (2010). Updated estimate of the growth curve of Western Atlantic bluefin tuna. *Aquat. Livi. Res.*, 23: 335-342.
- Richardson, D.E., Marancik, K.E., Guyon, J.R., Lutcavage, M.E., Galuardi, B., Lam, C.H., Walsh, H.J., Wildes, S., Yates, D.A., Hare, J.A. (2016). Discovery of a spawning ground reveals diverse migration strategies in Atlantic bluefin tuna (*Thunnus thynnus*). *PNAS*, 113: 3299-3304.
- Rooker, J.R., Alvarado, Bremer, J.R., Block, B.A., Dewar, H., De Metrio, G., Corriero, A., Kraus, R.T., Prince, E.D., Rodríguez Martín, E., Secor, D.H. (2007). Life History and Stock Structure of Atlantic Bluefin Tuna (*Thunnus thynnus*). *Rev. Fish. Sci.*, 15: 265–310.
- Russo, S., Torri, M., Patti, B., Musco, M., Masullo, T., Di Natale, M.V., Sarà, G., Cuttitta, A. (2022) Environmental conditions along tuna larval dispersion: Insights on the spawning habitat and impact on their development stages. *Water*, 14, 1568:1-16, doi.org/10.3390/w14101568.
- Sabatés, A., Olivar, M.P., Salat, J., Palomera, I., Alemany, F. (2007) Physical and biological processes controlling the distribution of fish larvae in the NW Mediterranean. *Prog. Oceanogr.*, 74: 355-376, doi:10.1016/j.pocean.2007.04.017.
- Satoh, K., Tanaka, Y., Iwahashi, M., 2008. Variations in the instantaneous mortality rate between larval patches of Pacific bluefin tuna *Thunnus orientalis* in the northwestern Pacific Ocean. *Fish. Res.*, 89: 248-256.
- Satoh, K., Masujima, M., Tanaka, Y., Okazaki, M., Kato, Y., Shono, H. (2014) Transport, distribution and growth of larval patches of Pacific bluefin tuna (*Thunnus orientalis*) in the northwestern Pacific Ocean. *Bull. Fish. Res. Agency Jpn.* 38:81–86.
- Schneider, C.A., Rasband, W.S., Eliceiri, K.W. (2012). NIH Image to ImageJ: 25 years of image analysis. *Nat. Methods*, 9: 671-675.
- Scott, G.P., Turner, S.C., Grimes, C.B., Richards, W.J., Brothers, E.B. (1993). Indices of larval bluefin tuna, *Thunnus thynnus*, abundance in the GOM: Modeling variability in growth, mortality, and gear selectivity: Ichthyoplankton methods for estimating fish biomass. *Bull. Mar. Sci.*, 53: 912-929.
- Secor, D.H., Dean, J.M., Campana, S.E. (1995). Recent developments in fish otolith research. Univ. of South Carolina Press, Columbia, S.C., USA.
- Secor, D.H., Wingate R.L., Neilson J.D., Rooker J.R., Campana S.E. (2008). Growth of Atlantic bluefin tuna: direct age estimates. *Col. Vol. Sci. Pap. ICCAT* 2008/84.
- Shiroza A., Malca E., Lamkin J.T., Gerard T., Landry M.R., Stukel M.R., Laiz-Carrión R. and Swalethorp R. (2021). Diet and prey selection in developing larvae of Atlantic bluefin tuna (*Thunnus thynnus*) in spawning grounds of the Gulf of Mexico. *J. Plank. Res.* 44(5):728-746, <https://doi.org/10.1093/plankt/fbab020>.

- Sponaugle, S. (2010). Otolith microstructure reveals ecological and oceanographic processes important to ecosystem-based management. *Environ. Biol. Fish.*, 89:221-238. doi: 10.1007/s10641-010-9676-z.
- Tilley, J.D., Butler, C.M., Suárez-Morales, E., Franks, J.S. and others (2016) Feeding ecology of larval Atlantic bluefin tuna, *Thunnus thynnus*, from the central Gulf of Mexico. *Bull. Mar. Sci.*, 92: 321–334.
- Uriarte, A., García, A., Ortega, A., de la Gándara, F., Quintanilla, J., Laiz-Carrión, R. (2016) Isotopic discrimination factors and nitrogen turnover rates in reared Atlantic bluefin tuna larvae (*Thunnus thynnus*): effects of maternal transmission. *Sci. Mar.*, 80(4), doi: <http://dx.doi.org/10.3989/scimar.04435.25A>
- Uriarte A., Johnstone, C., Laiz-Carrión R., García, A., et. al. (2019) Evidence of density-dependent cannibalism in the diet of wild Atlantic bluefin tuna larvae (*Thunnus thynnus*) of the Balearic Sea (N.W. Mediterranean). *Fish. Res.*, 212: 63-71.
- Varela, J.L., de la Gándara, F., Ortega, A., Medina, A. (2012) ^{13}C and ^{15}N analysis in muscle and liver of wild and reared young-of-the-year (YOY) Atlantic bluefin tuna. *Aquac.*, 354-355, 17–21.
- Varela, J.L., Cañavate, J.P., Medina, A., Mourente, G. (2019) Inter-regional variation in feeding patterns of skipjack tuna (*Katsuwonus pelamis*) inferred from stomach content, stable isotope and fatty acid analyses. *Mar. Env. Res.*, 152(104821), doi.org/10.1016/j.marenvres.2019.104821.
- Vélez-Belchí, P. and Tintoré, J. (2001) Vertical velocities at an ocean front. *Sci. Mar.*, 65 (1): 291-300.
- Watai, M., Ishihara, T., Abe, O., Ohshimo, S., Strussmann, C. A. (2017) Evaluation of growth-dependent survival during early stages of Pacific bluefin tuna using otolith microstructure analysis. *Mar. Freshwater Res.*, 68, 2008-2017.
- Watai, M., Hiraoka Y., Ishihara, T., Yamasaki, I., Ota, T., Ohsimo, S., Strüssmann (2018) Comparative analysis of the early growth history of Pacific bluefin tuna *Thunnus orientalis* from different spawning grounds. *Mar. Ecol. Prog. Ser.*, 607:207-220, doi.org/10.3354/meps12807.
- Wilson, S.G., Jonsen, I.D, Schallert, R.J., Ganong, J. E., Castleton, M. R., Spires, A. D, et al. (2015) Tracking the fidelity of Atlantic bluefin tuna released in Canadian waters to the Gulf of Mexico spawning grounds. *Can. J. Fish. Aquat. Sci.*, 72: 1–18, dx.doi.org/10.1139/cjfas-2015-0110.
- Wood, S. N. (2004). Stable and efficient multiple smoothing parameter estimation for generalized additive models. *J. Am. Stat. Assoc.*, 99(467).
- Wood, S. N. (2017). *Generalized Additive Models: An Introduction with R*, 2 edition. Chapman and Hall/CRC.
- Woodstock, M.S., Sutton, T.T., Frank, T., Zhang, Y. (2021) An early warning sign: trophic structure changes in the oceanic Gulf of Mexico from 2011-2018. *Ecol. Model.*, 445, 109509.

- Yúfera, M., Ortiz-Delgado, J.B., Hoffman, T., Sigüero, I., Urup, B., Sarasquete, C. (2014). Organogenesis of digestive system, visual system and other structures in Atlantic bluefin tuna (*Thunnus thynnus*) larvae reared with copepods in mesocosm system. *Aquac.*, 426-427: 126-137.
- Zygas, A., Malca, E. Gerard. T., Lamkin, J.T. (2015). Age-length relationship of larval skipjack tuna (*Katsuwonus pelamis*) in the Gulf of Mexico. ICCAT SCRS/2015/186.

CHAPTER 3: Influence of food quality on larval growth of Atlantic bluefin tuna (*Thunnus thynnus*) in the Gulf of Mexico¹

INTRODUCTION

Atlantic bluefin tuna (ABT, *Thunnus thynnus*) is the largest species of the tuna family (Scombridae), reaching sizes up to 4.6 m and 650 kg (Anonymous 2019). Adults of the western ABT stock migrate large distances from rich North Atlantic feeding grounds to spawn mainly in the oligotrophic waters of the Gulf of Mexico (GoM) between April and June (Fromentin & Powers, 2005, Rooker et al., 2008, Block 2019), which is believed to put their offspring in an optimal habitat for survival (Bakun 2013). Spawning appears to be mediated by sea surface temperature above ~24°C beyond the 200-m isobath and along the outer edges of anticyclonic eddies (Muhling et al., 2010, Domingues et al., 2016). The planktonic larvae, restricted to the upper 25 m of the water column, are subsequently challenged to grow rapidly, or perish due to starvation or predation, especially during the most vulnerable first weeks of life (Kimura et al., 2010, García et al., 2013, Shropshire et al., 2021).

Larval ABT habitat has been extensively studied and modeled in the GoM (Muhling et al., 2010, Lindo-Atichati et al., 2012, Laiz-Carrión et al., 2015, Domingues et al., 2016, Alvarez et al., 2021), as well as in the Mediterranean Sea (MED), where the eastern stock spawns (Alvarez-Beristegui et al., 2016, Ingram et al., 2017, Reglero et al., 2019). In the MED, García et al. (2006) examined DNA and protein ratios, and Ingram et al. (2017) incorporated environmental parameters into larval condition indices. The influence of habitat quality on larval growth has yet to be examined for the GoM. Higher growth rates generally lead to enhanced larval survival (Bergenius et al., 2002, Kimura et al., 2010). However, growth may be limited by the variable distribution of preferred zooplankton prey in a heterogeneous environment (McGruck 1986, Shiroza et al. 2021), and in warm oligotrophic systems like the GoM, high metabolic demand can easily lead to starvation under food-limiting conditions (Shropshire et al., 2021).

Otolith microstructure is routinely used in fisheries management and ecological modeling to quantify age and growth (Campana & Jones, 1992, Begg et al., 2005). Specifically, otoliths

¹ Malca, E., Shropshire, T.M., Landry M.R., Quintanilla, J.M., Laiz-Carrión, Shiroza, A., Stukel, M.R., Lamkin, J.T., Gerard, T.G., Swalethorp, R. Influence of food quality on larval growth of Atlantic bluefin tuna (*Thunnus thynnus*) in the Gulf of Mexico. J. Plankton Res., 44(5):747-762, doi.org/10.1093/plankt/fbac024.

provide a historical record of larval growth, with increments deposited daily and increment widths (IW, μm) being proportional to somatic growth (Panella 1971, Clemmesen 1994, Robert et al., 2007, Gleiber et al., 2020b). Similar to the early stages of other top pelagic predators like marlin, sailfish and swordfish, somatic growth rates of ABT larvae are highest during the first week of life (0.86 mm d^{-1} in days post hatch, dph) and decrease in the following week (0.62 mm d^{-1}) but remain rapid compared to most fishes (Malca et al., 2017). Larval daily increment formation has been validated for the closely related Pacific bluefin tuna (Foreman 1996, Itoh et al., 2000), and inferred for Southern bluefin tuna (Jenkins et al., 1990). Elevated temperature has been shown to enhance growth of larval tuna (Tanaka et al., 2006, Kimura et al., 2010, García et al., 2013) and has been identified as one the main abiotic driver of tuna distribution and recruitment (Alvarez et al., 2021). However, given the sub-tropical conditions of western ABT spawning grounds, prey availability may be more important than temperature for limiting growth (Jenkins et al., 1991, Tanaka et al., 2006, Shropshire et al., 2021).

Quantifying year-to-year differences in larval growth is relevant for annual estimates of ABT spawning biomass based on larval length distributions (Scott et al., 1993, Ingram et al., 2010, 2017) and may shed light on environmental drivers of larval survival. While substantial

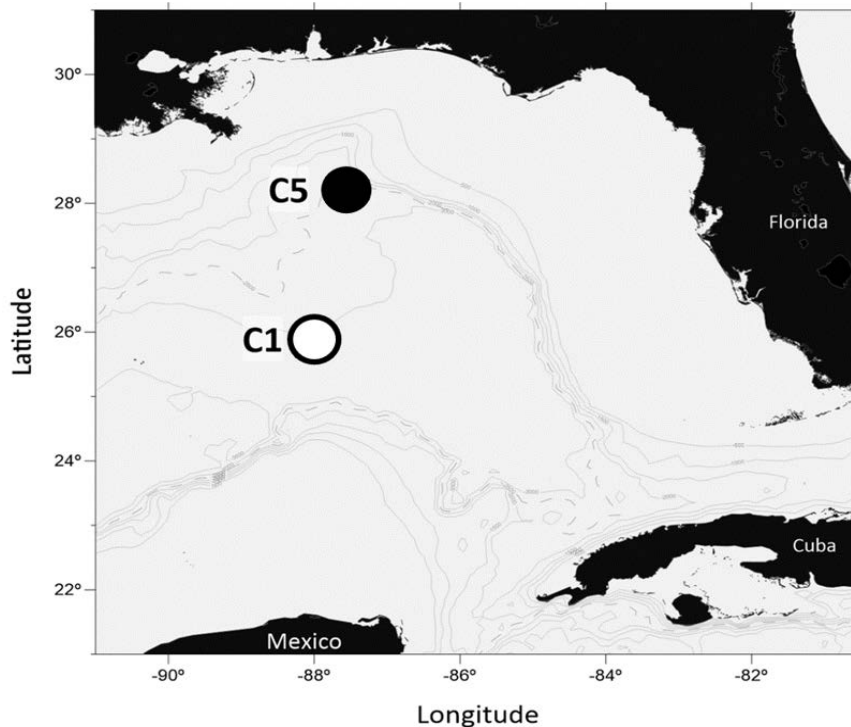


Figure 3.1. General study area in the northeastern Gulf of Mexico. Areas for net tow sampling during cycle experiment are indicated for survey NF1704, cycle 1 (C1, \circ) and NF1802, cycle 5 (C5, \bullet).

temporal variability in mean growth has not been observed in western ABT larvae aged previously from 2000 to 2012 (Malca et al., 2017), those analyses were for uneven sample sizes of specimens averaged over mixed locations and without knowledge of feeding conditions. The pairing of larval diet with otolith biometrics for the conditions experienced in discrete patches of larvae might more usefully reveal successful feeding strategies or point to factors that determine relative quality of feeding and growth environments (Gleiber et al., 2020a). ABT larvae are considered successful feeders in the sense of having daytime feeding incidences of up to 98-100% of at least one prey item in their stomach contents (Catalán et al., 2011, Llopiz et al., 2015, Tilley et al., 2016, Uriarte et al., 2019, Shiroza et al., 2021). However, there is little understanding of how the variability of their growth rates might be affected by their preferences for and availability of specific prey types.

Here, age-at-body size estimates are reported for GoM-spawned ABT larvae and compare full otolith growth trajectories between two cohorts, each tracked and sampled for several days in Lagrangian experiments. Larvae were collected as part of the BLOOFINZ-GoM Program (Bluefin Larvae in Oligotrophic Ocean Foodwebs: Investigating Nutrients to Zooplankton in the Gulf of Mexico) during 2017 and 2018 cruises in the peak ABT spawning month of May (Gerard et al., 2022). Somatic growth estimates from otolith microstructure were coupled to previously determined dietary analyses from the two nursery habitats (Shiroza et al., 2021) and to modeling outputs relating to food limitation and zooplankton biomass structure (Shropshire et al., 2021, Landry et al., 2021). The differences in somatic growth for early and late stage larvae were examined in relation to their shifting dietary preferences. This chapter's goals were to determine (i) how biometrics change with larval ABT ontogeny, and (ii) to determine the environmental drivers most important for regulating growth. In addition, the hypothesis that larval growth would be faster in the 2018 nursery area was tested because it was found to be richest in, and with the highest feeding incidences on the preferred prey (cladocerans) by the more developed postflexion larvae (Shiroza et al., 2021).

METHODS

Larval sampling and processing

Larval ABT were collected in the GoM on BLOOFINZ cruises NF1704 (10-13 May 2017) and NF1802 (15-19 May 2018) aboard the NOAA Ship *Nancy Foster* (Figure. 3.1). On each cruise, a larval patch was marked with satellite-tracked drifters and resampled the patch repeatedly over 4-5 days (hereafter, Cycle 1 (C1) in 2017 and Cycle 5 (C5) in 2018). A bongo-90 net frame (90-cm diameter, 505- μ m mesh nets) was towed obliquely from the sea surface to 25 m for ~10 min at ~ 2 knots. Depth was monitored with a SBE 39plus (Sea-bird Scientific) depth sensor at the end of the hydrowire, and volume filtered was measured by General Oceanics flow meters at the centers of each net. The plankton samples were preserved in 95% ethanol, which was replaced within 24 h and again in the laboratory for larger plankton volumes as needed. At sea, ~200 ABT larvae were removed and measured for standard length (SL, mm) and to determine the saltwater-to-95%-ethanol shrinkage curve across size classes throughout C1 and C5:

$$SL_{ethanol} = 0.907(SL_{saltwater}) + 0.047. \quad (1)$$

Gerard et al. (2022) provides the overall BLOOFINZ study design and survey details, including station positions and ABT larval catch (# net⁻¹) for each tow. Full details of the processing of stomach contents of larval tuna and zooplankton samples for biomass and taxonomic composition are available in Shiroza et al. (2021) and Landry & Swalethorp (2021).

ABT larvae were identified to three developmental stages (preflexion, flexion and postflexion) following Richards (2006). Ethanol-preserved larvae were measured for body size (SL, mm) and body depth (mm) with a Leica M205C dissecting microscope fitted with a Leica EC3 digital camera and image analysis software (Leica Application Suite, 4.3). SL was measured to the base of the caudal peduncle, while body depth was measured at the widest muscular height from the dorsal fin posterior of the anus when larval preservation allowed. Larval lengths were corrected for ethanol shrinkage using Equation 1 and dry weights (mg) were estimated subsequently for each larva using a dry-weight: saltwater-length relationship developed separately for each cycle (Eq. 2a and 2b for C1 (n=149) and C5 (n=45), respectively), where x is the $SL_{saltwater}$, mm. The subset of larvae of similar size distribution (not aged in this study) were

frozen at sea at $-80\text{ }^{\circ}\text{C}$ and dehydrated in a freeze dryer for 24 h following Laiz-Carrión *et al.*, 2019.

$$\text{Dry weight}_{C1} = 0.0113 e^{0.579x} \quad (2a)$$

$$\text{Dry weight}_{C5} = 0.0131 e^{0.5763x} \quad (2b)$$

Temperature ($^{\circ}\text{C}$), salinity (psu) and fluorescence (volts) profiles for the upper 25 m were determined from CTD casts conducted throughout C1 and C5. Relative fluorescence (volts) was uncalibrated, but close to mean Chlorophyll *a* values determined from extracted samples (mg m^{-3} , Selph *et al.*, 2021).

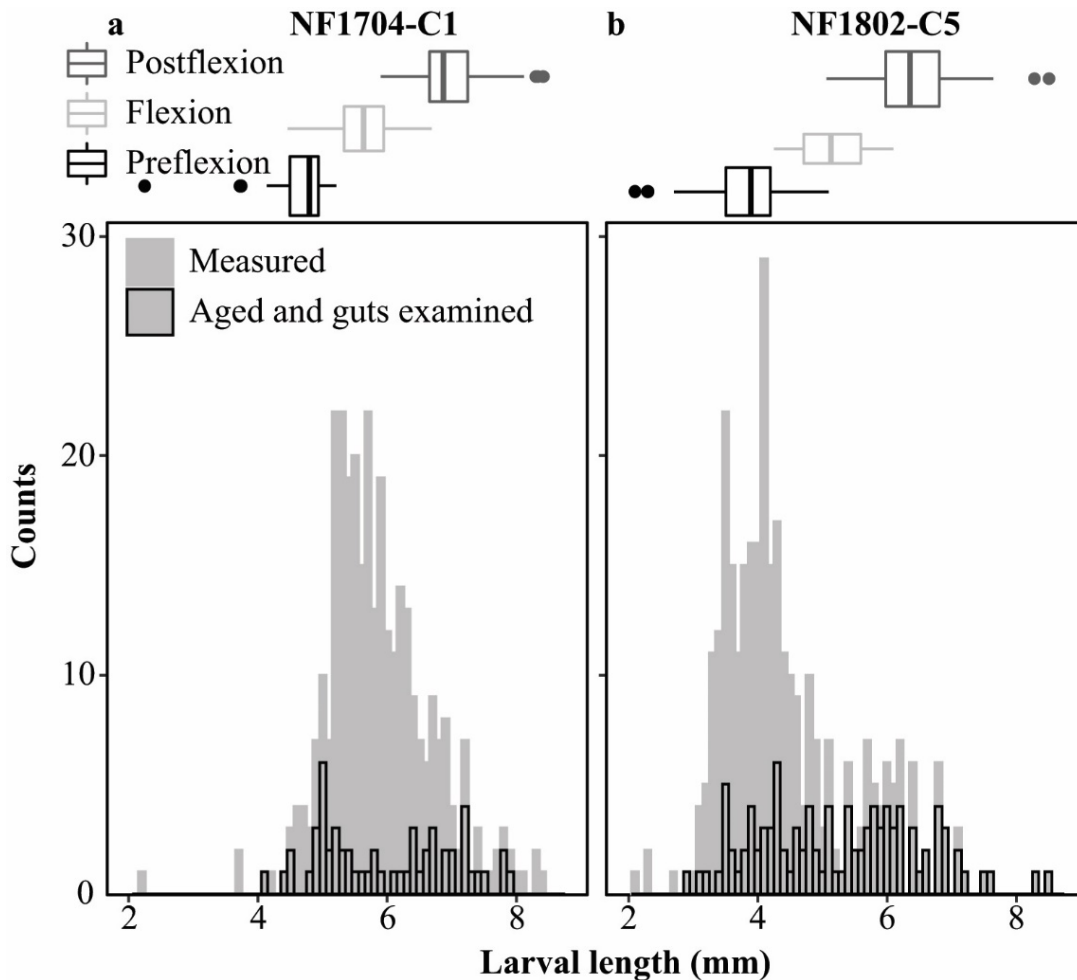


Figure 3.2. Histogram for bluefin tuna (*Thunnus thynnus*) larvae measured (mm) from a) cycle 1 (C1) and b) cycle 5 (C5) in the Gulf of Mexico. The boxplot indicates larval developmental stages preflexion, flexion and postflexion with corresponding larval length (SL, mm) from ethanol-preserved specimens (gray). Daytime-aged ABT larvae with gut contents examined are also indicated.

Otolith analyses

The largest otolith pairs (sagittal) were extracted from the cranial cavity of ABT larvae using sharpened glass probes and allowed to air dry. Otoliths were fixed with one drop of mounting medium (Flo-Texx™), distal side facing up. One randomly selected sagitta was chosen for age estimation. If the selected sagitta was cracked or otherwise damaged, the corresponding sagitta was aged. All otoliths were examined at 400 to 1000x in immersion oil (transmitted light) with a compound microscope (Zeiss A.1), digital camera and calibrated image analysis software (Image Pro Plus 7 or Image Pro Plus 10).

Table 3.1. ANCOVA summary (upper panel) for larval *Thunnus thynnus* biometrics. Linear mixed model (lower panel) considering full otolith increment width history from all larvae. Asterisk indicates significant results at the 0.05 level. For the linear mixed model, early growth is 1-7 days post hatch (dph), and late growth is 8-15 dph. Number inside parenthesis indicates number of ABT considered for cycle 1 and cycle 5 (C1, C5 respectively).

| ANCOVA | F | R² | ρ |
|--|----------|----------------------|-----------|
| Overall somatic growth: length at age | 959.4 | 0.830 | < 0.001 * |
| Cycle C1 vs C5 | 0.411 | 0.829 | 0.5223 |
| Overall otolith growth: OR _{Log} at age | 1510.8 | 0.885 | < 0.001 * |
| Cycle C1 vs C5 | 0.5617 | 0.885 | 0.455 |
| OR _{Log} at age residuals and length at age residuals | 314.02 | 0.614 | < 0.001 * |
| Cycle C1 vs C5 | 0.0604 | 0.610 | 0.806 |
| Weight _{Log} at age | 535.77 | 0.738 | < 0.001 * |
| Cycle C1 vs C5 | 4.460 | 0.738 | 0.036 |
| Depth _{Log} at age | 648.12 | 0.805 | < 0.001 * |
| Cycle C1 vs C5 | 0.367 | 0.803 | 0.545 |
| Linear Mixed Model | | | |
| Increment width early growth, C1 (102) vs C5 (103) | 17.056 | NA | < 0.001 * |
| Increment width late growth, C1 (93) vs C5 (64) | 4.336 | NA | 0.039 * |

Daily increments were counted along the otolith radius (OR) twice by a single experienced reader. Since most ABT otoliths do not have a clear hatch mark, a minimum distance of 7 μm from the central core was designated as the starting point (Jenkins & Davis, 1990, García et al., 2013), and estimated increments were added along the OR until reaching the first observed increment. The last increment is often obscured by light microscopy artifacts and is less discernable (Campana & Jones, 1992), particularly for larger otoliths. To address this issue in age determination, a terminal increment was added if there was space for one along the OR. Measurement precision was calculated using Chang's (1982) coefficient of variation (CV) adjusted for age. Hereafter, age refers to days post hatch (dph).

Recent otolith growth (μm) was calculated from the average of the last three completed increments, which has been shown to characterize larval conditions prior to collection (Clemmensen 1994, Shulzitski et al., 2015, Gleiber et al., 2020a). Incomplete increments were excluded from further analyses.

Larval gut contents and prey availability

Larvae selected for ageing were also examined for gut contents as reported in Shiroza *et al.* (2021). ABT larvae examined in this section were preserved, measured and staged in the same manner as mentioned previously. Briefly, the gut contents from daytime caught larvae were examined and characterized into nine taxonomic categories of prey: Ciliophora, Podonidae, Copepoda nauplii, Calanoida, Corycaeidae, Other Copepoda, Appendicularia, unidentified fish larvae, and other prey. Ingested carbon weights (mg C) for these taxa were then estimated from length-dry weight conversion factors in Table S1 of Shiroza et al. (2021) for each individual larva. Gut content data also provide estimates of prey size range as a function of larval length, which can be used to estimate total prey biomass from measured zooplankton biomass. For all aged larvae, prey size length ranged from 80 to 914 μm .

During the BLOOFINZ cruises, bulk mesozooplankton biomass ($\mu\text{g C m}^{-3}$) were measured in multiple size classes (0.2-0.5, 0.5-1, 1-2, 2-5, > 5 mm) (Landry & Swalethorp, 2021). Measurements were made for each cycle during day and night hours; however, only daytime tows are considered here because larval ABT are visual feeders. A 1-m diameter ring net (0.2-mm mesh) was towed obliquely through the euphotic zone (100 m at C1, 135 m at C5), and

Table 3.2. Names and descriptions of variables included in the generalized additive model selection process and their data sources.

| Variable Name | Variable Definition | Data Sources |
|---------------------------------|--|---|
| <i>Dietary metrics</i> | | |
| Ingested prey | Sum of all prey in larval gut | |
| Ingested preferred prey | Sum of prey preferred by all larval sizes in gut (copepod nauplii and cladocerans) | Shiroza et al. (2021) |
| Ingested prey C | Sum of all prey carbon (C) weights in gut | |
| Ingested preferred prey C | Sum of preferred prey C weights in gut | |
| <i>Prey habitat</i> | | |
| Large Zooplankton Biomass (LZB) | Mesozooplankton biomass (0.2-1 mm, $\mu\text{g C m}^{-3}$) from upper 25 m | Field estimates Landry et al. (2021) |
| Large Prey Biomass (LPB) | Portion of LZB within larval-specific prey size range defined as a function of larval length SL (mm) | Field estimates Landry et al. (2021). SL from Shiroza et al. (2021) |
| Small Zooplankton Biomass (SZB) | Microzooplankton biomass (0.002-0.2 mm, $\mu\text{g C m}^{-3}$) estimated from measured LZB multiplied by the ratio of SZB to LZB estimated from a biogeochemical model | Field estimates and Shropshire et al. (2021) |
| Small Prey Biomass (SPB) | Portion of SZB within larval specific prey size range defined as a function of larval length SL (mm) | Field estimates and Shropshire et al. (2021). SL from Shiroza et al. (2021) |
| Food Limitation Index (FLI) | Ratio of metabolic requirement to assimilated ingestion, values >1 indicate prey-limited habitat | Field estimates and Shropshire et al. (2021) |
| <i>Abiotic variables</i> | | |
| Temperature | Temperature °C, 0-25m | |
| Salinity | Salinity psu, 0-25m | Gerard et al. (2022) |
| Fluorescence | Fluorescence v, 0-25m | |
| Cycle | 2 levels: C1, C5 | |

the cod end contents were size-fractionated through nested Nitex screens. Here, the mesozooplankton biomass was examined from 0.2 to 1 mm given the overlap with prey size range of aged larvae. A bongo-20 was towed in the upper 25 m of the water column with 0.05- and 0.2-mm meshes to record bulk biomass of smaller zooplankton, and to identify, count and measure prey in both nurseries (see Shiroza et al., 2021). Sampling with both net configurations provides measurements zooplankton biomass from 0.05 to 1 mm, which fully encompasses the planktivore prey fields for all aged larvae (see Table 3.4).

To provide an additional estimate of the small zooplankton biomass (SZB, 0.002-0.2 mm range), observed mesozooplankton biomass in the 0.2-1.0 mm range (herein referred to large zooplankton biomass, LZB) was adjusted to the top 25 m of the water column and scaled using the ratio of SZB to LZB estimated by a three-dimensional biogeochemical model NEMURO²-GoM (Shropshire et al., 2020). The NEMURO-GoM model was designed to simulate zooplankton biomass distribution in the GoM and has been extensively validated using remote and in situ measurements including over two decades of zooplankton biomass measurements collected by the Southeast Area Monitoring and Assessment Program (SEAMAP). The ratio of LZB to SZB was determined from daily climatologies generated by the model at each sample location and day of the year over the 20-y simulation (1993-2012). An advantage of the LZB and SZB was that they could be estimated for each ABT larval sampling location, as bulk zooplankton net tows did not accompany every larval net tow. For more information on NEMURO-GoM see Shropshire et al. (2020). Two additional variables were calculated from SZB and LZB that estimated the respective prey biomasses defined as a function of ABT-larval length for small prey biomass (SPB) and for large prey biomass (LPB), respectively (see Table 3.4).

Lastly, to evaluate prey availability, a Food Limitation Index (FLI, Shropshire et al., 2021) was computed for all aged larvae. The index is defined as the ratio of metabolic requirement to assimilated ingestion where values >1 indicate prey limitation. The ingestion formulation includes many terms but is primarily a function of sensory radius and prey biomass. Prey biomass is estimated using in situ LZB and estimated SZB along with estimates of prey size range as a function of larval length. Sensory radius is modeled as a function of prey size and larval length using a recently determined anatomical relationship for visual acuity (Hilder et al.,

² North Pacific Ecosystem Model for Understanding Regional Oceanography (Kishi et al., 2007)

2019). Metabolic requirement is estimated primarily as a function of larvae age and temperature. Specifically, metabolic requirement is derived from the first derivative of the age to weight relationship with assumptions regarding gross growth and assimilation efficiencies. In situ temperature values were obtained from the nearest sampling station for each cycle and are used to scale estimates of metabolic requirement. For more information on FLI formulations see Shropshire et al. (2021). Collectively, FLI values along with estimates of prey biomass and in situ measurements of mesozooplankton biomass are the metrics used to investigate drivers of differences in larval growth potential.

Data analysis and modeling approach

Data and statistical tests were carried out in R 4.0.3 (R Core Team, 2022). Least squares regressions were calculated for best fits of the following metrics to age: length, OR, body depth (mm), dry weight (mg), mean IW (μm), recent growth (μm), and residuals for age-at-length and OR at age. Analyses of covariance (ANCOVA) were carried out using age as a continuous covariate and log-transformed biometric variables when required to meet normality assumptions; overall growth was examined comparing the slopes between C1 and C5. Finally, recent growth between stages and cycles were analyzed in separate ANCOVAs with age as a continuous covariate to test for any significant interactions.

To test for differences in larval growth between C1 and C5, the otolith microstructure was analyzed for full growth trajectories with a linear mixed model using the nlme package (Pinheiro et al., 2014). Following the design outlined in Swalethorp et al. (2016) and Malanski et al. (2020), the model was fit to the data with otolith IW as the dependent variable and cycle as independent. Increment number was nested by individual larvae and included as a random effect, with cycle included as a fixed effect. The otolith growth trajectories were divided in two groups using 7 dph as a cutoff because this is when the IWs for C1 and C5 intersect. The random effects were applied to both model intercepts and slopes. To correct for autocorrelation and non-independence of the consecutive otolith IW measurements (Chambers & Miller, 1995, Campana, 1996), the model was refitted with an autocorrelation structure with increment number as the continuous time covariate using the corCAR1 function (Fox & Weisberg, 2015). Since larvae differed in number of growth increments (unbalanced design), the maximum likelihood was used to estimate slopes and model significance (Plant 2012).

The effect of variables (diet, prey availability, and temperature) on recent otolith IW was examined using generalized additive models (GAMs) with a Gaussian distribution. GAMs are non-parametric, generalized linear models with flexibility to handle both linear and complex relationships between the explanatory and response variables within the same environment (Wood 2004, 2017). All models were constructed using the *mgcv* library in R. Variables included in model selection are listed in Table 3.2. The model selected recent IW as the dependent variable for the subset of larvae ($n=139$) with all considered dietary metrics measured or estimated.

The dietary metrics considered are the abundance and corresponding carbon (C) mass of all ingested prey and of preferred ingested prey. Preferred prey are the sum of the two prey categories, copepod nauplii and podonids, most preferred across all larval sizes. Concurrent, zooplankton prey biomass (small and large), FLI, and hydrographic variables were also included.

To account for potential correlations between explanatory variables, correlations (Spearman's correlation matrix, $\rho > 0.6$) between all potential explanatory variables were identified and strongly correlated variables were modeled against the response in single-variable GAMs. The Akaike Information Criterion (AIC) (Akaike 1974) of the single-variable GAMs were compared between correlated variable pairs, and the variable with the lowest AIC was included in the final model selection process. After the set of non-correlated explanatory variables was identified, overall multi-collinearity was assessed using the variance inflation factor (VIF) with three as cutoff. Smoothing functions were applied to continuous predictor variables restricted to 4 knots to avoid overfitting.

To select a final model, the restricted maximum likelihood (REML) method was used as it applies a double penalty to smooth terms and allows for removal of variables with minor predictive values (Marra & Wood, 2011). Model diagnostics and residuals were checked for potential deviations from normality and homogeneity of variance.

RESULTS

In total, 30 and 38 bongo-90 tows were taken during cycles C1 and C5, and ABT larvae were aged from 18 and 20 stations, respectively (Figure 3.1). Aged larvae represented similar times during the peak month of the ABT spawning season in both years. Back-calculating spawning from observed ages indicates that adult ABT spawning events occurred between 24

April through 4 May 2017 for C1, and 29 April through 13 May 2018 for C5. Four larvae between 13 and 15 dph, one from C1 and 3 from C5, were found to be piscivorous, the first time that larval ABT piscivory has been established from direct observations.

The most salient difference between the two cycles was that larval abundances at C5 were almost 14 times higher than C1. Despite very narrow ranges, both temperature (24.19 – 25.95 °C at 25-m depth) and salinity (35.6 – 36.43 psu), differed significantly between cycles (Wilcox, $p < 0.001$), with C1 having slightly cooler and more saline conditions consistent with

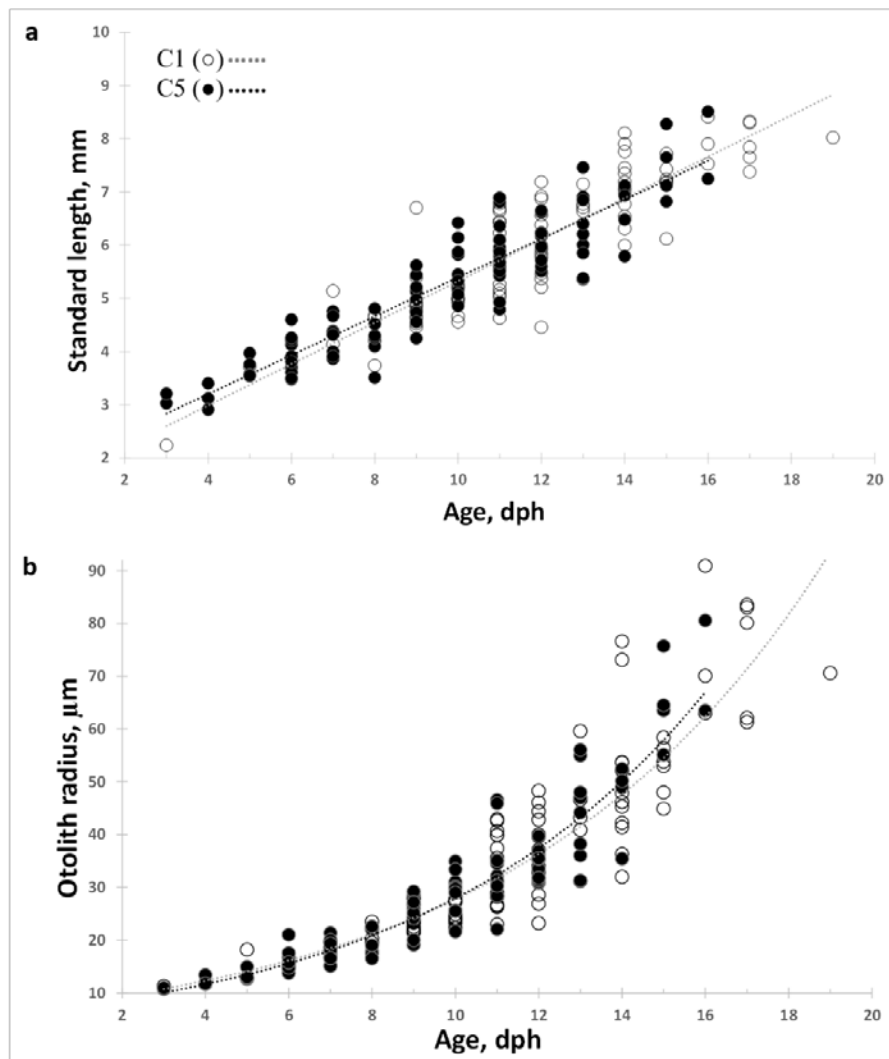


Figure 3.3. Least squares regressions for aged *Thunnus thynnus* larvae examined for a) body size (SL, mm) at-age, (days post hatch, dph), b) otolith radius (μm) at-age for cycle 1 (C1, \circ), and cycle 5 (C5, \bullet). Linear regressions are shown for C1 (\cdots) and C5 (\cdots) for length at-age $y_{C1} = 0.39x + 1.43$, $R^2 = 0.78$; $y_{C5} = 0.37x + 1.74$, $R^2 = 0.86$ and the exponential regression for OR at-age $y_{C1} = 7.19e^{0.14x}$, $R^2 = 0.83$, $y_{C5} = 6.52e^{0.15x}$, $R^2 = 0.91$, respectively.

an offshore environment. Fluorescence (also measured at 25-m depth) did not differ between sites (t-test = -2.921, df = 14.164, p = 0.995) although C1 had overall lower values (see abiotic variables in Table 3.4).

Shrinkage for freshly measured ABT larvae was measured for the first time and found to be $9.24\% \pm 3.5$ (average \pm SD) when preserved in 95% ethanol (Equation 1). This average includes larvae caught during both surveys, within C1 and C5 as well as outside the cycles to extend the fresh size range (2.45 – 9.64 mm SL) of larvae collected.

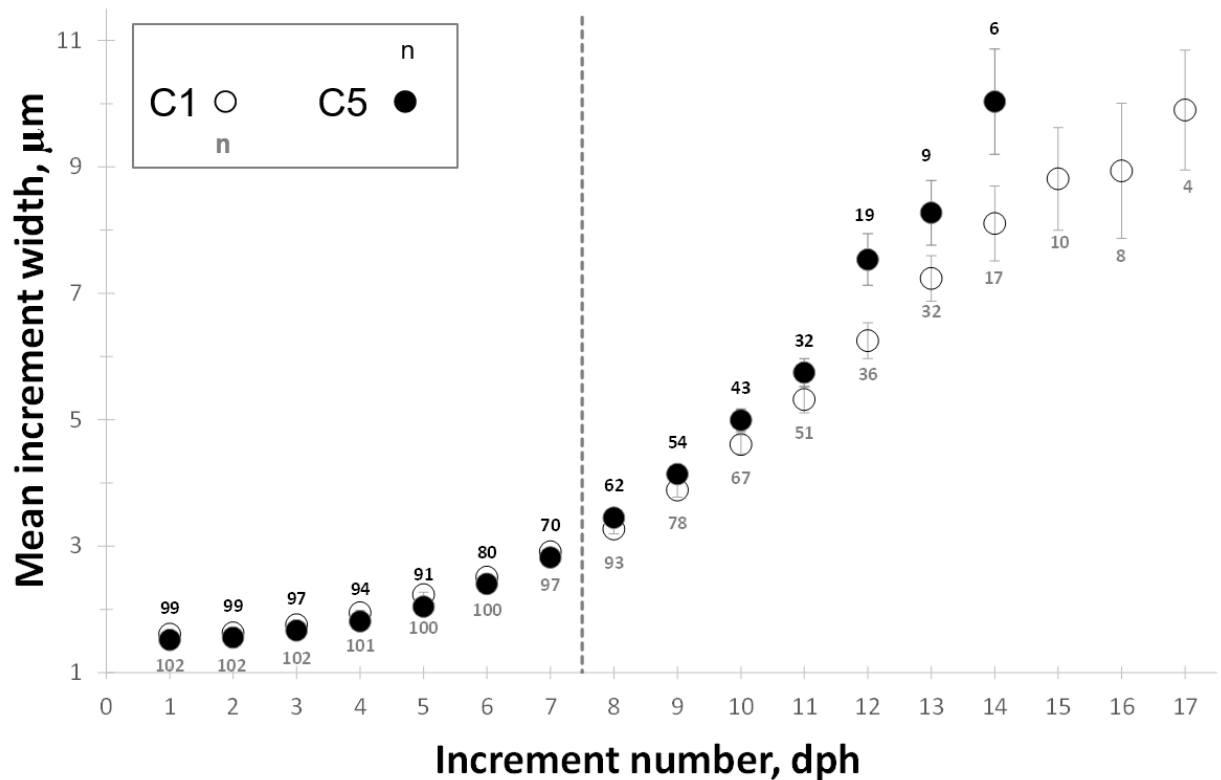


Figure 3.4. a) Mean increment width trajectories (μm) at increment number (days post hatch, dph) for *Thunnus thynnus* from cycles C1 (\circ) and C5 (\bullet). Error bars indicate standard error and are plotted when at least five larvae were included. The dashed vertical (---) line placed between 7 and 8 dph indicates a significant observed change in increment width (μm) between C1 and C5 larvae and roughly corresponds with onset of flexion.

Biometrics and growth

In total, 198 daytime ABT larvae were aged from both cycles, with a subset of 158 of the same larvae examined for stomach contents. For C1, the 98 aged larvae were 3 - 17 dph with one larvae at 19 dph. While for C1 and $3.84 \% \pm 4.47$ for C5. Four C5 larvae were excluded from further analysis because they did not meet ageing precision criteria ($CV > 10 \%$, from Chapter 2). Developmental stage distribution of the aged larvae were 20 preflexion, 30 flexion and 49 postflexion larvae for C1 and 32 preflexion, 30 flexion and 37 postflexion for C5 (Figure 3.2a, and 3.2b respectively). Preflexion larvae ranged from 3 to 10 dph (6.9 ± 2.0 dph). The youngest larva to reach flexion was 7 dph and the oldest flexion larva was 14 dph (10.2 ± 1.6 dph). Postflexion larvae were 9 dph and older (11.5 ± 1.0 dph).

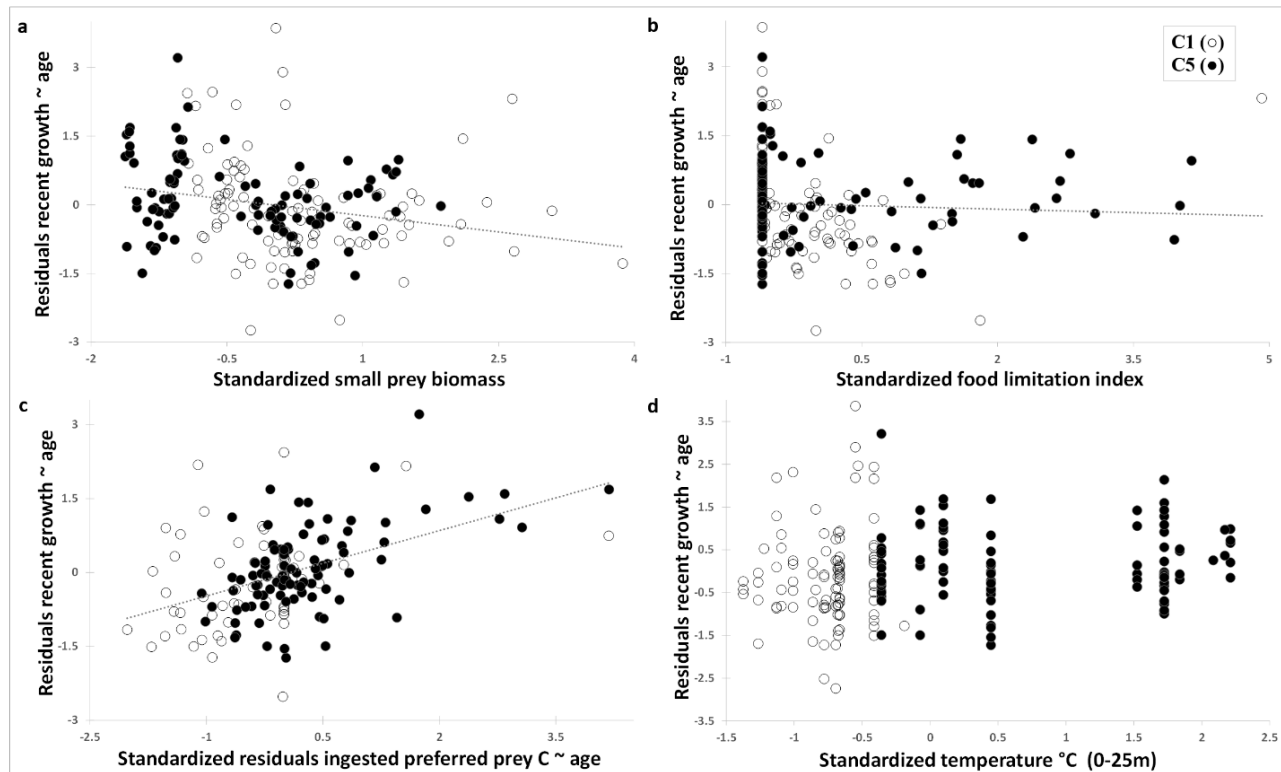


Figure 3.5. Least squares regressions for aged *Thunnus thynnus* larvae from cycles C1 (○) and C5 (●) examined for standardized residuals of recent otolith growth at-age (y-axis) and standardized a) small prey biomass, b) food limitation index (FLI), c) residual of ingested preferred prey carbon at-age, and d) temperature °C from 0 - 25 m.

Larval biometrics from the two cycles overlapped both with respect to length and otolith radius (OR, Figure 3.3a and 3.3b). There were no difference in mean larval somatic growth rates between C1 and C5 (0.358 vs 0.368 mm SL d⁻¹, Table 3.1). Body depth was measured only on undamaged larvae (n=157) and is reported here for western ABT larvae for the first time. On average, C1 larvae were slightly heavier, had greater body depth (Figure 3.6a, and 3.6b) and were older compared to C5; however, older C5 larvae (> 12 dph) were slightly heavier than C1 larvae of the same age. Least squares regressions for length relative to age and for OR-at-age residuals relative to length-at-age residuals did not differ between cycles (Figure 3.6c, Table 3.1), meaning that the body length relative to otolith growth patterns were consistent between C1 and C5 larvae, on average. Body depth, weight and OR-at-age all showed exponential relationships (Figure 3.3b, and 3.6) and had linear fits (significant positive slopes) when log-transformed (Table 3.1). Although C5 larvae appeared thinner compared to C1, neither body depth, weight or OR differed significantly between cycles for the larvae examined (Table 3.1).

Table 3.3 Generalized additive model statistics summary for recent increment width (IW, μm). The effect of the parametric coefficients on recent IW (top panel). The estimated significance levels of the smooth functions (lower panel); ΔDE is the loss in percent deviance explained caused by dropping the variable, “edf” is the estimated degrees of freedom for smoothing terms shown on lower panel. An asterisk (*) denotes statistical significance ($\alpha = 0.001$).

| Parametric coefficients | Estimate | Standard Error | p-value |
|--------------------------------|---|-----------------------|----------------|
| Intercept | -0.03 | 0.06 | 0.634 |
| Smooth Function | ΔDE (%) | Edf | p-value |
| Small prey biomass | 14.8 | 1.880 | <0.001* |
| Food limitation index | 13.4 | 2.390 | <0.001* |
| Ingested preferred prey C | 10.4 | 1.870 | <0.001* |
| Temperature | 4.3 | 1.658 | <0.020* |

Sagittal growth trajectories examined using a linear mixed model showed that average growth (assessed as IW) was significantly larger in early (1-7 dph) stage larvae for C1 compared to C5 (Figure 3.4, Table 3.1). Thereafter, the relationship shifted, with IW being significantly

larger in 8-15 dph larvae in C5. Similarly, recent IW (last three increments) also diverged around 7 dph (not shown).

Explained growth

The available biotic and abiotic variables were explored that could regulate growth using a GAM approach (Figure 3.8 a-d). Since IW was the only growth estimate found to differ between cycles (Table 3.1), and since differences in the possible explaining variables listed in Table 3.2 were generally greater between than within cycles, the GAM analysis was carried out using recent IW (average of the three most recent IWs). Recent IW-at-age was highly correlated to both length-at-age and body depth-at-age underlining its appropriateness as a historical and recent growth metric (Figure 3.7a and 3.7b). Because diet was an important variable, four larvae with damaged or empty guts were not included in this analysis. Consequently, diet and age were analyzed for 59 and 95 daytime-collected and aged larvae from C1 and C5, respectively.

The best model fit was achieved using the four variables: small prey biomass (SPB), FLI, ingested preferred prey C, and average temperature, which explained 44.3% of the recent IW variance (Figures 3.5, 3.8, and Table 3.3). The most important explaining variable was estimated SPB, which surprisingly decreased with increasing recent IW, suggesting that other size categories could be more important. Indeed, although estimated LPB fell out of the model, that was mainly because it was positively correlated to FLI ($r = -0.59$), which did a better job of explaining the residual recent IW variance. The second most important variable, FLI, indicated larval growth rate was sensitive to food limitation. In addition, ingested preferred prey C also explained a significant amount of the residual variance, showing that the larvae grew faster with more of the preferred prey ingested. Interestingly, the abundances of preferred prey ingested or as well as total ingested prey C and abundances did poorly at explaining recent IW variance. Although *in situ* temperature was also significant, the positive relationship to recent IW was weak in comparison to the other variables. Both fluorescence and salinity were correlated with temperature and fell out of the model.

Environmental cycle differences

Since greater zooplankton or prey biomass could not be directly linked to faster growth in the GAM *in situ* zooplankton availability was indirectly compared between the two cycles. The mesozooplankton biomass (sizes 0.05 – 1.0 mm) for C1 and C5 were not significantly different

Table 3.4. Daytime prey group biomass from cycles C1 and C5 collected using 0.055- and 0.2-mm mesh size plankton nets. Ring nets sampled 0-100 m during C1 and from 0-133 m during C5. Bongo-20 sampled from 0-25m. Bottom panel indicates mean values for temperature, salinity and relative fluorescence (volts) for the upper 25 m determined from CTD casts. Asterisk (*) indicates significant results at the 0.05 level for t-test; double asterisk (**) indicates Wilcoxon test.

| | Cycle | | Gear | Reference | t test | ρ |
|---|--|---------------------|--|---------------------------|--------|----------|
| <i>In situ</i> bulk zooplankton sizes (mm) | C1 | C5 | | | | |
| | $\mu\text{g C m}^{-3} \pm \text{SD}$ | | | | | |
| 0.05 - 0.2 | 643.77 \pm 156.0 | 421.85 \pm 137.26 | Bongo-20 (0.05 μm mesh), 0-25 m depth | In situ | 1.64 | 0.18 |
| 0.2 - 0.5 | 377.8 \pm 116.8 | 763.5 \pm 443.5 | Ring net (0.2-mm mesh), 0-100/135 m depth | Landry & Swalethorp, 2021 | -1.698 | 0.150 |
| 0.5 - 1.0 | 637.1 \pm 363.4 | 729.3 \pm 623.9 | | | -0.226 | 0.830 |
| <i>In situ</i> preferred taxa > 0.2 mm | $\mu\text{g C m}^{-3} \pm \text{SD}$ | | | | | |
| Copepod nauplii | 0.3 \pm 0.3 | 0.8 \pm 0.6 | Bongo-20 (0.2-mm mesh), 0-25 m depth | Shiroza, et al. (2021) | -1.326 | 0.242 |
| Cladocera | 1.3 \pm 1.9 | 48.5 \pm 19.5 | | | -4.083 | 0.01* |
| Calanoid | 127.7 \pm 30.4 | 376.9 \pm 92.8 | | | -4.386 | 0.007* |
| Appendicularia | 0.6 \pm 0.4 | 0.9 \pm 0.5 | | | -0.696 | 0.518 |
| Abiotic variables | Mean \pm SD | | | | | |
| Temperature, $^{\circ}\text{C}$ | 24.49 \pm 0.13 | 25.23 \pm 0.44 | CTD, 0-25m | Gerard, et al. (2022) | 1** | < 0.001* |
| Salinity, psu | 36.40 \pm 0.01 | 35.90 \pm 0.27 | | | 180** | < 0.001* |
| Fluorescence, volt | 0.07 \pm 0.002 | 0.07 \pm 0.002 | | Selph, et al. (2021) | 2.921 | 0.995 |

(Table 3.4). Overall, C5 had more mesozooplankton biomass in the 0.2 – 1.0 mm range, however C1 had a greater biomass of smaller mesozooplankton in the 0.05 -0.2 mm range. Since much of

this total biomass is not part of ABT larval diet, the in situ availability of specific taxa that Shiroza et al. (2021) identified as the preferred ABT larval prey were examined. C5 had consistently higher C biomass of the preferred taxa, podonids and calanoid copepods (Table 3.4).

Although most appendicularians and copepod nauplii may be too small to be efficiently caught by the 0.200 mm mesh sized net used, and did not differ significantly between cycles, C5 did contain more of them as well. In addition, the majority of C5 larvae (61%) experienced warmer temperatures ($> 25^{\circ}\text{C}$), which could also allow larvae to grow wider increments reflecting faster growth.

DISCUSSION

This study provides new information on the growth of ABT larvae in their GoM spawning grounds. By comparing two sites that differed in temperature and food availability, the conditions that were most important for regulating larval growth were identified. Furthermore, a newly proposed ABT larval food limitation index (FLI) was validated with field values. Below the findings are discussed in relation to environmental conditions and compared with other published studies.

ABT larval growth

All biometrics changed significantly as the larvae grew older, with larval length, body weight and OR all continuously increasing during the first 17 days of larval life. Body depth, also referred to as muscular height and, is reported here for the first time, increased exponentially during early life. These findings are consistent with other studies on the ontogenetic development of larval ABT (Malca et al., 2017, García et al., 2017, Hernandez et al., 2021). Small preflexion stage larvae were not well represented at C1 compared to C5 and could have affected the slope at the base end of the growth curves. Nonetheless, biometrics were not significantly different between the two nursery areas, indicating that surviving larvae from cycles C1 and C5 grew similarly on average for the size range examined. However, growth curves for the two cycles

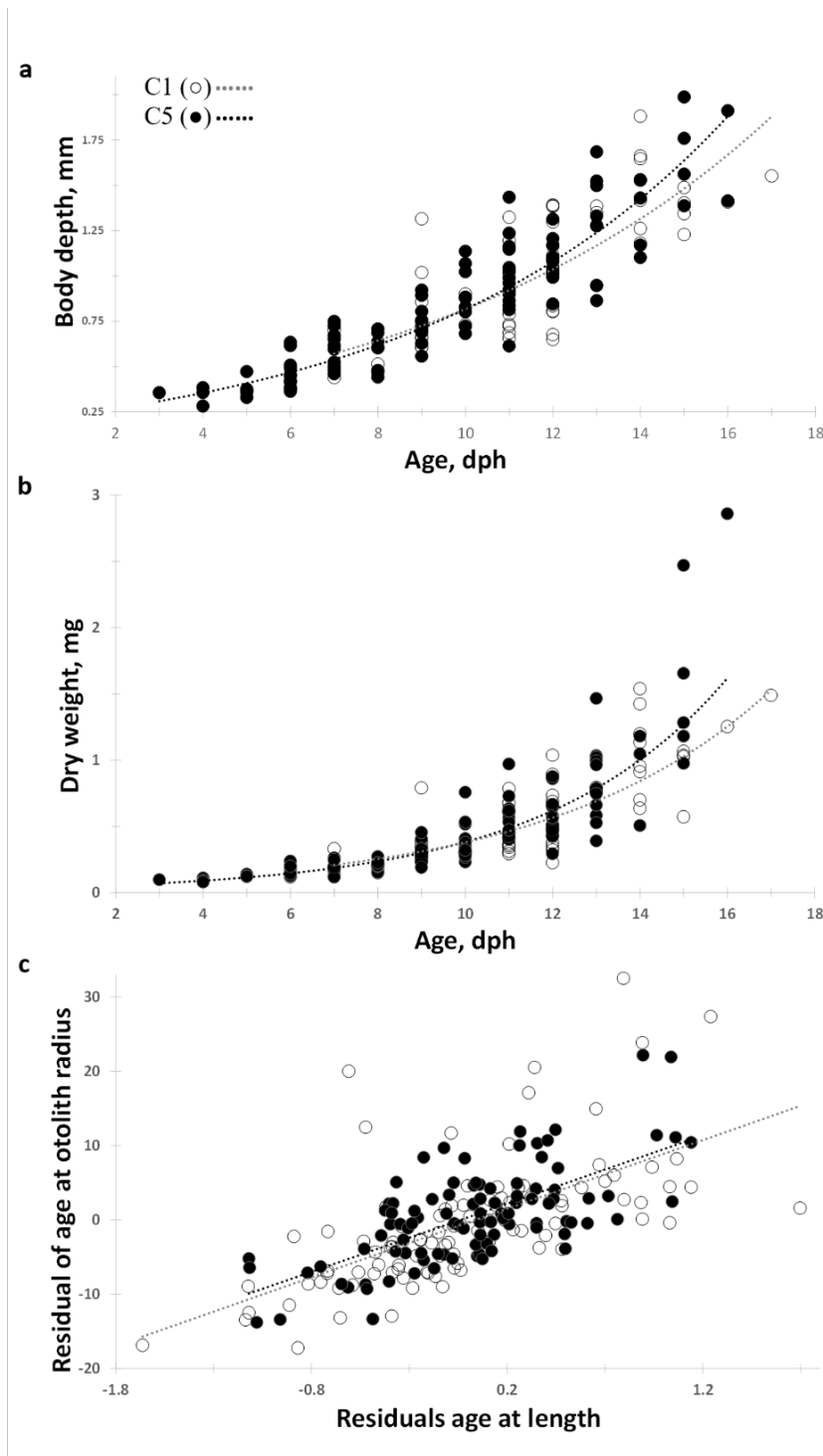


Figure 3.6. Least squares regressions for aged *Thunnus thynnus* larvae for a) body depth (mm) at-age and b) dry weight (mg) at-age and c) residuals of age-at-length vs residuals otolith radius at-age for C1 (○) and C5 (●) from NF1704 and NF1802. Weights were converted from length at weight relationships from Equation 2a and 2b. Exponential curves for C1 (····) and C5 (---) for age and depth were $y_{C1} = 0.26e^{0.12x}$, $R^2 = 0.66$, $y_{C5} = 0.21e^{0.14x}$, $R^2 = 0.85$ and for age at weight $y_{C1} = 0.04e^{0.22x}$, $R^2 = 0.77$, $y_{C5} = 0.04e^{0.23x}$, $R^2 = 0.86$. Linear regression for age-at-length residuals vs age-at-otolith residual $y_{C1} = 9.24x - 0.34$, $R^2 = 0.40$ and $y_{C5} = 9.17x + 0.34$, $R^2 = 0.45$

intersected between 8 and 14 dph, when larvae are in the flexion stage. Since larvae undergo substantial transformation in morphology, foraging capabilities and diet during flexion (Morote et al., 2008, Shiroza et al., 2021), this could indicate that conditions essential for preflexion and postflexion larval growth differed between the two nursery areas. Combining larvae from both cycles, the average growth rate of 0.37 mm SL d⁻¹ is somewhat lower than previously reported estimates from the GoM, although the ages reported here include individual dph corrections calculated for the first time. The dph corrections account for observed variability among larvae associated with estimating the missing increments between 7 μ m from the otolith core to the first observed increment. On average, 2.29 \pm 0.94 day were added to increment counts. Malca et al., (2017) reported larval growth rates of 0.46 mm SL d⁻¹ in larvae collected throughout the northern and eastern GoM in 2000-2012 based on raw increment counts alone. Despite this disparity, average growth rates (SL ~ dph) reported in this study are 18% lower than those in 2012 (0.55 vs 0.67 mm d⁻¹). The average growth rates reported in Malca et al. (2017) were corrected for dph by adding two days to increment counts. Compared to other ABT larval studies, these rates are slightly lower, but similar to those reported for other tuna species (0.3-0.51 mm d⁻¹, Jenkins & Davis, 1990, Lang et al., 1994, Tanaka et al., 2006, Zygias et al., 2015, Gleiber et al., 2020a, 2020b). The slower growth rates of GoM ABT larvae in 2017-2018 reflect a spatially restricted sampling effort spanning 3 days during daytime-collections. These short cycles likely included small subsets of all cohorts from the 2017 and 2018 spawning seasons. In Malca et al. (2017), larvae were aged from multiple water masses that included over 100 larvae aged from samples collected at temperatures > 27 °C. In contrast, the mixed-layer temperatures for C1 and C5 ranged from 24.1 to 25.9 °C.

Residual analysis of recent otolith IW-at-age, body depth-at-age and length-at-age revealed a high correlation among all three growth metrics. While it is generally assumed that otolith growth tracks somatic growth, this may not be the case for some species during certain developmental periods or under specific environmental conditions (e.g., Morales-Nin 2000, Swalethorp et al., 2016). Nevertheless, these results support the use of IW and recent IW for assessing the full history and recent growth differences in wild-caught ABT larvae. IW increased exponentially during the first 14 dph, but growth curves intersected between 7 and 8 dph for the two cycles, suggesting more favorable growth conditions for preflexion larvae during C1. Conversely, during the flexion and postflexion stage conditions were more favorable in the C5

nursery area. IWs were comparable to those reported by Malca et al. (2017) for the GoM in 2012 only during the first two days post hatch, after which they were much narrower. However, IWs were comparable to Balearic Sea ABT larvae during the first 11 days and then widened (García et al., 2013). Ontogenetic changes impact growth (Hare & Cowen, 1995), and should be

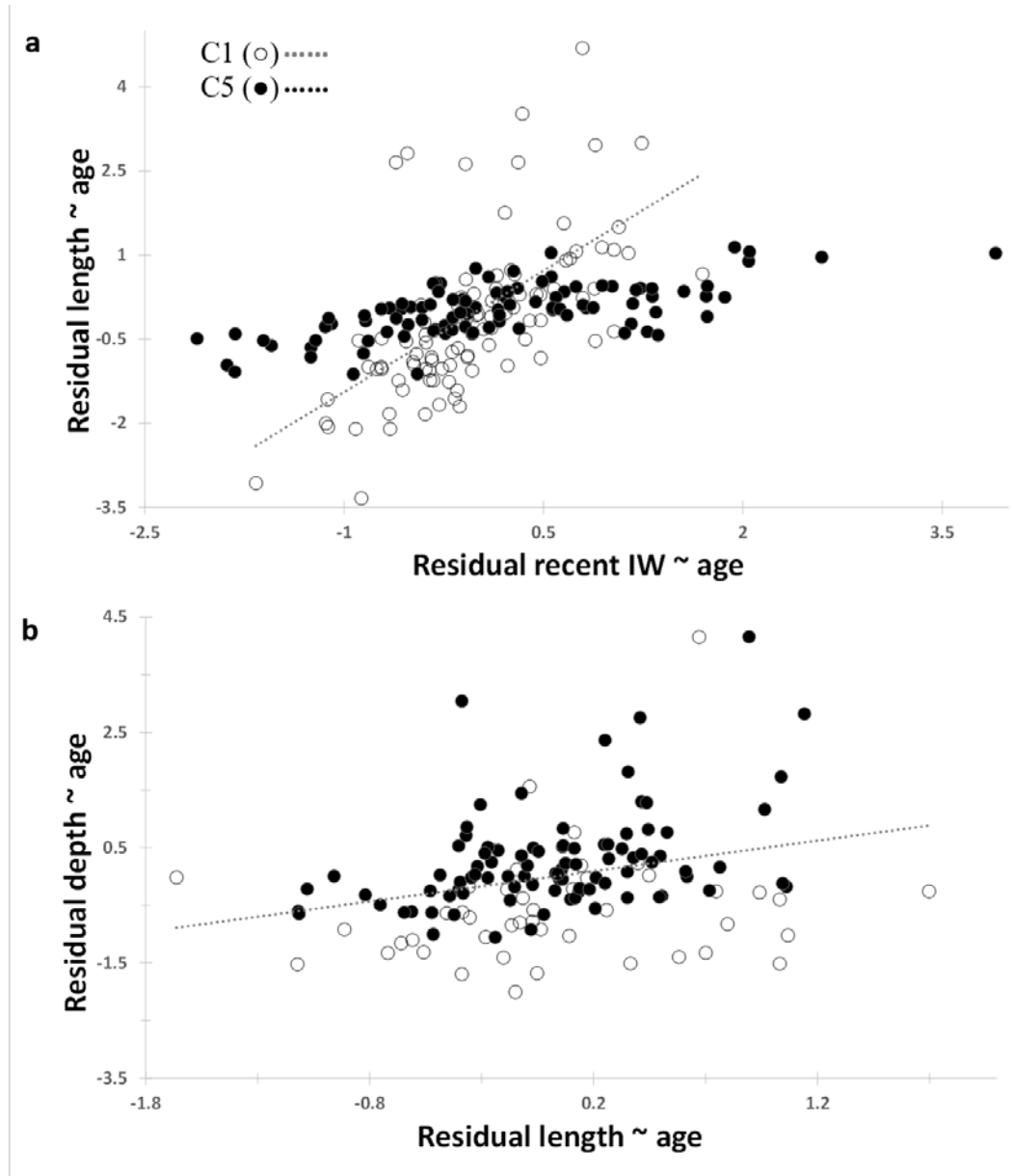


Figure 3.7. Least squares regressions for aged *Thunnus thynnus* larvae for recent increment width (μm) at-age residuals (x-axis) and a) body length at age residuals, b) body depth at-age residuals.

considered vital during otolith microstructure studies. It is possible that maternal investment could have differed between C1 in 2017, C5 in 2018 and other studies. Maternal investment has

the capacity to affect larval survival and growth later in life (Berkeley et al., 2004, Masuma 2009). Although a maternal effect has been proposed for growth of ABT larvae (Uriarte et al., 2016, Laiz-Carrión et al., 2019), it has not yet been established (Medina 2020).

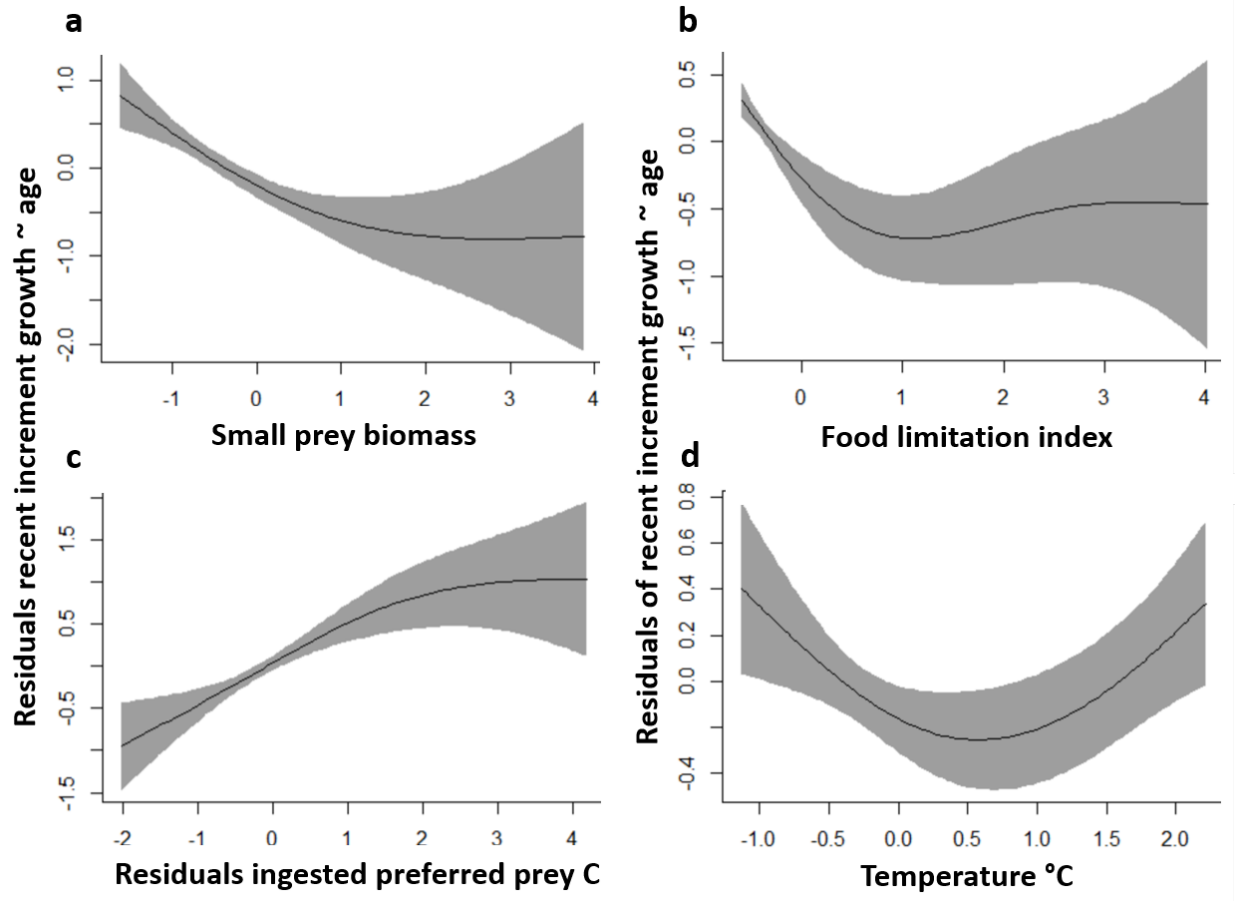


Figure 3.8. General additive model results for the individual additive effects of four smoothing terms on the standardized residual of otolith growth (3-day mean of recent otolith increment width, μm) (y-axis) for 139 *Thunnus thynnus* larvae from the Gulf of Mexico: a) small prey biomass b) food limitation index c) ingested preferred prey C representing biomass of copepod nauplii and cladocerans, and d) temperature $^{\circ}\text{C}$ (0- 25 m). All variables were standardized to zero mean and unit variance. Model AIC = 308.58 with 44.3 % of deviance explained. The grey-shaded areas indicate 95% confidence intervals.

Environmental drivers of growth

In addition to potential maternal effects, the availability of zooplankton prey is generally considered important for sustaining larval growth (Houde 1987, Houde 2008). For ABT larvae of a given size or developmental stage, prey need to be of a suitable size, catchability and

nutritional quality (Cushing 1990, Robert et al., 2013). Within the thermal range that ABT larvae are adapted, higher temperatures can support faster development if food is sufficient to support the increased metabolic and growth demand. The importance of these and other measured variables was tested using data and data products from C1 and C5 (Table 3.2). The GAM approach revealed that greater food limitation negatively impacted recent larval IW. The multivariate Food Limitation Index (FLI), which is indicative of sufficiency of zooplankton biomass of suitable larvae-specific size to support ingestion rates that satisfy metabolic requirements, (Shropshire et al., 2021) was determined for each individual larvae based on its size and location. Not surprisingly, it was among the best explanatory variables for larval growth, which supports its use in assessing ABT larval habitat quality (Shropshire et al., 2021). Interestingly, however, a direct positive relationship was not found between estimates of prey biomass availability and larval growth. SPB, which only considers the fraction of 0.002-0.2 mm zooplankton that falls within the prey size spectra of larvae (Shropshire et al., 2021), was negatively correlated with recent IW. This is surprising since much of the prey ingested by aged larvae in this study fell within this size range. The LPB, which considers the 0.2-1.0 mm fraction within the larval prey size spectra, fell out of the GAM model, but only because it was strongly and negatively correlated to FLI. Considering this, availability of larger-sized prey, such as other larval fishes, may be important in regulating growth. Some gut content studies either exclude size classes that may be piscivorous or remove larval fishes from diet contributions due to degradation and uncertainty of body length needed in carbon-length conversion factors (Gleiber et al., 2020b). This practice neglects evidence that fast-growing larvae such as ABT begin targeting other fishes as soon as opportunity and larval development align. The four piscivorous ABT larvae included in this study show that prey > 1mm are targeted. Although these precocious larvae had larval fishes in their guts, these were likely first time captures as the corresponding IW were within range of other larvae of the same age and size. Piscivorous larvae could have had larger recent IW had the prey in their guts been fully digested at time of capture.

It can be difficult to detect significant relationships between fish larval growth and bulk estimates of zooplankton available as prey (Robert et al., 2009, Swalethorp et al., 2016). One of the main issues is that fish larvae are nonrandom predators, feeding selectively on specific prey taxa and sizes available to them (Robert et al., 2009, Robert et al., 2013, Swalethorp et al., 2016, Shiroza et al., 2021). This study lacked robust *in situ* estimates of preferred prey taxa availability

covering the entire prey size spectra of the larvae to include in the GAM. Younger, smaller larvae feed extensively on prey not quantitatively sampled by a 0.2 mm mesh bongo net, and 0.05-0.2 mm samples for taxonomic analysis were only collected on C5. However, diet information on feeding success was expressed here as the amount of prey carbon each larvae had ingested. Using this information, ingestion of calanoid nauplii and Podonidae, the two most preferred prey taxa by developing larvae (Shiroza et al., 2021), was positively correlated to recent IW. Interestingly, only including ingested preferred taxa explained growth variability substantially better than when including all ingested prey. This is a significant finding as it highlights the importance of considering prey taxa and sizes that are positively selected by larval fish, not only bulk zooplankton, when assessing nursery habitat quality and its potential for supporting growth and survival.

Temperature was the weakest explanatory variable for larval growth, likely reflecting the narrow range of habitat temperatures sampled in this study, all well within the optimal range for ABT larvae (Muhling et al., 2010, Domingues et al., 2016). Even though temperature has been found to be a principal driver of larval growth (Satoh et al., 2013), if prey availability limits feeding success (i.e. ingested prey), it becomes more important (Swailethorp et al., 2016). The intersection of all growth curves between the two nursery areas coincided with the important transition of larval flexion suggested that C1 had better conditions to support preflexion larval growth, while C5 had better conditions for flexion and postflexion growth. As previously mentioned, this study lacked estimates of preferred prey taxa availability in the 0.05-0.2 mm fraction from C1. However, small zooplankton biomass was highest at C1 within this size range (Table 3.4), suggesting that more of the preferred copepod nauplii and small calanoid copepodites could have been available there. Preflexion larvae were also found to feed significantly on ciliates (Shiroza et al., 2021) and could have been feeding on other microplankton, which are hard to detect in stomach contents but can provide important feeding opportunities for first-feeding fish (Scura & Jerde, 1977, Overton et al., 2010). C1 had the highest concentrations of ciliates and large autotrophs, including dinoflagellates (Landry et al., 2021, Selph et al., 2021, Shiroza et al., 2021). Considering the more oligotrophic conditions at C1 compared to C5, which had a stronger connection to the nutrient and plankton rich northeastern shelf (Gerard et al., 2022), it is expected that plankton communities would be

shifted towards the smaller median sizes preferred by first-feeding larvae. However, C1 prey communities did not match the larval ontogenetic shift in prey preferences.

For flexion and postflexion larvae, C5 was significantly richer in the preferred larger Podonidae and calanoids. This richness explains why larvae at this developmental stage grew significantly faster at C5. It also further emphasizes the importance of advection of shelf zooplankton communities into ABT larval nurseries (Kelly et al., 2021, Landry & Swalethorp, 2021) to support faster larval growth and likely survival, since faster growing individuals are more adept at avoiding predators and less likely to starve (Tanaka et al., 2006, Watai et al., 2017).

CONCLUSION

The growth of larval ABT in the GoM and its environmental drivers were investigated in two developmental stages and compared with a contrasting nursery area that differed in prey availability. All growth biometrics examined increased as the larvae grew older, but their trajectories differed between areas. The principal drivers of this growth were related to food limitation/availability and feeding success. As a significant finding, the ingestion of preferred prey (Copepoda nauplii and Cladocera) better explained growth variability than total ingestion. While mean growth rates were similar, one nursery habitat appeared better suited to faster growth of preflexion stage larvae, while the other had faster growth of flexion and postflexion larvae due to greater availability of the preferred prey sizes and taxa of more developed larvae. These findings underline the importance in considering ontogenetic differences in preferred prey rather than bulk zooplankton biomass when assessing habitat quality, and that growth limitation can occur at different larval ages among nursery areas that vary in both the quantity and composition of food resources.

REFERENCES

- Akaike H. (1974) A new look at the statistical model identification. *IEEE Trans. Automat. Contr.*, 19, 716–723.
- Alvarez, I., Rasmuson, L. K., Gerard, T., Laiz-Carrión, R., Hidalgo, M., Lamkin, J. T., Malca, E., Ferra, C. et al. (2021) Influence of the seasonal thermocline on the vertical distribution of larval fish assemblages associated with Atlantic bluefin tuna spawning grounds. *Oceans*, 2, 64–83.
- Alvarez-Berastegui, D., Hidalgo, M., Tugores, M., Reglero, P., Aparicio-González, A., Ciannelli, L., Juza, M., Murre, B. et al. (2016) Pelagic seascape ecology for operational fisheries oceanography: modelling and predicting spawning distribution of Atlantic bluefin tuna in Western Mediterranean. *ICES J. Mar. Sci.*, 73, 1851–1862.
- Anonymous, (2019). Report of the standing committee on research and statistics (SCRS). ICCAT, Madrid, Spain.
https://www.iccat.int/Documents/Meetings/Docs/2019/REPORTS/2019_SCRS_ENG.pdf.
- Bakun, A. (2012) Ocean eddies, predator pits and bluefin tuna: implications of an inferred ‘low risk–limited payoff’ reproductive scheme of a (former) archetypical top predator. *Fish Fish.*, 14, 424–438.
- Begg, G., Campana, S., Fowler, A., Suthers, I. (2005). Otolith research and application: Current directions in innovation and implementation. *Mar. Freshwater Res.*, 56, 477–483.
- Bergenius, M. A. J., Meekan, M. G., Robertson, R. D. and McCormick, M. I. (2002) Larval growth predicts the recruitment success of a coral reef fish. *Oecologia*, 131, 521–525.
- Berkeley, S. A., Chapman, C., Sogard, S. M. (2004) Maternal age as a determinant of larval growth and survival in a marine fish, *Sebastes melanops*. *Ecology*, 85, 1258–1264.
- Block, B. A. (2019) The future of bluefin tunas: ecology, fisheries management, and conservation. John Hopkins University Press, Baltimore, MD, USA, 346 pp.
- Campana, S.E. (1996). Year-class strength and growth rate in young Atlantic cod (*Gadus morhua*). *Mar. Ecol. Prog. Ser.*, 135:21–26.
- Campana, S. E. and Jones, C. (1992) Measurement and interpretation of the microstructure of fish otoliths. In: Stevenson, D. K. and Campana, S. E. (eds) Otolith microstructure examination and analysis. *Can. Spec. Publ. Fish. Aquat. Sci.*, 117, 59–71.
- Catalán, I. A., Tejedor, A., Alemany, F. and Reglero, P. (2011) Trophic ecology of Atlantic bluefin tuna *Thunnus thynnus* larvae. *J. Fish Biol.*, 78, 1545–1560.
- Chambers, R.C., Miller, T.J. (1995) Evaluating fish growth by means of otolith increment analysis: special properties of individual-level longitudinal data. D.H. Secor J.M. Dean S.E.

- Campana (Eds) Recent Developments in Fish Otolith Research, University of South Carolina Press, pp. Columbia, 155–176.
- Chang, W. Y. B. (1982) A statistical method for evaluating the reproducibility of age determination. *Can. J. Fish. Aquat. Sci.*, 39, 1208–1210.
- Clemmesen, C. (1994) The effect of food availability, age or size on the RNA/DNA ratio of individually measured herring larvae: laboratory calibration. *Mar. Biol.*, 118, 377–382.
- Cushing, D. H. (1990) Plankton production and year-class strength in fish populations - an update of the match / mismatch hypothesis. *Adv. Mar. Biol.*, 26, 249-293.
- Domingues, R., Goni, G., Bringas, F., Muhling, B., Lindo-Atichati, D. and Walter, J. (2016) Variability of preferred environmental conditions for Atlantic bluefin tuna (*Thunnus thynnus*) larvae in the Gulf of Mexico during 1993–2011. *Fish. Oceanogr.*, 25, 320–336.
- Fromentin, J. M. and Powers, J. E. (2005) Atlantic bluefin tuna: population dynamics, ecology, fisheries and management. *Fish Fish.*, (6): 281–306.
- Foreman, T. (1996) Estimates of age and growth, and an assessment of ageing techniques, for northern bluefin tuna (*Thunnus thynnus*) in the Pacific Ocean. *Bull. IATTC*, 21:74.
- Fox J., Weisberg S. (2015) Mixed-effects models in R: an appendix to an R companion to applied regression, Vol 1. SAGE Publications, Thousand Oaks, CA.
- García, A., Cortés, D., Ramírez, T., Rifika, F., Alemany, F., Rodríguez, J. M., Carpena, A., Alvarez, J. P. (2006) First data on growth and nucleic acid and protein content of field-captured Mediterranean bluefin (*T. thynnus*) and albacore (*T. alalunga*) larvae: a comparative study. *Sci. Mar.*, 70, 67–78.
- García, A., Cortés, D., Quintanilla, J., Ramirez, T., Quintanilla, L., Rodríguez, J. M. and Alemany, F. (2013) Climate-induced environmental conditions influencing interannual variability of Mediterranean bluefin (*Thunnus thynnus*) larval growth. *Fish. Oceanogr.*, 22: 273–287.
- García, A., Laiz-Carrión, R., Uriarte, A., Quintanilla, J., Morote, E., Rodriguez, J., Alemany, F. (2017). Differentiated stable isotopes signatures between pre- and post-flexion larvae of Atlantic bluefin tuna (*Thunnus thynnus*) and of its associated tuna species of the Balearic Sea (NW Mediterranean). *Deep Sea Res., Part II*, 140: 18-24.
- Gerard, T., Lamkin, J. T., Kelly, T. B., Knapp, A. N., Laiz-Carrión, R., Malca, E., Selph, K. E., Shiroza, A. et al. (2022) Bluefin larvae in Oligotrophic Ocean Foodwebs, Investigations of Nutrients to Zooplankton: overview of the BLOOFINZ-Gulf of Mexico program. *J. Plankton Res.*, 44(5): 600-617.
- Gleiber, M. R., Sponaugle, S., Robinson, K. and Cowen, R. (2020a) Food web constraints on larval growth in subtropical coral reef and pelagic fishes. *Mar. Ecol. Prog. Ser.*, 650, 19–36.

- Gleiber, M.R., Sponaugle, S., Cowen, R. K. (2020b) Some like it hot, hungry tunas do not! Implications of temperature and plankton food web dynamics on growth and diet of tropical tuna larvae. *ICES J. Mar. Sci.*, 77 (7-8):3058–3073, <https://doi.org/10.1093/icesjms/fsaa201>.
- Ingram Jr., G.W., Alvarez-Berastegui, D., Reglero, P., Balbín, R., García, A. (2017) Incorporation of habitat information in the development of indices of larval bluefin tuna (*Thunnus thynnus*) in the Western Mediterranean Sea (2001–2005 and 2012–2013). *Deep Sea Res., Part II*, 140, 203-211. <https://doi.org/10.1016/j.dsr2.2017.03.012>.
- Ingram Jr., G. W., Richards, W. J., Lamkin, J. T. and Muhling, B. A. (2010) Annual indices of Atlantic bluefin tuna (*Thunnus thynnus*) larvae in the Gulf of Mexico developed using delta-lognormal and multivariate models. *Aquat. Living Resour.*, 23, 35-47.
- Hare, J. A., and Cowen, R. K. (1995). Effect of age, growth rate, and ontogeny on the otolith size–fish size relationship in bluefish, *Pomatomus saltatrix*, and the implications for back-calculation of size in fish early life history stages. *Can. J. Fish Aquat. Sci.*, 52, 1909–1232.
- Hernández, C. M., Richardson, D. E., Rypina, I. I., Chen, K., Marancik, K.E., Shulzitski, K., Llopiz, J.K. (2021) Support for the Slope Sea as a major spawning ground for Atlantic bluefin tuna: evidence from larval abundance, growth rates, and particle-tracking simulations. *Can. J. Fish Aquat. Sci.* <https://doi.org/10.1139/cjfas-2020-0444>.
- Hilder, P. E., Battaglione, S.C., Hart, N.S., Collin, S.P., Cobcroft, J.M. (2019) Retinal adaptations of southern bluefin tuna larvae: implications for culture. *Aquacult.*, 507, 222-232.
- Houde, E. D. (1987) Early life dynamics and recruitment variability. *Am. Fish. Soc. Symp.*, 2, 17-29.
- Houde, E. D. (2008) Emerging from Hjort’s shadow. *J. NW. Atl. Fish. Sci.*, 41, 53-70.
- Itoh, T., Shiina, Y., Tsuji, S., Endo, F., Tezuka, N., 2000. Otolith daily increment formation in laboratory reared larval and juvenile bluefin tuna *Thunnus thynnus*. *Fish. Sci.* 66, 834 -839.
- Jenkins, G. P. and Davis, T. L. O. (1990) Age, growth rate, and growth trajectory determined from otolith microstructure of southern bluefin tuna *Thunnus maccoyii* larvae. *Mar. Ecol. Prog. Ser.*, 63, 93-104.
- Jenkins, G. P., Young, J. W. and Davis, T. L. O. (1991) Density dependence of larval growth of a marine fish, the southern bluefin tuna, *Thunnus maccoyii*. *Can. J. Fish. Aquat. Sci.*, 48, 1358-1363.
- Kelly, T. B., Knapp, A. N., Landry, M. R., Selph, K. E., Shropshire, T. A., Thomas, R. and Stukel, M. R. (2021) Lateral advection supports nitrogen export in the oligotrophic open-ocean Gulf of Mexico. *Nature Comm.* 12: 3325, <https://doi.org/10.1038/s41467-021-23678-9>.

- Kimura, S., Kato, Y., Kitagawa, T. and Yamaoka N. (2010) Impacts of environmental variability and global warming scenario on Pacific bluefin tuna (*Thunnus orientalis*) spawning grounds and recruitment habitat. *Prog. Oceanogr.*, 86, 39–44.
- Kishi, M. J., Kashiwai, M., Ware, D. M., Megrey, B. a., Eslinger, D. L., Werner, F. E., et al. (2007) NEMURO-a lower trophic level model for the North Pacific marine ecosystem. *Ecol. Model.*, 202, 12–25, <https://doi.org/10.1016/j.ecolmodel.2006.08.021>.
- Laiz-Carrión, R., Gerard, T., Uriarte, A., Malca, E., Quintanilla, J.M., Muhling, B.A., Alemany, F., Privoznik, S. L. et al. (2015) Trophic ecology of Atlantic bluefin tuna (*Thunnus thynnus*) larvae from the Gulf of Mexico and NW Mediterranean spawning grounds: a comparative stable isotope study. *PLoS One*, 10(9):122, e0133406, doi:10.1371/journal.pone.0133406.
- Laiz-Carrión, R., Gerard, T., Suca, J.J., Malca, E., Uriarte, A., Quintanilla, J.M., Privoznik, S.L., Llopiz, J.K., et al. (2019) Stable isotope analysis indicates resource partitioning and trophic niche overlap in larvae of four tuna species in the Gulf of Mexico. *Mar. Ecol. Prog. Ser.*, 619:53-68. <https://doi.org/10.3354/meps12958>.
- Landry, M. R., Selph, K. E., Stukel, M. R., Swalethorp, R., Kelly, T. B., Beatty, J. L. and Quackenbush, C. R. (2021) Microbial food web dynamics in the oceanic Gulf of Mexico. *J. Plankton Res.*, 44(5): 638-655.
- Landry, M. R. and Swalethorp, R. (2021) Mesozooplankton biomass, grazing and trophic structure in the bluefin tuna spawning area of the oceanic Gulf of Mexico. *J. Plankton Res.*, 44(5): 677-691, doi:10.1093/plankt/fbab008.
- Lang, K.L., Grimes, C.B., Shaw, R.F. (1994) Variations in the age and growth of yellowfin tuna larvae, *Thunnus albacares*, collected about the Mississippi River plume. *Environ. Biol. Fish.*, 39, 259–270.
- Lindo-Atichati, D., Bringas, F., Goni, G., Muhling, B., Muller-Karger, F. E., Habtes, S. (2012) Varying mesoscale structures influence larval fish distribution in the northern Gulf of Mexico. *Mar. Ecol. Prog. Ser.*, 463: 245–257.
- Llopiz, J. K., Muhling, B. A. and Lamkin, J. T. (2015) Feeding dynamics of Atlantic bluefin tuna (*Thunnus thynnus*) larvae in the Gulf of Mexico. *Coll. Vol. Sci, Pap., ICCAT*, 71: 1710–1715.
- Malca, E., Muhling, B. A., Franks, J., García, A., Tilley, J., Gerard, T., Ingram, Jr., W. and Lamkin, J. T. (2017) The first larval age and growth curve for bluefin tuna (*Thunnus thynnus*) from the Gulf of Mexico: comparisons to the Straits of Florida, and the Balearic Sea (Mediterranean). *Fish. Res.*, 190, 24–33.
- Malanski, E., Munk, P., Swalethorp, R., Nielsen, G. T. (2020) Early life characteristics of capelin (*Mallotus villosus*) in the subarctic-arctic transition zone. *Estuar. Coast. Shelf Sci.*, 240: 106787.

- Marra, G., and Wood, S. N. (2011) Practical Variable Selection for Generalized Additive Models. *Comput. Stat. Data Anal.*, 55, 2372–2387.
- Masuma, S. (2009) Biology of Pacific bluefin tuna inferred from approaches in captivity. *Collect Vol. Sci. Pap. ICCAT*, 63, 207-229.
- McGruck, M.D. (1986). Natural mortality of marine pelagic fish eggs and larvae: role of spatial patchiness. *Mar. Ecol. Prog. Ser.*, 34: 227-242.
- Medina, A. (2020) Reproduction of Atlantic bluefin tuna. *Fish Fish.*, 21, 1109-1119.
- Morales-Nin, B. (2000) Review of the growth regulation processes of otolith daily increment formation. *Fish. Res.*, 46, 53-67.
- Morote, E., Olivar, M. P., Pankhurst, P. M., Villate, F. and Uriarte, I. (2008) Trophic ecology of bullet tuna *Auxis rochei* larvae and ontogeny of feeding-related organs. *Mar. Ecol. Prog. Ser.*, 353, 243-254.
- Muhling, B. A., Lamkin, J. T. and Roffer, M. A. (2010) Predicting the occurrence of Atlantic bluefin tuna (*Thunnus thynnus*) larvae in the northern Gulf of Mexico: building a classification model from archival data. *Fish. Oceanogr.*, 19, 526–539.
- Overton, J. L., Meyer, S., Støttrup, J. G., Peck, M. A. (2010) Role of heterotrophic protists in first feeding by cod (*Gadus morhua*) larvae. *Mar. Ecol. Prog. Ser.*, 410, 197-204.
- Pannella, G. (1971) Fish otoliths: daily growth layers and periodical patterns. *Science*, 173, 1124–1127.
- Pinheiro, J., Bates, D., DebRoy, S., Sarkar, D. and R Core Team. (2014) nlme: linear and nonlinear mixed effects models. <http://CRAN.R-project.org/package=nlme>.
- Plant, R.E. (2012) Spatial data analysis in ecology and agriculture using R. CRC Press Boca Raton, FL, pp. 684.
- Reglero, P., Balbín, R., Abascal, F. J., Medina, A., Alvarez-Berastegui, D., Rasmuson, L., Mourre, B., Saber, S., et al. (2019) Pelagic habitat and offspring survival in the eastern stock of Atlantic bluefin tuna. *ICES J. Mar. Sci.*, 76, 549–558.
- Richards, W. (2006) Early Stages of Atlantic Fishes: An Identification Guide for the Western Central North Atlantic. CRS Press, Boca Raton, FL, USA, 600 pp.
- R Core Team. 2022. R: A Language and Environment for Statistical Computing. R Foundation for Statistical Computing, Vienna, Austria. <https://www.R-project.org/>
- Robert, D., Castonguay, M., Fortier, L. (2007) Early growth and recruitment in Atlantic mackerel *Scomber scombrus*: discriminating the effects of fast growth and selection for fast growth. *Mar. Ecol. Prog. Ser.*, 337, 209–219.

- Robert, D., Castonguay, M., Fortier, L. (2009) Effects of preferred prey density and temperature on feeding success and recent growth in larval mackerel of the southern Gulf of St. Lawrence. *Mar. Ecol. Prog. Ser.*, 377, 227-237.
- Robert, D., Murphy, H. M., Jenkins, G. P., Fortier, L. (2013) Poor taxonomical knowledge of larval fish prey preference is impeding our ability to assess the existence of a “critical period” driving year-class strength. *ICES J. Mar. Sci.*, 71, 2042-2052.
- Rooker, J. R., Secor, D.H., De Metrio, G., Schloesser, R., Block, B.A., Neilson, J.D. (2008). Natal homing and connectivity in Atlantic bluefin tuna populations. *Science*, 322, 742-744.
- Satoh, K., Tanaka, Y., Masujima, M., Okazaki, M., Kato, Y., Shono, H. and Suzuki, K. (2013) Relationship between the growth and survival of larval Pacific bluefin tuna, *Thunnus orientalis*. *Mar. Biol.*, 160, 691–702.
- Scott, G. P., Turner, S. C., Grimes, C. B., Richards, W. J., Brothers, E. B. (1993) Indices of larval bluefin tuna, *Thunnus thynnus*, abundance in the GOM; modeling variability in growth, mortality, and gear selectivity. *Bull. Mar. Sci.*, 53, 912–929.
- Scura, E. D. and Jerde, C. W. (1977) Various species of phytoplankton as food for larval northern anchovy, *Engraulis mordax*, and relative nutritional value of dinoflagellates *Gymnodinium splendens* and *Gonyaulax polyedra*. *Fish. Bull.*, 75, 577-583.
- Selph, K. E., Swalethorp, R., Stukel, M. R., Kelly, T. B., Knapp, A. N., Fleming, K., Hernandez, T. and Landry, M. R. (2021) Phytoplankton community composition and biomass in the oligotrophic Gulf of Mexico. *J. Plankton Res.*, 44(5):618-637, <https://doi.org/10.1093/plankt/fbab006>
- Shiroza, A., Malca, E., Lamkin, J. T., Gerard, T., Landry, M. R., Stukel, M. R., Laiz-Carrión, R. and Swalethorp, R. (2021) Diet and prey selection of Atlantic Bluefin Tuna (*Thunnus thynnus*) larvae in spawning grounds of the Gulf of Mexico. *J. Plankton Res.*, 44(5): 728-746, doi:10.1093/plankt/fbab020.
- Shropshire, T. A., Morey, S. L., Chassignet, E. P., Bozec, A., Coles, V. J., Landry, M. R., Swalethorp, R., Zapfe, G. et al. (2020) Quantifying spatiotemporal variability in zooplankton dynamics in 759 the Gulf of Mexico with a physical-biogeochemical model. *Biogeosci. Discuss.*, 17, 760, 3385–3407.
- Shropshire, T. A., Morey, S. L., Chassignet, E.P., Karnauskas, Coles, V.J., Malca, E., Laiz-Carrión R., Fiksen, O., Reglero P., Shiroza, A., Quintanilla, J.M., Gerard T., Lamkin J.T., Stukel, M.R. (2021). Trade-offs between risks of predation and starvation in larvae make the shelf break an optimal spawning location for Atlantic bluefin tuna. *J. Plankton Res.*, 44(5): 782-798, doi.org/10.1093/plankt/fbab041.
- Shulzitski, K., Sponaugle, S., Hauff, M., Walter, K., Alessandro, E. K. and Cowen, R. K. (2015) Close encounters with eddies: oceanographic features increase growth of larval reef fishes during their journey to the reef. *Biol. Lett.*, 11, 20140746, doi:10.1098/rsbl.2014.0746.

- Swalethorp, R., Malanski, E., Dalgaard Agersted, M., Gissel Nielsen, T. and Munk, P. (2015) Structuring of zooplankton and fish larvae assemblages in a freshwater-influenced Greenlandic fjord: influence from hydrography and prey availability. *J. Plankton Res.*, 37: 102–119.
- Swalethorp, R., Nielsen, T. G., Thompson, A. R., Møhl, M. and Munk, P. (2016) Early life of an inshore population of West Greenlandic cod *Gadus morhua*: spatial and temporal aspects of growth and survival. *Mar. Ecol. Prog. Ser.*, 555: 185-202.
- Tanaka, Y., Satoh, K., Iwahashi, M., Yamada, H. (2006) Growth-dependent recruitment of Pacific bluefin tuna *Thunnus orientalis* in the northwestern Pacific Ocean. *Mar. Ecol. Prog. Ser.* 319, 225–235.
- Tilley, J. D., Butler, C. M., Suárez-Morales, E., Franks, J. S., Hoffmayer, E. R., Gibson, D., Comyns, B. H., Ingram, Jr., G. W. et al. (2016) Feeding ecology of larval Atlantic bluefin tuna, *Thunnus thynnus*, from the central Gulf of Mexico. *Bull. Mar. Sci.*, 92, 321–334.
- Uriarte, A., García, A., Ortega, A., De La Gándara, F., Quintanilla, J., Laiz-Carrión, R. (2016). Isotopic discrimination factors and nitrogen turnover rates in reared Atlantic bluefin tuna larvae (*Thunnus thynnus*): effects of maternal transmission. *Sci. Mar.*, 80: 447-456.
- Uriarte, A., Johnstone, C., Laiz-Carrión, R., García, A., Llopiz, J. K., Shiroza, A., Quintanilla, J. M., Lozano-Peral, D. et al. (2019) Evidence of density-dependent cannibalism in the diet of wild Atlantic bluefin tuna larvae (*Thunnus thynnus*) of the Balearic Sea (NW-Mediterranean). *Fish. Res.*, 212, 63-71.
- Watai, M., Ishihara, T., Abe, O., Ohshimo, S., Strussmann, C. A. (2017) Evaluation of growth-dependent survival during early stages of Pacific bluefin tuna using otolith microstructure analysis. *Mar. Freshwater Res.*, 68, 2008-2017.
- Wood, S. N. (2004). Stable and efficient multiple smoothing parameter estimation for generalized additive models. *J. Am. Stat. Assoc.*, 99(467).
- Wood, S. N. (2017). *Generalized Additive Models: An Introduction with R*, 2 edition. Chapman and Hall/CRC.
- Zygas, A.J., Malca, E., Gerard, T., Lamkin, J. T. (2015) Age-length relationship of larval skipjack tuna (*Katsuwonus pelamis*) in the Gulf of Mexico. *Col. Vol. Sci. Pap. ICCAT*. 186/2015, pp 8.

CHAPTER 4: Larval growth of Atlantic bluefin tuna in transient mesoscale oceanographic features of the Gulf of Mexico

INTRODUCTION

The mesoscale oceanography in the Gulf of Mexico (GoM) is determined mainly by Loop Current (LC) dynamics associated with intermittent anticyclonic rings that form after northward LC intrusions into the GoM (Bakun 2012, Johnston et al., 2019). Figure 4.1a illustrates the GoM's main circulatory features along with five mesoscale oceanographic features, regions, or conditions that influence the nursery areas of ABT: (1) anticyclonic region (AR), (2) anticyclonic boundary (AB), (3) cyclonic boundary (CB), (4) cyclonic region (CR), and (5) Common Water (CW).

Anticyclonic flow, lower chlorophyll, and warm Caribbean waters characterize the LC and the accompanying intrusions (Ward & Tunnell, 2017) into the GoM. These anticyclonic rings have downwelling centers, with divergent and upwelling boundary regions. Anticyclonic rings pinch-off, propagate westward, have a ~150 km radius, and can last from days up to a year (Elliott 1982, Forristall et al., 1992, Lindo-Atichati et al., 2012). In contrast, cyclonic eddies have opposite characteristics, with clockwise circulation, upwelling conditions, relatively enhanced nutrients in the center, and downwelling occurring at the boundary regions.

These mesoscale features introduce dynamic currents that interact throughout the GoM and enhance regional geostrophic energy. Variations in the nutrient composition between features affects the trophic cascade (Bakun 2012). Ultimately, upwelling associated with mesoscale features influences primary and secondary productivity. Convergent areas may concentrate prey and predators for larvae and juvenile fishes in the typically oligotrophic offshore GoM region (Ortner et al., 1978, Fratantoni et al., 1998, McGillicuddy et al., 1998, Shropshire et al., 2021).

ABT is a large pelagic species that undergo extensive migrations between foraging grounds in the North Atlantic towards spawning grounds in the GoM and Mediterranean Sea (Rooker et al., 2007). The International Commission for the Conservation of Atlantic Tunas (ICCAT) manages ABT as two separate stocks divided by the 45° west longitude. Multiple studies examining fishery-dependent catch, chemical (Rooker et al., 2008), tagging (Block et al., 2005, Hanke et al., 2019), and genetics (Johnstone et al., 2021, McDowell, et al., 2022) point to

the existence of two ABT stocks (with intermittent mixing reported by Díaz-Arce et al., 2022). The western stock spawns mainly in the GoM, while the eastern stock spawns in the Mediterranean Sea (Muhling et al., 2013). Recent management measures (Anonymous, 2015, 2019) have aimed to reduce widespread overfishing and there are signs of population increase in both the eastern and western Atlantic (Anonymous 2015).

Previous ABT ageing efforts for the western stock reported large variation among individual larval growth (Brothers et al., 1983, Malca et al., 2017, 2022). Larval somatic growth is evaluated by examining otolith microstructure patterns, growth trajectories, and increment width (IW, μm) (Jenkins & Davis, 1990, Swalethorp et al., 2016). The average between the last two or three increments before collection has been utilized to evaluate and model growth in the larval environment (Gleiber et al., 2020b, Malca et al., 2022) and larval growth indicate that this variation determines larval survival (Searcy & Sponaugle 2001, Tanaka et al., 2006, Perez & Munch, 2010). Larval bluefin tuna experience strong selection pressures and must outgrow the vulnerable larval stage in order to survive (Bakun 2012, Pepin et al., 2014). Growth-dependent survival has been documented for bluefin tunas (Jenkins et al., 1991, Watai et al., 2018) using otolith-derived age estimates. Despite decades of larval surveys, inter-annual variability and growth-dependent survival has not been documented rigorously for ABT.

Mesoscale circulation features have been proposed as critical nursery habitats for larval fishes, particularly for bluefin tuna larvae (Bakun 2006, 2012). Western larval ABT habitat has been characterized as warm (23-28 °C), low chlorophyll areas ($< 0.2 \text{ mg m}^{-3}$) in the upper ~20m of the water column (Muhling et al., 2013, Habtes et al., 2014, Alvarez et al., 2021) within a very limited spatiotemporal (April-June), and environmental envelope (Muhling et al., 2010, Habtes et al., 2014, Domingues et al., 2016). A decade ago, Lindo-Atichati et al. (2012) determined that between 1992-2008, larval ABT were most abundant first, in the boundaries of AB and second in CW features of the open Ocean-GoM (Figure 4.1a and 4.1b). Adult spawning behavior ostensibly places larvae in boundary regions (Bakun 2012), suggesting that there may exist specific survival advantages for ABT larvae associated with these habitats. Habitat modeling frameworks that included representative larval parameters have recently characterized ABT mortality and survival in the GoM (Shropshire et al., 2020b, 2021). Interestingly, this model predicted higher mortality in anticyclonic circulation features and slightly lower mortality for CW and cyclonic habitats (Shropshire et al., 2021). CW has been defined as neither cyclonic,

anticyclonic, nor shelf-region (Lindo-Atichati et al., 2012, Johnston et al., 2019). The links between early life history dynamics, the environment, and recruitment variability are largely unresolved despite significant advances in the understanding of ABT spawning habitat.

Larval and early juvenile ABT prey on small copepoda nauplii, calanoid copepods, podonids, and like most scombrids, rely heavily on appendicularians (Morote et al., 2008, Llopiz et al., 2010, Catalán et al., 2011, Tilley et al., 2016, Shiroza et al., 2021). Although high displacement volumes of plankton in the frontal areas of the anticyclonic LC suggest that prey availability may provide opportunities for enhanced feeding and growth (Richards et al., 1989, 1993), size-selective preferences are essential to avoid starvation in the youngest larvae, while predation avoidance is key for older larvae (Shropshire et al., 2021). Gut content and ambient microzooplankton comparisons revealed that larval ABT can be highly selective (Shiroza et al., 2021) and may modify their feeding behavior accordingly. The same ABT larvae with preferred prey in their guts also grew faster than larvae with suboptimal prey (Malca et al., 2022).

In this study, larval ABT growth curves were developed and inter-annual variability between cohorts was assessed. Second, feature-specific growth curves were developed to compare inter-feature growth and examine size-specific growth between the youngest vs. oldest larvae. The goal was to ascertain whether these entrained larvae experience the benefit of increased growth in specific mesoscale features. Lastly, gut contents were examined from the 2016 aged ABT larvae to explore feeding dynamics within mesoscale features.

METHODS

Multi-year survey and larval collections

Larval ABT were collected during three NOAA Southeast Area Monitoring and Assessment Program (SEAMAP) Spring Plankton surveys in the northern GoM during the peak of the spawning seasons for western ABT. Since 1982, the Spring SEAMAP Plankton surveys have occupied a systematic grid (~30 nm apart) targeting the early life stages of ABT to assess distribution, occurrence, and abundance in the GOM. All surveys were conducted aboard the NOAA Ship *Oregon II*, with survey numbers OR312, OR317, and OR322 from 2015, 2016, and 2017, respectively (each year will reference each dataset henceforth). All surveys conducted 24-h operations to cover the extent of potential spawning grounds in the northern GoM. Since 1982,

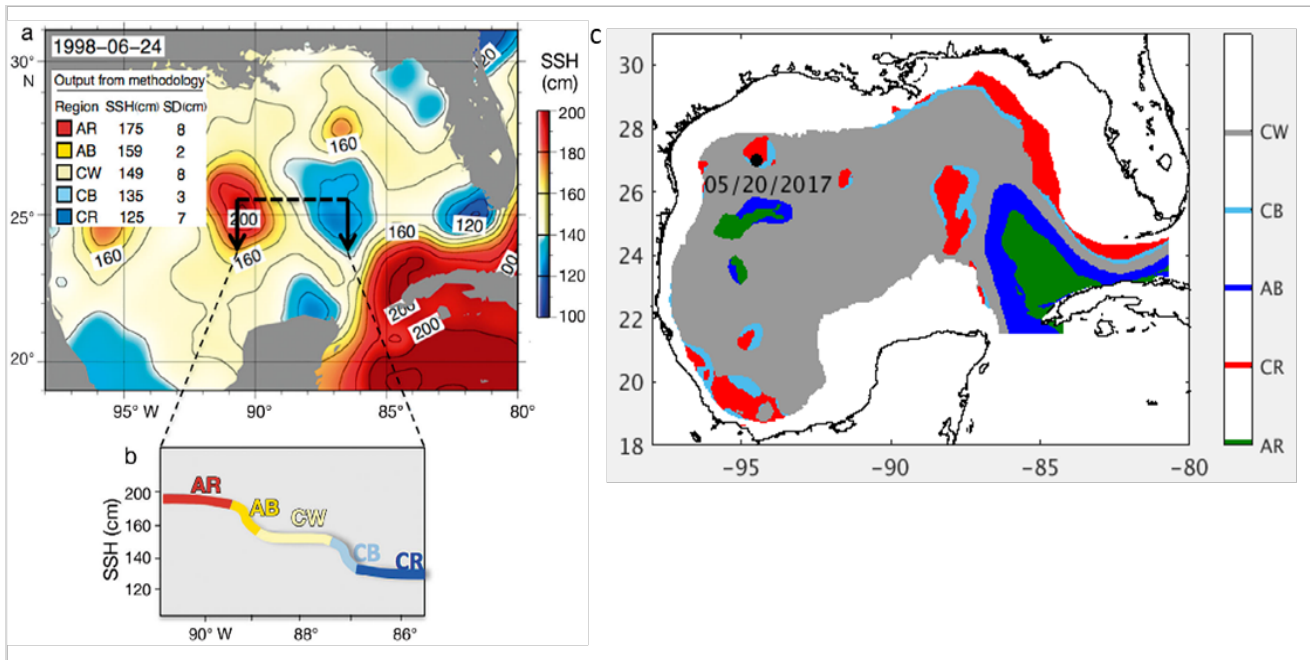


Figure 4.1. Schematic representation of the mesoscale features types in the Gulf of Mexico from Lindo-Atichati et al. (2012). a) Mean sea surface height (SSH, cm) values for mesoscale features and b) corresponding SSH (cm) for longitudes (~91°- 85°W). c) Collection location for one *Thunnus thynnus* larva (●) from CR on 20 May 2017. Feature types are shown for (1) anticyclonic region (AR), (2) anticyclonic boundary (AB), (3) cyclonic boundary (CB), (4) cyclonic region (CR), and (5) Common Water (CW). The majority of the open GoM > 200 m depth was classified as CW (grey). Image from panel b provided by Taylor Shropshire, and is used with permission.

the Spring Plankton surveys have occupied a systematic grid (~30 nm apart) to assess the distribution, occurrence, and abundance of the early life stages of ABT.

During each survey, a 61-cm bongo frame fitted with 0.335-mm mesh nets (B61 hereafter), and a 1 × 2 m neuston (NN hereafter) frame fitted with a 0.950-mm mesh net were towed at each station. Starting in 2009, subsurface gear was added, fitted with 0.505-mm mesh nets towed for ~10 min from the sea surface to 10 m depth. A SBE19 SEACAT profiler above the frames monitored depth in real time. In 2016, the subsurface gear was a 1 × 2 m neuston frame (S10 hereafter). While in 2016 and 2017, the 61-cm bongo was used as the subsurface gear (SB61 hereafter), see Table 4.1. The B61, S10, and SB61 nets had flowmeters (General Oceanics, Inc.) attached at the center of each net to record volume filtered (m^3) to standardize ABT catches into larval abundances ($ind. 1000^{-1} m^{-3}$). Plankton samples were preserved in 95% ethanol, which was replaced within 24 h. At each station, a CTD (SBE 9plus, Sea-Bird Scientific) recorded vertical profiles of temperature ($^{\circ}C$) and salinity (psu), Table 4.1. CTD casts were processed (SBE Data Processing, Sea- Bird Scientific) and were binned to 1-m depth

intervals (see Millet et al., 2015, 2016, and 2017 for additional survey methods). Contours of sea surface temperature and salinity were constructed in Surfer 9 (Golden Software, Inc., Golden Co), using the kriging method of interpolation (Figure 4.2).

SEAMAP plankton samples were processed at the Polish Sorting Center (Morski Instytut Rybacki (MIR) - Zakład Sortowania i Oznaczania Planktonu (ZSIOP). Protocols require larval scombrids identified to the lowest taxonomic level possible using morphological characteristics. *Katsuwonus pelamis* and ABT have diagnostic pigmentation and morphological characteristics that are sufficient for visual identifications (Richards 2005). Larval blackfin (*Thunnus atlanticus*) and yellowfin (*T. albacares*) tuna are difficult to identify to species level, therefore blackfin and yellowfin tuna were combined as *Thunnus* spp. Prior to ABT larval handling for subsequent analyses, larval identification was confirmed by another senior taxonomist.

Mesoscale feature types and ageing

Mesoscale feature types were determined for the positive ABT stations during the three larval surveys (2015, 2016, and 2017) following Domingues et al. (2016). This study utilized the same code that Domingues et al. (2016) used in their feature assignments to assign a location of interest (latitude, longitude, and date) to a mesoscale feature. Domingues et al. (2016) utilized a dynamic criteria that included geostrophic velocity and SSH from the ~4 km HYbrid Coordinate Ocean Model (HYCOM) daily output “expt_32.5,” (www.hycom.org, Chassignet et al., 2007). Mesoscale feature type designations were overlain with larval ABT distribution and abundance for each year. Station coordinates and day of year were assigned to five potential mesoscale feature types: (1) anticyclonic region (AR), (2) anticyclonic boundary (AB), (3) cyclonic boundary (CB), (4) cyclonic region (CR), and (5) Common Water (CW).

A subset of larvae within the range of larval size distribution during each cruise was selected for ageing. Larvae were first identified to three developmental stages (preflexion, flexion, and postflexion) following Richards (2006). Each larva was measured for body size (body length, mm hereafter). Specifically, ABT were measured from the snout tip to the tip of the notochord for reflexion larvae, to notochord flexion, and postflexion stages were measured to base of the caudal peduncle. Larval measurements were conducted using a dissecting microscope (Leica M205C, Leica Microsystems) fitted with a digital camera (Leica EC3, Leica Microsystems) and image analysis software (Leica Application Suite 4.3, Leica Microsystems).

Table 4.1. Summary of plankton gear sampled in 2015, 2016, and 2017. Stations with positive catches / total tows are shown. Larval *Thunnus thynnus* (ABT) aged and the gear that it was collected from is shown. Mean Scombridae densities (ind. 1000⁻³m⁻³) ± SD for ABT, *Thunnus* spp., and *Katsuwonus pelamis* for each year. Mean temperature, salinity, and fluorescence is shown.

| | All | 2015 | 2016 | 2017 |
|---|---------------------|--|---------------------|---------------------|
| Plankton nets | | Stations with positive ABT/ no. of tows | | |
| Gear | B61 | 21/108 | 36/86 | 22/88 |
| | SB61 | - | 50/92 | 12/76 |
| | NN* | 17/103 | 36/62 | 11/68 |
| | S10 | 34/93 | - | - |
| Gear (ABT aged) | 319 | B61 (8) | B61 (31) | NN (2) |
| | | <u>S10 (97)</u> | <u>SB61 (111)</u> | <u>SB61 (38)</u> |
| | | 105 | 142 | 72 |
| Tuna abundances (ind. 1000 m⁻³) | | Mean ± SD | | |
| <i>Thunnus thynnus</i> | 8.20 ± 31.12 | 4.72 ± 23.13 | 18.32 ± 60.8 | 2.94 ± 10.14 |
| <i>Thunnus</i> spp. | 7.65 ± 21.75 | 9.95 ± 28.28 | 6.7 ± 12.78 | 5.56 ± 19.23 |
| <i>Katsuwonus pelamis</i> | 3.25 ± 12.59 | 2.51 ± 5.4 | 5.51 ± 21.42 | 2.05 ± 5.31 |
| Environmental parameters | Mean (range) | Mean | | |
| Temperature, °C | 26.36 (23 - 28.43) | 26.73 | 26.46 | 25.75 |
| Salinity, psu | 35.8 (28 - 36.6) | 35.77 | 35.64 | 36.05 |

Otolith analyses

Sagittal otoliths were selected for ageing because they are the largest and have been previously aged for ABT. Otoliths were examined at 1000× in immersion oil (transmitted light) with a compound microscope (A.1, Zeiss Microscopy), a digital camera, and with calibrated image analysis software (Image Pro Plus 7, Media Cybernetics). Daily increments were measured twice along the longest axis or the otolith radius (OR, μm) by an experienced reader. Marginal (incomplete) increments were not included in further analysis and an increment was considered marginal if the last increment was thinner than the penultimate increment. Three days were added to final increment counts following Chapter 2's age-adjustment analysis. Hereafter,

age refers to days post hatch (dph) which coincides with onset of exogenous feeding and has been estimated from otolith microstructure (Brothers et al., 1983, Malca et al., 2022). The precision between the two reads was evaluated using the coefficient of variation (CV, Chang 1982) after adjusting increment counts for age. Instantaneous growth rates (mm dph^{-1}) were calculated by dividing body length by dph. Mean increment width (IW, μm) was the average of all increments while excluding incomplete increments. Recent otolith growth (μm) was calculated from the average of the last two completed increments, which has been shown to characterize larval conditions prior to collection (Clemmensen 1994, Shulzitski et al., 2015, Malca et al., 2022). Larvae with less than two complete increments were excluded from further analyses.

Otolith trajectories were analyzed by comparing the respective otolith microstructure patterns (mean increment growth at-age and recent growth-at age) for younger (1-8 daily increments) vs. older larvae (+12 increments) between years and feature type for the first six increments (9 dph). Daily increment growth (μm) trajectories were calculated only for samples with more than ten observations and were compared regarding increment number to avoid any uncertainty with age-adjustments.

Larval ABT diet

Larval guts were examined for a subset of the aged 2016 ABT from daytime sampling only because tunas are visual predators that feed mainly during daytime (Llopiz & Cowen, 2009, Llopiz et al., 2010). A representative distribution of body lengths was examined and gut content analysis followed Shiroza et al. (2021). The alimentary canal from esophagus to anus was removed using forceps and a scalpel. Then, the digestive tract was carefully opened using insect pins, and its contents were isolated following Govoni et al. (1968) and Llopiz et al. (2010). Distinguishing features of ingested prey were often degraded due to digestion and compaction, thus identifications were conducted to the lowest possible taxonomic level. Prey type per taxon was tallied and feeding incidence was calculated as the proportion of larvae with prey present inside the gut. Five larvae with empty guts were excluded from all other analyses and prey was measured to the nearest 0.1 mm.

Statistical analysis

Data explorations and statistical tests were carried out in R 4.0.3 (R Core Team, 2022). Least squares regressions were calculated for best fits of somatic and otolith metrics (body length, OR, and otolith IW) and for the residuals of length-at-age vs. residuals of OR-at-age. Analyses of covariance (ANCOVA) were conducted using age as a continuous covariate and log-transformations for biometric (e.g., OR, recent growth) variables were used as needed to meet normality requirements. Growth was also evaluated by comparing the slope (mm day^{-1}) of the linear least squares regressions between years and between mesoscale feature types.

Recent otolith growth was the otolith metric selected to examine potential environmental effects on larval growth. Log-transformed recent otolith growth was regressed on larval length (recent growth-at-age) using least squares regressions between years, and feature types in separate ANCOVAs, with age as a continuous covariate. For larval growth and mesoscale feature type analyses, only CW and CR were compared in 2015 and 2016 because in 2017, only the CW feature type was sampled. Environmental parameters (SST, SSS) along with ABT abundance 1000^{-1} m^{-3} were also examined to assess ambient influences on larval growth, or density-dependent growth during the three years.

RESULTS

Survey and larval collections

During each larval survey, some stations in the SEAMAP grid were not completed due to mechanical issues (e.g., ship repairs, gear and or equipment malfunction), or due to weather-related difficulties. Although the number of net tows and gear type varied, the majority of the SEAMAP grid was sampled yearly. During the most affected survey (2017), nine stations were cancelled. Nonetheless, during the three years combined, over 2000 ABT larvae were collected under relatively ordinary sampling conditions for this type of fisheries oceanographic surveys (Table 4.1). Among the gear utilized, the most successful gears at catching ABT larvae were the 'subsurface' gears (SB61 and S10). Stations positive for ABT catches ranged from 15% to 58% net tow⁻¹ and larval ABT catches (and abundance) was significantly different ($p < 0.05$, Wilcoxon) between years.

The 2016 survey collected the most larvae (18.3 ind. 1000^{-1} m^{-3}), followed by the 2015 survey (4.72 ind. 1000^{-1} m^{-3}), with the 2017 survey having the lowest catches (2.94 ind. 1000^{-1} m^{-3}). Interestingly, ABT abundances between the 2016 and 2017 survey did not differ ($p > 0.05$, Wilcoxon) (Figure 4.2). The NN gear is not included in previous abundances because it lacked a flowmeter however, positive ABT catches were on average ~30% from the NN gear. Larval ABT abundances (1000^{-1} m^{-3}) were highest from CW and CR feature types in most years followed by CB feature type. The lowest ABT abundances were from AR, followed by AB.

During the SEAMAP surveys, other larval tunas (e.g., *Auxis* spp., *Euthynnus alletteratus*, *Scomber colias*, and *Scomberomorus* spp.) were also collected. However, only *Thunnus* spp. and *K. pelamis* were consistently found to co-occur with ABT larvae (Table 4.1). Relative to ABT abundances, *Thunnus* spp. were at least twice as abundant in 2015 and 2016. However, in 2017, ABT dominated the *Thunnus* assemblages. *Thunnus* spp., *K. pelamis* and ABT co-occurred only 13% in 81 net tows while *K. pelamis* co-occurred with ABT only in 17% of all net tows.

Abiotic conditions

Environmental conditions were significantly different with respect to SST between years ($p < 0.05$, Wilcoxon), with SST differing by ~ 5 °C within surveys. The 2017 survey had cooler and more saline conditions (e.g., almost -1 °C) than 2015 and 2016 (Table 4.1). While SSS did not differ between 2015 and 2016 ($p > 0.05$, Wilcoxon), it significantly differed ($p < 0.05$, Wilcoxon) between 2015 and 2017, and between 2016 and 2017.

The environment within the mesoscale feature types was variable among the three SEAMAP surveys in 2015, 2016, and 2017 (Figure 4.2). Within each survey, anticyclonic features (AB and AR) had warmer SST (~ +1 °C) and higher SSS, while cyclonic eddies (CB and CR) had cooler temperatures (~ -1 to -3 °C) with intermediate SSS. CW had intermediate SST but had the lowest SSS. Finally, SST and SSS were significantly different (ANCOVA, $p < 0.05$) between years for both age-at-length and recent growth-at-age comparisons. Posthoc comparisons for SST indicated that 2015 and 2016 had a positive increase of growth (age-at-length and recent growth-at-age) with SST while in 2017 this was not detected. Posthoc comparisons for SSS indicated that only 2015 had a positive increase on growth, but only for recent growth-at-age.

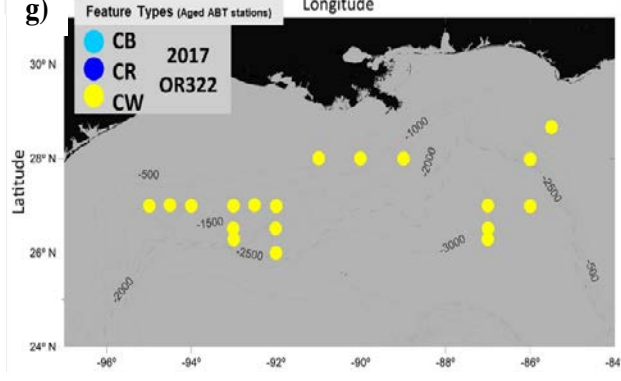
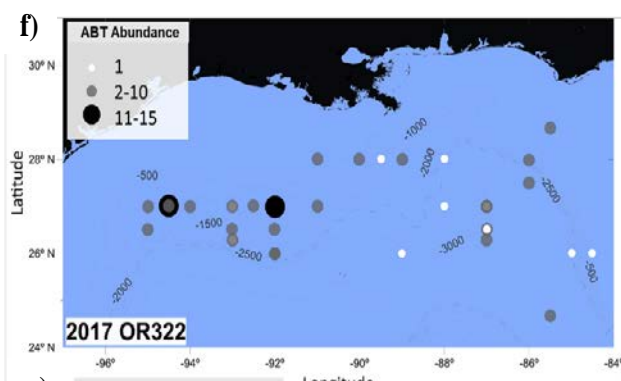
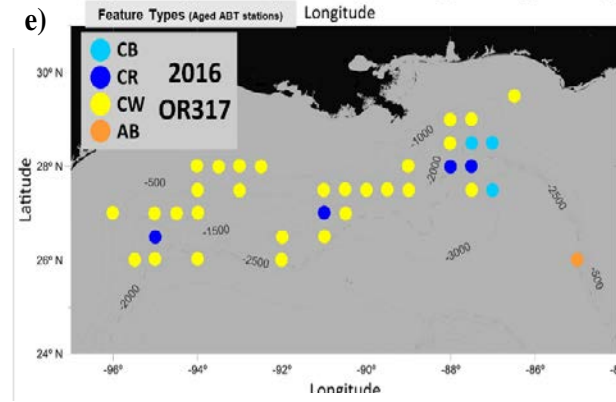
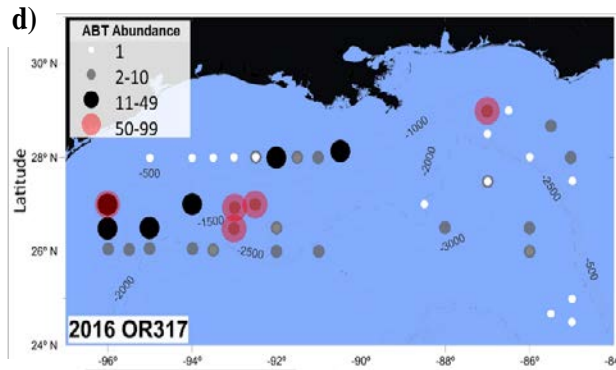
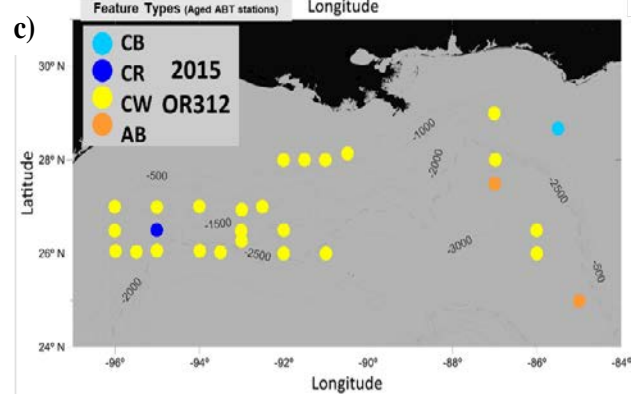
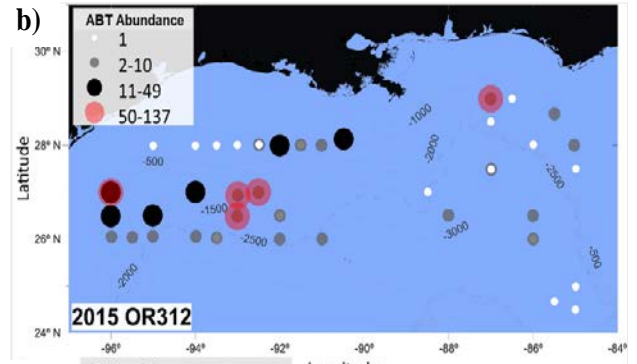
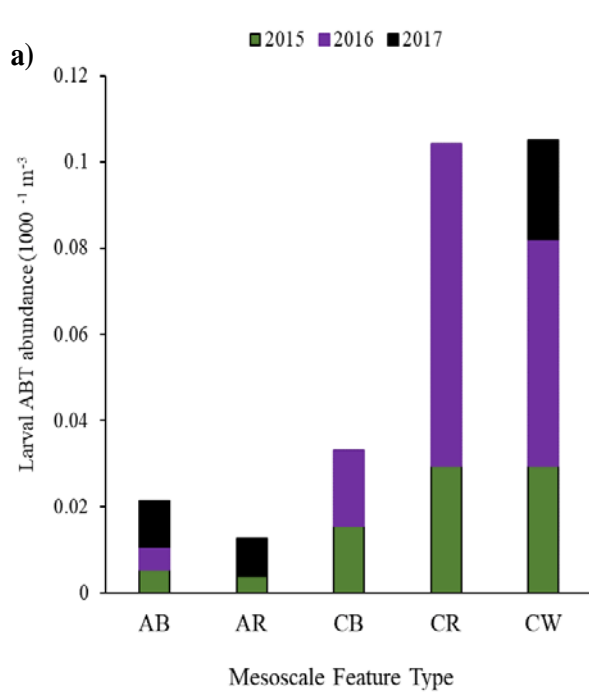


Figure 4.2. Abundances of larval *Thunnus thynnus* (ABT) during 2015, 2016, and 2017 along with bathymetry (m) contours in the open Gulf of Mexico. Panel (a) shows abundances $1000^{-1} m^{-3}$ for ABT-positive stations. Panels (b-g) indicate ABT catches from aged individuals. The station's mesoscale feature types are indicated: anticyclonic boundary (AB, orange), cyclonic boundary (CB, light blue), cyclonic region (CR, blue), and Common Water (CW, yellow).

Mesoscale feature types and ageing

During the surveys, all five feature types occurred in the northern GoM with different abundances each year (Figure 4.2a). ABT larvae were collected in all mesoscale feature types, but no larvae were aged from the AR feature type. In total, 319 larvae were aged mostly (> 80%) collected from CW, with only 17% (n = 55) from CR. Few ABT larvae (10) were aged from AB and CB mesoscale feature types, therefore in subsequent feature type comparisons, only CW and CR were analyzed in 2015 and 2016. In contrast, in 2017, all aged larvae were from CW feature type (Table 4.2).

ABT were 5 to 19 dph, with similar age and length distributions across years. Four aged larvae were excluded because they had high CVs (> 10%), and three larvae only had one increment, and were excluded only for recent growth analyses. Larger larvae (> 7.5 mm) were very sparse and only 16 were aged. None of these older individuals were from the 2015 survey. In 2016, larger larvae were collected, four of which had more than 13 increments (~15 dph).

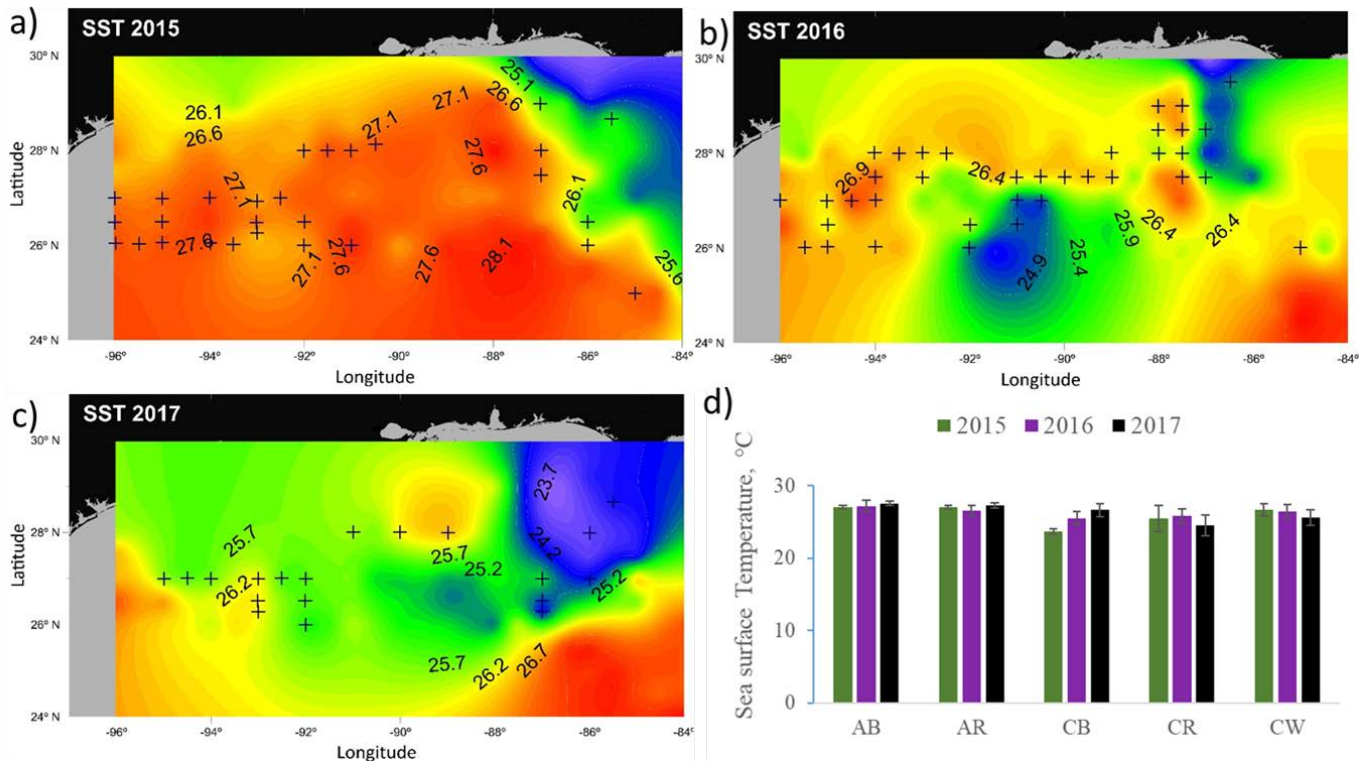


Figure 4.3. Sea surface temperature (SST, °C) for 2015, 2016, and 2017 (a-c) and for mean \pm SD in the five oceanographic mesoscale feature types: anticyclonic boundary (AB), anticyclonic region (AR), cyclonic boundary (CB), cyclonic region (CR), and Common Water (CW). Positive symbols (+) indicate stations with *Thunnus thynnus* aged in this chapter and SST are from CTD vertical casts at ~5 m depth.

Table 4.2. Summary of stations in five oceanographic feature types: anticyclonic boundary (AB), anticyclonic region (AR), cyclonic boundary (CB), cyclonic region (CR), and Common Water (CW). The number of aged *Thunnus thynnus* (ABT) are shown in (). Mean \pm SD for somatic (age, body size), and otolith metrics for recent growth (last two completed increments as a proxy for recent growth). The range of the otolith radius is also shown.

| Dataset | Aged ABT | Feature Type (ABT aged) AB / AR / CB / CR / CW | Age, dph | Size, mm | Otolith radius, μm (range) | Recent growth, μm |
|---------|----------|---|---------------|-----------------|--|------------------------------|
| 2015 | 105 | 11 (2) / 9 (0) / 2 (1) / 5 (18) / 81 (84) | 10 \pm 2.44 | 4.62 \pm 1.3 | 10.8 - 87.5 | 4.07 \pm 2.68 |
| 2016 | 142 | 15 (1) / 9(0) / 4 (6) / 6 (37) / 85 (98) | 11 \pm 2.93 | 5.15 \pm 1.34 | 11.3 - 102.1 | 4.03 \pm 2.20 |
| 2017 | 72 | 6 (0) / 7(0) / 2(0) / 4(0) / 66(72) | 9 \pm 2.94 | 4.45 \pm 1.38 | 11 - 66.5 | 3.26 \pm 2.13 |

Overall, least squares regressions were linear and age-at-length comparisons were not significantly different between years (ANCOVA, $\rho > 0.05$), (Figure 4.4a and 4.4b). However, growth rates (slopes) were larger for 2015 (0.51 mm day⁻¹), while in 2016 and 2017, the slopes were similar (0.41, and 0.45 mm day⁻¹, respectively). In addition, age-at-length and recent growth-at-age comparisons were not significantly different within years relative to overall ABT abundances 1000⁻¹ m⁻³ (ANCOVA, $\rho > 0.05$) likely indicating that density dependent growth was not taking place.

Given that, the least squares regressions for age-at-length residuals vs. OR-at-age residuals were not significantly different (ANCOVA, $\rho < 0.05$) between years, larval somatic growth was assumed to be relative to otolith growth, and was compared directly for recent growth comparisons. Recent growth-at-age was significantly different (ANCOVA, $\rho < 0.05$) between years. Tukey's posthoc test indicated that larvae from 2015 had significantly faster recent growth ($\rho < 0.05$) when compared to the other two years. Recent growth-at-age for 2016 and 2017 did not differ between years. Similarly, OR-at-age followed the same pattern than recent growth-at-age, further emphasizing that 2015 larvae grew faster.

Growth in mesoscale feature type was variable (Figure 4.6). In 2015, the CR vs. CW comparison was significantly different (ANCOVA, $\rho < 0.05$) with CW larvae growing faster for both for age-at-length and with recent growth-at-age (Figure 4.5a and 4.5c). In 2016, the CR vs. CW comparison was not significantly different for neither age-at-length or recent growth-at-age (Figure 4.5b and 4.5d). A limitation of these comparisons was not only the low number of aged

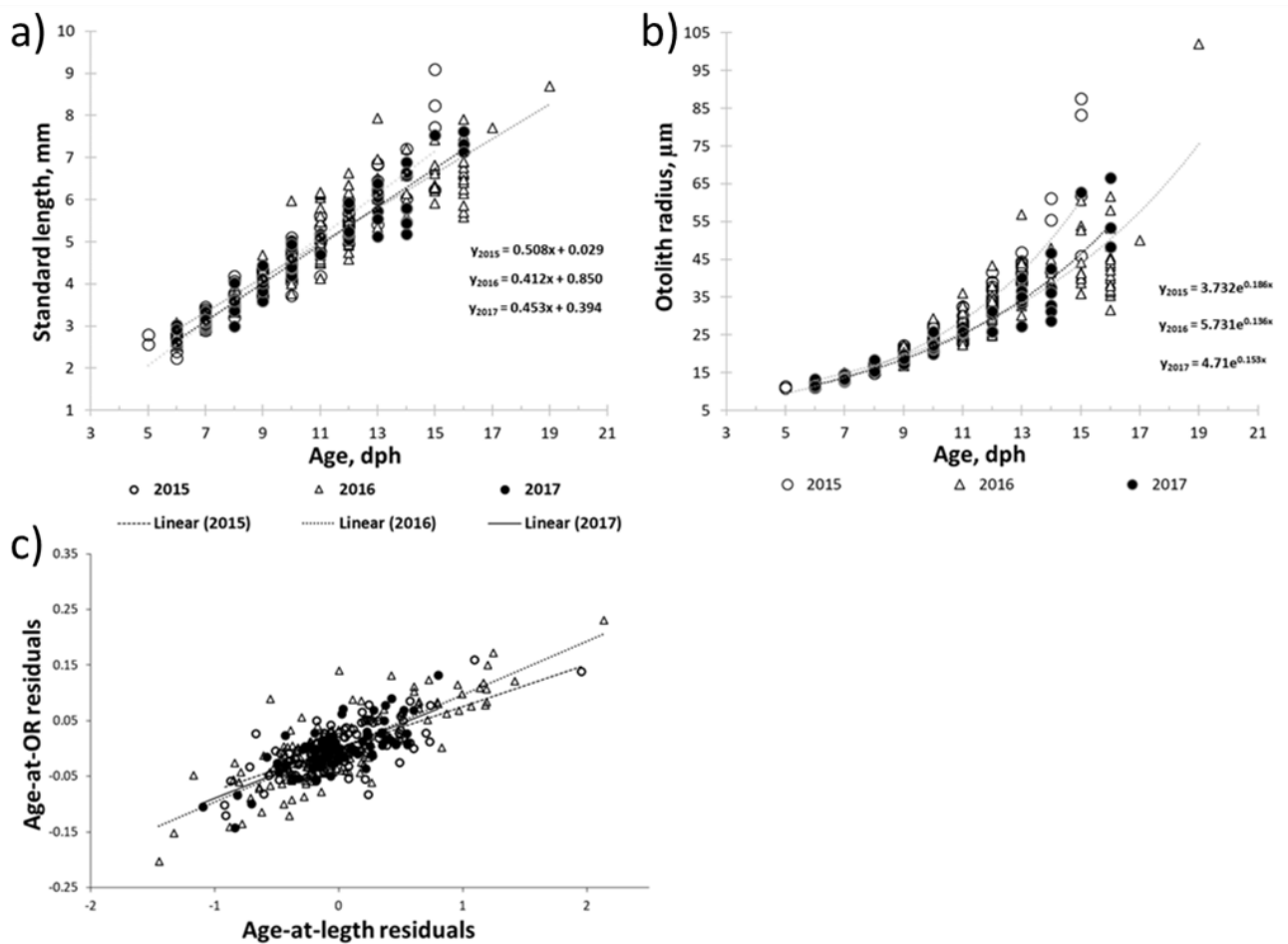


Figure 4.4. Growth curves for *Thunnus thynnus* (a) SL (mm) vs. age (days post hatch, dph), b) otolith radius (μm) vs. age (dph), and c) otolith size-at age residuals vs. SL-at-age residuals for years 2015, 2016, 2017.

ABT larvae available in 2015 from CR, but also that the corresponding length distribution was narrow (< 2 mm). Nonetheless, in both 2015 and 2016, the overall slopes of the CW least squares regressions for age-at-length and recent growth-at-age were larger than for CR (Figure 4.5b and 4.5d).

Otolith microstructure trajectories

Otolith microstructure for recent growth-at-age was larger for 2015, but very similar between 2015 and 2016 (4.06 ± 2.68 and 4.03 ± 2.20 μm respectively). In 2017, mean recent growth was almost 1 μm smaller (3.26 ± 2.13 μm). Overall, daily IW growth trajectories increased with ontogeny, with surprisingly smaller variability among older larvae (+12 dph). IW

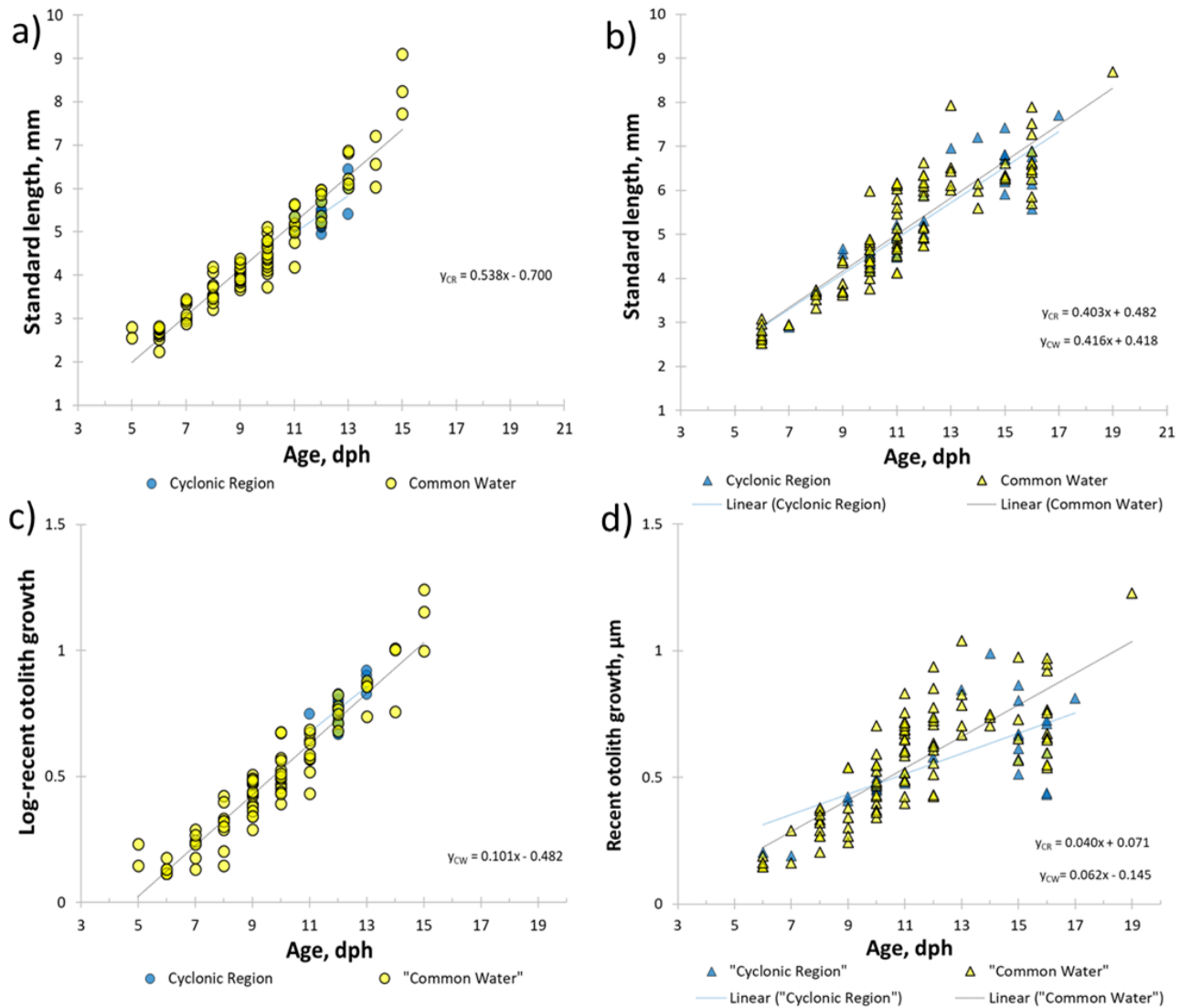


Figure 4.5. Growth curves for *Thunnus thynnus* for SL (mm) vs. age (days post hatch, dph) for cyclonic region, CR (blue) vs Common Water, CW (yellow) for a) 2015 ○ (CR= 18, CW=84) and b) 2016 △(CR = 37, CW=98). Recent increment (μm) vs. SL (mm) are shown for c) 2015 (CR= 18, CW=84) and d) 2016 (CR = 37, CW=98).

were not significantly different -at-age between younger larvae compared to older larvae (Figure 4.6). The 2016 and 2017 IW trajectories were examined together because recent growth in 2015 was significantly faster. In this 2016 and 2017 combined comparison, younger larvae consistently grew faster than older larvae, and older larvae had a very similar IW trajectory during the first three increments until increment 4 (7 dph) after which the trajectories no longer track each other with IW slowing down by ~30% in older larvae.

Larval ABT diet

The three most abundant prey taxa found in 100 larval ABT guts examined from 2016 were copepod nauplii (25%), appendicularians (24%), and calanoid copepods (23%) (Table 4.3). Overall, larval ABT had a 98% feeding incidence, with only three among 100 larvae having empty guts. Copepod nauplii were ingested most often by preflexion larvae, augmenting with copepodites with ontogeny. Postflexion larvae also consumed copepod nauplii and copepodites, however, they had the most diverse diet, which included appendicularians, ciliates, and other crustaceans (Table 4.3). In addition, calanoid copepods were consumed during all larval stages. The average prey size was $0.30 \text{ mm} \pm 0.01$ (SE), with the smallest prey measured 0.06 mm, and the largest prey measured 0.96 mm. Two larvae collected in CB and AB were excluded from statistical comparisons because too few individuals were collected in those two feature types.

In CW and CR, larvae ingested one to eight prey items, and the three ABT larvae had the highest number of prey (15, 17, and, 20), all from CW. Also in CW, gut fullness indices were 1 (at least one prey item) or 2 (full gut), with only 9% completely full (index 3). In CR, gut fullness was mostly at index 2, with only 25% at index 1, and only one larva had completely full guts. From the two larvae examined from the CB feature type, one larva had an empty gut (index 0) while the other had completely full guts (index 3).

Although copepod nauplii, appendicularians, and calanoid copepods were the most abundant prey in both mesoscale feature types, CW had larger percentage of all three when compared to CR (Table 4.3). Notably, ciliates (ciliophora) were less abundant, but found in both feature types. Similarly, appendicularians, calanoid copepods, copepod nauplii were ingested in very similar proportions in both CW and CR. In contrast, *Farranula gracilis* were ingested only in CR while cladocerans and copepodites were ingested mainly in CW. Overall, larvae from CW had diets that were more diverse (euryphagous) and included more prey types than CR (Table 4.3). Younger larvae (preflexion) had faster recent growth when large prey sizes were ingested despite having less overall prey-at-age. Older larvae had higher prey abundances in their guts.

Although growth curves did not significantly differ between the CR and CW feature types in 2016, the number of prey was significantly higher in CR (Wilcoxon test, $\rho = 0.024$). Larval CR had a larger proportion of the three most abundant taxa when compared to the dietary contents of CW larvae. Interestingly, recent growth did not differ with prey number or prey size (ANCOVA, $\rho > 0.05$). Recent growth-at-age also did not differ between CR and CW (t-test = 0.41, $\rho > 0.05$) although, recent growth within each feature increased with prey abundance and maximum prey size.

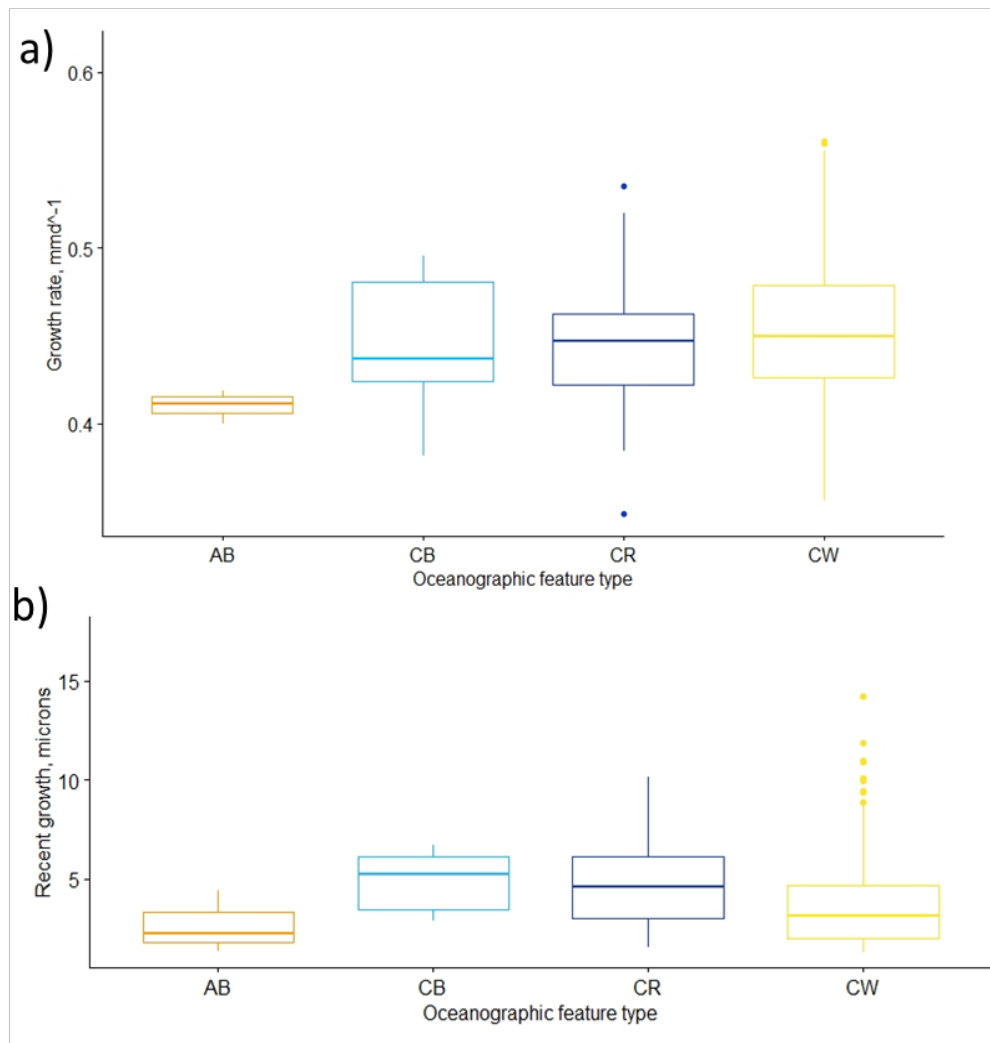


Figure 4.6. a) Growth rates (mm d^{-1}) in each oceanographic feature type AB, CB, CR, and CW for anticyclonic boundary, cyclonic boundary, cyclonic region, and Common Water, respectively for aged larval *Thunnus thynnus* otolith microstructure. b) Recent growth, μm shown for each feature type.

DISCUSSION

During the three years examined in this study (2015, 2016, and 2017), ABT larvae grew on average at 0.51 mm d^{-1} . First, inter-annual comparisons highlighted that the 2015 larvae grew fastest when compared to 2016 and 2017, and that temperature influenced larval somatic and otolith growth. Second, CR and CW feature types were associated with differential growth rates in the 2015 and 2016 cohorts. Specifically, ABT growth in CW was faster with larger recent growth in the two years, but the differences between CR and CW were marginal. Lastly, larval ABT dietary contents from 2016 had a 98% feeding incidence with some differences in prey abundance between CR and CW. Given that larvae from CW grew faster and had sufficient prey in their guts, this study proposes that CW is highly suitable habitat for larval ABT development in the northern GoM.

Larval abundances in the GoM

The Spring SEAMAP Plankton surveys sampled the GoM during the peak of the ABT spawning seasons yearly with at least 33% ABT-positive stations. ABT were collected throughout the northern GoM, with more abundant stations in the western GoM, particularly in 2015 and 2016 (Figure 4.2). Despite mechanical issues, the 2017 survey was able to sample in the eastern and western GoM however, the 2017 survey collected the lowest larval ABT abundances ($0.021 \text{ } 1000^{-1} \text{ m}^{-3}$) for all years. Larval ABT abundances (1000^{-1} m^{-3}) differed between 2015 and 2016, but did not differ between 2015 and 2017.

Larval ABT catches have been highly variable during the 40 years of the SEAMAP surveys (Ingram et al., 2010). One of the reasons for the higher catches in recent years (including the three years of this study) can be attributed to a shift in sampling protocols. Starting in 2009, a subsurface plankton tow was added to the SEAMAP protocols. The subsurface (upper 10 m, Habtes et al., 2014) gear was almost twice as effective at catching ABT in 2015, while in 2016 it was 22% more effective. Strangely, in 2017, the subsurface gears were less effective than the standard bongo tows (B61). Overall, the survey's catches were higher than previous years (1990-2006). During those years, only approximately 11% of stations were ABT-positive (Muhling et al., 2010), which is less than half of this study's positive percentage of catches. It is difficult to find ABT in sufficient numbers to examine larval dynamics, mainly due to their inherently patchy

distributions (Satoh et al, 2014, Gerard et al., 2022), and although they aggregate in frontal regions, the size of the patch has yet to be determined.

Recruitment and larval dynamics

Recruitment of marine species determines the size of adult populations (Cushing 1990). Recruitment is not solely determined by body length and larval growth of a year class; instead, recruitment is influenced by several multifaceted factors that interact at different scales (Houde 2008, Pepin et al., 2014). Some of the ways to disentangle the influence of these factors is by examining inter-annual differences along different gradients. In this study, inter-annual differences between ABT were not statistically apparent when initially examining age-at-length comparisons between 2015, 2016, and 2017 (Figure 4.4) however, different growth strategies were revealed when recent growth-at-age was analyzed between years. First, the 2015 cohort had significantly larger recent growth when compared to ABT larvae born in 2016 and 2017 (Figure 4.5a and 4.5b). Within 2015, CW larvae had faster recent growth when compared to CR. One of the potential explanations for this enhanced growth may be due to intermediate values of plankton volumes (mL) and combined larval fish taxa found in CW. CR had double (53%) the amount of aggregated plankton and more than double (64%) the amount of fish taxa than CW. Thus, the CR feature had a much larger concentration of prey (and predators), which may negatively influence larval survival. In 2016, larvae in CW and CR grew similarly, however recent growth-at-age was larger for CW larvae with the caveat that CR had lower number of larvae aged that year.

Observed larval growth estimates for the 2015, 2016, and 2017 cohorts (0.51, 0.41, and 0.45 mm d⁻¹, respectively) were mostly similar to growth rates from previous growth estimates from the GoM. The growth rates derived from ABT sampled during 2000-2012, 0.46 mm increment⁻¹ (Malca et al., 2017) were very similar, with larvae also preserved in ethanol. Contrastingly, the 2015-2016 growth rates were faster than from that reported by Malca et al. (2022) from 2017 and 2018, 0.39 and 0.37 mm d⁻¹, respectively. These 2017 and 2018 ABT were preserved following similar protocols, and despite this similarity in larval preservative and otolith analyses, 2015-2017 growth rates were 23% higher.

Otolith microstructure has exposed differences in age-at-length and recent growth-at-age patterns in ABT (Malca et al., 2017), as well as the influence of temperature on ABT growth in the western Mediterranean (García et al., 2013), while mesoscale oceanographic features have been shown to influence larval *K. pelamis* survival in the Straits of Florida (Gleiber et al., 2020a). In the GoM, temperature has recently been shown to influence larval ABT recent growth even within narrow (1 °C) SST differences (Malca et al., 2022). In this study, SST was

Table 4.3. Dietary analysis for *Thunnus thynnus* prey from the 2016 survey in the northern Gulf of Mexico. Prey counts indicate the mesoscale feature type at time of collection. The three features types are cyclonic boundary (CB), cyclonic region (CR), and Common Water (CW) are shown.

| Taxa | CB | CR | CW | Total |
|-------------------------------|-----------|-----------|-----------|--------------|
| Class Copepoda | | 4 | 17 | 21 |
| nauplii | 6 | 46 | 74 | 126 |
| Egg | | | 10 | 10 |
| Order Calanoida | 2 | 46 | 71 | 119 |
| Pontellidae | | | 2 | 2 |
| Scolecithrichidae | | | | |
| <i>Scolecithrix danae</i> | | | 1 | 1 |
| <i>Calocalanus</i> spp. | | | 1 | 1 |
| <i>Nannocalanus minor</i> | | 1 | | 1 |
| <i>Clausocalanus furcatus</i> | | 1 | 4 | 5 |
| Order Cyclopoida | | | | |
| Suborder Ergasilida | | | | |
| Corycaeidae | | 2 | 4 | 6 |
| <i>Farranula gracilis</i> | | 12 | 8 | 20 |
| <i>Oncaea</i> spp. | | 1 | 2 | 3 |
| Suborder Poecilostomatoida | | | 3 | 3 |
| <i>Oithona</i> spp. | | | 4 | 4 |
| Cirripedia nauplii | | | 2 | 2 |
| Order Euphausiacea (Egg) | | 4 | 1 | 5 |
| Class Cladocera | | 1 | 8 | 9 |
| Phylum Ciliophora | | 16 | 16 | 32 |
| Subphylum Radiolaria | | 1 | 1 | 2 |
| Order Siphonophorae | | | 1 | 1 |
| Class Appendicularia | | 43 | 79 | 122 |
| Unidentified | N/A | 8 | 6 | 14 |
| Total prey in stomachs | | | | 509 |

influential in 2015 and 2016 by driving overall age-at-length and recent growth-at-age for ABT larvae. In these two years, SST was positively associated with faster growth. Increasing SSS in contrast, had a negative influence on larval growth, particularly for recent growth of the 2015 cohort. There was also a negative trend in larval growth with increasing SSS for both 2016 and 2017. However, the effect was not significant. Contrary to previous GoM ABT studies, the SST ranged (~ 4 °C) within each of the years aged and a temperature gradient was captured that may have allowed a significant influence of temperature on larval growth. In 2017 however, SST was lower throughout the survey, and perhaps this smaller temperature differences obscured any temperature-driven influence on larval growth. However, smaller recent growth-at-age point to temperature likely (negatively) influencing larval somatic growth.

Otolith microstructure trajectories

The daily IW growth trajectories observed for 2016 and 2017 reflect the highly variable growth strategies between ABT larval age groups. While the first three increments were forming, younger larvae deposited otolith material (grew) faster than older larvae (Figure 4.7a). This trend may seem straightforward, as selective pressures have been shown to increase larval growth (Bakun 2012, Ishihara et al., 2019, Gleiber et al., 2020a). However, after increment four, the daily IW growth trajectories between younger and older larvae decoupled. Next, older larvae appeared to slow down comparably and mean IW slowed down by $\sim 30\%$ (Figure 4.7a). During ABT development, increment four (7 dph) coincides with the onset of flexion stage (Richards 2005, Malca et al., 2022). During the flexion stage, ABT larvae substantially increase their swimming capacity, and perhaps these precocious young larvae are unable to find sufficient prey to meet metabolic demands that accompany ingesting larger prey. In contrast, the older larvae in Figure 2.7a have slightly slower rates that may reflect decreased metabolic demands that may align with lower prey availability in the GoM.

In the otolith trajectories comparing CW and CR, low number of CR larvae indicated high uncertainty during the first five increments however, at increment seven, the recent growth-at-age for CW is greater than CR. The conditions in CR revealed twice as much plankton volumes and likely brought competition for resources that typically result in starvation or predation. Otolith trajectories have also been shown to differ significantly for *T. orientalis* larvae from two contrasting environmental conditions (Ishihara et al., 2019) and have been utilized as a

tool to examine growth rates in *T. maccoyii* in the Indian Ocean (Jenkins & Davis, 1990). Including otolith trajectories incorporates the wide variability in size-at-age with more abundant measurements of daily increment growth, which are typically thousands of observations (as opposed to $n = 319$ aged ABT). Individualized otolith trajectories based on otolith microstructure may provide a way to improve the predictive capacity of otolith-based growth analyses.

Mesoscale feature types and ageing

Larval growth is constrained by multiple factors. Yearly fluctuations in larval abundances have been linked to habitat variability and to mesoscale oceanographic features (García et al., 2013, Lindo-Atichati et al., 2012, Domingues et al., 2016, Russo et al., 2022). Although abiotic conditions and the number of feature types was variable for ABT-positive stations among years, all stations that collected ABT larvae consistently remained within the threshold of SST and SSS that previous studies have characterized as favorable ABT larval habitat (Muhling et al., 2010, Lindo-Atichati et al., 2012, Domingues et al., 2016). CW was the most common oceanographic condition associated with positive ABT catches during 2015, 2016, and 2017. It would appear that CW has been underestimated as one of the vital habitats that is most often inhabited by ABT larvae. This study found that faster growth rates were associated with CW conditions when compared to CR. However, in reality, the majority (80%) of larval growth rates examined in this study reflect mostly larval growth in CW – especially for the 2017 survey in which 100% of ABT-positive stations were collected inside the CW feature type. CW is therefore of high importance as a larval nursery for ABT larvae born in the GoM. Unlike the cyclonic eddies that concentrate biological productivity and predators (Bakun 2012, Domingues et al., 2016), the ABT larvae inside CW habitats may experience reduced predation despite constrained prey abundances. Fast larval growth is tightly coupled with increased survival (Satoh et al., 2008, Watai et al., 2017, Gleiber et al., 2020a). Individuals in unfavorable conditions for larval development will likely struggle (or perish) during the vulnerable first weeks of life prior to transitioning to the juvenile stage. For ABT, the environmental conditions associated with CW may offer several advantages including prey availability and sufficient temperatures to sustain larval growth.

The major limitation of this study is that anticyclonic mesoscale feature types (AR and AB) were uncommon during the three years examined. There were few instances of sampling in

AB feature types. During the three surveys combined, only 32 and 25 stations were characterized as AB and AR, respectively. In these uncommon feature types, ABT abundances were low (10% and < 2%, respectively) relative to the total number of ABT collected in each survey. These findings appear to contradict previous habitat modeling that found more larval ABT at anticyclonic feature types during the late 90s into early 2000s (Domingues et al., 2016). Perhaps the current distance between SEAMAP stations (30 nm) is adequate to observe trends and patterns for the larvae that spawn throughout the peak of the spawning season; however, to observe the fine-scale dynamics of mesoscale features, stations would need to be closer together (~5-10 nm).

Variations for age-at-length estimates (dph) during the first week of larval life can result in different growth rates and introduce error into already variable abundance estimates (Ingram et al., 2017). Larval growth curves are usually calculated utilizing observations of several (dozen to hundreds of larvae) and reflect somatic growth as well as environmental influences that may propel or hinder larval development. In this study, larvae were aged from multiple locations throughout the GoM. The 2015-2017 growth rates were sourced from over 20 stations and reflect the average range of conditions (temperature, salinity, prey abundance, competition, and predation) for the GoM during each spawning season. In targeted sampling efforts, such as in 2017 and 2018, a narrower envelope is encompassed, likely with less variable conditions. Perhaps this disparate sampling strategy can explain the low growth rates observed for larval ABT born in the GoM in Malca et al. (2022) for 2017 and 2018.

Larval ABT diet

Otolith-derived metrics have been combined with dietary prey abundances to provide insights into survival and recruitment dynamics (Young & Davis, 1990, Sponaugle 2010, Malca et al., 2022). After the posthatch stage and during the preflexion larval stage, in addition to adequate abiotic conditions, prey availability becomes a critical bottleneck for larval survival. During the ABT spawning seasons, the open ocean GoM is an oligotrophic environment with warming spring temperatures (> 24 °C) that support larval survival. Despite the lower productivity of the offshore environment, several gut content studies from this basin have resulted in very high feeding incidences (95 - 99%) for ABT larvae (Tilley et al., 2014, Llopiz et al., 2015, Shiroza et al., 2021). ABT larvae appear to be highly successful predators that exploit

prey with lower nutritional quality (appendicularians, ciliates) in addition to copepods. Such zooplankton are more readily available throughout ontogeny and likely support ABT early life dynamics.

Copepod nauplii, appendicularians and calanoid copepods were the most abundant prey found in larval ABT diet, particularly in CW. Appendicularians have high growth rates and short generation times (~4 d) (Llopiz et al., 2010) when compared to crustaceans. Interestingly, cladocerans and cirripeds have been identified as important prey in previous ABT gut content analysis (Tilley et al., 2016, Shiroza et al., 2021), yet they were minimally found in the 2016 guts. A potential explanation for large abundances of cladocerans and cirripeds in this study is that some of the collection sites in Tilley et al. (2016) and Shiroza et al. (2021) were located along a frontal zone or near the shelf. In these conditions, cirripeds and cladocerans can be more abundant.

Larval growth in 2016 was not significantly influenced by prey number, or prey size however, recent growth-age increased with both metrics. The very high feeding incidence (98%) observed for larvae from CR and CW feature types indicate that these two features were more than adequate to sustain larval survival. If CR plankton volumes from 2016 agree with observed larger plankton volumes in 2015 at CR, then CR from 2016 would have higher relative abundance of prey in larval ABT diet. Although CR may concentrate more prey, the increased metabolic demands that occur with higher growth rates may become reduced by cooler SST in cyclonic eddies. This hypothesis requires further examination, however it may be a possible explanation for the high-observed growth rates (Figure 4.6) in cyclonic eddies (CB and CR). Prey preferences likely partition prey resources of tuna species, and potentially life-stage separation, that may allow for co-occurrence of multiple cohorts simultaneously while minimalizing cannibalistic behavior.

The results of this study support larval survival estimates proposed by Shropshire et al., (2021) from a larval ABT individual based model (IBM) coupled with a physical-geochemical model that incorporated estimates of realistic zooplankton dynamics in the GoM. The IBM estimated that larval survival was highest in cyclonic eddies (CB and CR) and CW when compared to anticyclonic eddies (AR and AB). The IBM predicted that on average, $1.09 \pm 0.39\%$ (SE) of ABT larvae survived in CB, while $1.09 \pm 0.39\%$ survived at the CR, and $0.82 \pm 0.17\%$ in CW (Shropshire et al., 2020a). Survival in AB was predicted to be the lowest ($0.05 \pm 0.06\%$)

than all other regions except for AR ($0.02 \pm 0.05\%$). Additional ABT ageing efforts that can characterize larval growth within anticyclonic conditions (AB and AR) may provide additional evidence to evaluate larval growth in the five feature types that occur in the GoM during the spawning season.

Larval nutrition and growth dynamics are challenging to reconstruct during the larval stage. A positive correlation between feeding success (fuller guts) and larval growth (faster growth rate) is an example of the growth-survival paradigm. In this study, this paradigm was not observed mainly because both faster and slower growing ABT had full guts. At least for the 2016 cohort, prey consumed was similar to previous studies, with marked lower abundances of cladocerans. Overall, larvae had larger recent growth-at-age, although the proportion of faster-growing larvae was less than half of all larvae aged. This may be an indication that despite high feeding incidences, there were food-limiting conditions during all years. Another explanation for the lower proportion of larvae growing faster may be due to lower abundances of preferred prey encountered in the 2016 survey. Unfortunately, abundances for small zooplankton (microzooplankton) were not available during these three surveys to evaluate background prey abundances. Piscivory was not observed in these larval guts examined, as it is rare to observe in wild collections and occurs after 13 dph (Malca et al., 2022). Larger larvae are scares in ABT larval studies likely because their visual and swimming capacities may allow them to evade plankton nets to some extent.

CONCLUSION

In this study, larval growth was compared between CR and CW. CW was the most spatially prevalent habitat, but exhibited intermediate ecological preferability, with warm temperatures that enhanced larval ABT growth in the 2015 and 2016 cohorts examined. In 2017, lower temperatures likely decreased larval growth. If ABT survival depended only on anticyclonic habitat conditions, perhaps the survival of the species would not be as likely. CR larvae also grew fast, though environmental conditions were more variable when compared to CW. Fast growth has been found to be critical for larvae to survive to the juvenile stage; however, for ABT, fast larval growth rates that are supported by prey availability is likely the best habitat to ensure that the most larvae may survive. The fastest growth found in the youngest larvae was not matched by older larvae suggesting that younger larvae experience higher mortality levels in the GoM. Perhaps the most precocious larvae have larger metabolic needs that cannot be sustained within the food-limited conditions of the GoM Common Waters.

REFERENCES

- Alvarez, I., Rasmuson, L. K., Gerard, T., Laiz-Carrión, R., Hidalgo, M., Lamkin, J. T., Malca, E., Ferra, C. et al. (2021) Influence of the seasonal thermocline on the vertical distribution of larval fish assemblages associated with Atlantic bluefin tuna spawning grounds. *Oceans*, 2: 64–83.
- Anonymous (2015) Report of the Standing Committee on Research and Statistics (SCRS), International Commission for the Conservation of Atlantic Tunas (ICCAT), Madrid, Spain.
- Anonymous (2019) Report of the Standing Committee on Research and Statistics (SCRS), International Commission for the Conservation of Atlantic Tunas (ICCAT), Madrid, Spain.
- Bakun, A. (2006). Fronts and eddies as key structures in the habitat of marine fish larvae: opportunity, adaptive response and competitive advantage. *Sci. Mar.* 70(s2): 105-122.
- Bakun, A. (2012) Ocean eddies, predator pits and bluefin tuna: implications of an inferred ‘low risk–limited payoff’ reproductive scheme of a (former) archetypical top predator. *Fish Fish.*, 14, 424-438.
- Block, B. A., Teo, S.L.H., Walli, A., Boustany, A., Stokesbury, M. J. W., Farwell, C. J., et al. (2005) Electronic tagging and population structure of Atlantic bluefin tuna. *Nature*, 434(7037): 1121-1127, doi: 10.1038/nature03463.
- Brothers, E.B., Prince, E.D., Lee, D.W., (1983). Age and growth of young-of-the-year bluefin tuna, *Thunnus thynnus*, from otolith microstructure. In: Prince ED and Pulos LM eds. Procedures of the international workshop on age determination of oceanic pelagic fishes: tunas, billfishes, and sharks. NOAA Tech. Repos. N. M. F. S. 8, 49–60.
- Catalán I.A., Tejedor, A., Alemany, F., Reglero, P. (2011) Trophic ecology of Atlantic bluefin tuna *Thunnus thynnus* larvae. *J. Fish. Biol.*, 78: 1545–1560.
- Chang, W. Y. B. (1982) A statistical method for evaluating the reproducibility of age determination. *Can. J. Fish. Aquat. Sci.* 39, 1208–1210.
- Chassignet, E. P., H. E. Hurlburt, O. M. Smedstad, G. R. Halliwell, P. J. Hogan, A. J. Wallcraft, R. Baraille, and R. Bleck. (2007) The HYCOM (hybrid coordinate ocean model) data assimilative system. *J. Mar. Syst.*, 65: 60–83. doi:10.1016/j.jmarsys.2005.09.016.
- Clemmesen, C. (1994) The effect of food availability, age or size on the RNA/DNA ratio of individually measured herring larvae: laboratory calibration. *Mar. Biol.*, 118, 377–382.
- Cushing, D. H. (1990) Plankton production and year-class strength in fish populations - an update of the match / mismatch hypothesis. *Adv. Mar. Biol.*, 26, 249-293.
- Domingues, R., Goni, G., Bringas, F., Muhling, B., Lindo-Atichati, D. and Walter, J. (2016) Variability of preferred environmental conditions for Atlantic bluefin tuna (*Thunnus thynnus*) larvae in the Gulf of Mexico during 1993–2011. *Fish. Oceanogr.*, 25, 320–336.

- Díaz-Arce, N., Fraile, I., Abid, N., Addis, P., Deguara, S., Sow, F.N., Hanke, A., et al. (2022) Insights in the Stock Mixing Dynamics of Atlantic Bluefin Tuna in the North Atlantic. *Biol. Life Sci. Forum*, 13, 30, doi.org/10.3390/blsf2022013030.
- Drass, D.M. (2009) Southeast area monitoring and assessment program 2009 spring plankton survey. Cruise Rep. 1- 45 (GU-09-02).
- Elliott, B.A. (1982). Anticyclonic rings in the Gulf of Mexico. *J. Phys. Oceanogr.* 12: 1292–1309.
- Forristall, G.Z., Schaudt, K.J., Cooper, C.K. (1992) Evolution and kinematics of a Loop Current eddy in the Gulf of Mexico during 1985. *J. Geophys. Res.*, 97: 2173–2184.
- Fratantoni, P.S., Lee, T.N., Podesta, G.P., and Muller-Karger, F. (1998) The influence of Loop Current perturbations on the formation and evolution of Tortugas eddies in the southern Strait of Florida. *J. Geophys. Res.*, 103(C11): 24,759–24,799.
- García, A., Cortés, D., Quintanilla, J., Ramirez, T., Quintanilla, L., Rodríguez, J. M. and Alemany, F. (2013) Climate-induced environmental conditions influencing interannual variability of Mediterranean bluefin (*Thunnus thynnus*) larval growth. *Fish. Oceanogr.*, 22: 273–287.
- Gerard, T., Lamkin, J. T., Kelly, T. B., Knapp, A. N., Laiz-Carrión, R., Malca, E., Selph, K. E., Shiroza, A. et al. (2022) Bluefin larvae in Oligotrophic Ocean Foodwebs, Investigations of Nutrients to Zooplankton: overview of the BLOOFINZ-Gulf of Mexico program. *J. Plankton Res.*, 44(5): 600-617.
- Gleiber, M. R., Sponaugle, S., Robinson, K. and Cowen, R. (2020a) Food web constraints on larval growth in subtropical coral reef and pelagic fishes. *Mar. Ecol. Prog. Ser.*, 650, 19–36.
- Gleiber, M.R., Sponaugle, S., Cowen, R. K. (2020b) Some like it hot, hungry tunas do not! Implications of temperature and plankton food web dynamics on growth and diet of tropical tuna larvae. *ICES J. Mar. Sci.*, 77 (7-8):3058–3073, <https://doi.org/10.1093/icesjms/fsaa201>.
- Govoni, J. J., Boehlert, G. W. and Watanabe, Y. (1968) The physiology of digestion in fish larvae. *Environ. Biol. Fishes*, 16: 59–77.
- Habtes, S., Muller-Karger, F., Roffer, M., Lamkin, J.T., Muhling, B.A. (2014) A comparison of sampling methods for larvae of medium and large epipelagic fish species during spring SEAMAP ichthyoplankton surveys in the Gulf of Mexico. *Limnol. Oceanog. Meth.*, 12, 86–101.
- Hanke, A., Guenette, S. & Lauretta, M. (2019) A summary of bluefin tuna electronic and conventional tagging data. *Collect. Vol. Sci. Pap. ICCAT* 75, 1587–1621.
- Hernández, C. M., Richardson, D. E., Rypina, I. I., Chen, K., Marancik, K.E., Shulzitski, K., Llopiz, J.K. (2021) Support for the Slope Sea as a major spawning ground for Atlantic bluefin tuna: evidence from larval abundance, growth rates, and particle-tracking simulations. *Can. J. Fish Aquat. Sci.* <https://doi.org/10.1139/cjfas-2020-0444>.

- Hiraoka, Y., Okochi, Y., Ohshimo, S., Shimose, T., Ashida, H., Sato, T., et al. (2019) Lipid and fatty acid dynamics by maternal Pacific bluefin tuna. PLoS ONE 14(9): e0222824. <https://doi.org/10.1371/journal.pone.0222824>.
- Houde, E.D. (2008) Emerging from Hjort's Shadow Evaluation of ecosystem based reference points for Atlantic Menhaden in the Northwest Atlantic Ocean View project: Emerging from Hjort's Shadow. J.N.W. Atl. Fish. Sci., vol. 41, pp. 53-70.
- Ingram Jr., G. W., Richards, W. J., Lamkin, J. T. and Muhling, B. A. (2010) Annual indices of Atlantic bluefin tuna (*Thunnus thynnus*) larvae in the Gulf of Mexico developed using delta-lognormal and multivariate models. Aquat. Living Resour., 23, 35-47.
- Ingram Jr., G.W., Alvarez-Berastegui, D., Reglero, P., Balbín, R., García, A. (2017) Incorporation of habitat information in the development of indices of larval bluefin tuna (*Thunnus thynnus*) in the Western Mediterranean Sea (2001–2005 and 2012–2013). Deep Sea Res., Part II, 140, 203-211. <https://doi.org/10.1016/j.dsr2.2017.03.012>.
- Jenkins G.P. and Davis, T.L.O. (1990) Age, growth rate, and growth trajectory determined from otolith microstructure of southern bluefin tuna *Thunnus maccoyii* larvae. Mar. Ecol. Prog. Ser., 63: 93-104.
- Jenkins, G. P., Young, J. W. and Davis, T. L. O. (1991) Density dependence of larval growth of a marine fish, the southern bluefin tuna, *Thunnus maccoyii*. Can. J. Fish. Aquat. Sci., 48, 1358–1363.
- Jochens, A., DiMarco, S. (2008) Physical oceanographic conditions in the deepwater Gulf of Mexico in summer 2000-2002. Deep-Sea Res II 55: 2541–2554.
- Johnston, M., Milligan, R.J., Easson, C.G., Penta, B., DeRada, S., Sutton, T. (2019) An empirically-validated method for characterizing pelagic habitats in the Gulf of Mexico using ocean model data. Limnol. & Oceanogr. Methods., 17(6): 363-375, doi.org/10.1002/lom3.10319.
- Johnstone, C., Pérez, M., Malca, E., Quintanilla, J.M., Gerard, T., Lozano-Peral, D., Alemany, F., Lamkin, J.T., et al. (2021) Genetic connectivity between Atlantic bluefin tuna larvae spawned in the Gulf of Mexico and in the Mediterranean Sea. PeerJ, 9, e11568. <https://doi.org/10.7717/peerj.11568>.
- Kodama, T., Hirai, J., Tawa, A., Ishihara, T. and Ohshimo, S. (2020) Feeding habits of the Pacific bluefin tuna (*Thunnus orientalis*) larvae in two nursery grounds based on morphological and metagenomic analyses. Deep-Sea Res., Part II, 175: 104745.
- Lamkin, J. T., Muhling, B. A., Malca, E., Laiz-Carrion, R., Gerard, T., Privoznik, S., Liu, Y., et al. (2015) Do western Atlantic bluefin tuna spawn outside of the Gulf of Mexico? Results from a larval survey in the Atlantic Ocean in 2013. Coll. Vol. Sci. Pap. ICCAT, 7: 1736–1745.
- Lindo-Atichati, D., Bringas, F., Goni, G., Muhling, B., Muller-Karger, F. E. and Habtes, S. (2012) Varying mesoscale structures influence larval fish distribution in the northern Gulf of Mexico. Mar. Ecol. Prog. Ser., 463: 245–257.

- Llopiz, J. K. (2013) Latitudinal and taxonomic patterns in the feeding ecologies of fish larvae: a literature synthesis. *J. Mar. Syst.*, 109: 69–77.
- Llopiz, J. K., Richardson, D. E., Shiroza, A., Smith, S. L. and Cowen, R. K. (2010) Distinctions in the diets and distributions of larval tunas and the important role of appendicularians. *Limnol. Oceanogr.*, 55: 983–996.
- Llopiz, J. K. and Cowen, R. K. (2009) Variability in the trophic role of coral reef fish larvae in the oceanic plankton. *Mar. Ecol. Prog. Ser.*, 381: 259–272.
- Llopiz, J. K., Muhling, B. A. and Lamkin, J. T. (2015) Feeding dynamics of Atlantic bluefin tuna (*Thunnus thynnus*) larvae in the Gulf of Mexico. *Coll. Vol. Sci, Pap., ICCAT*, 71: 1710–1715.
- Malca, E., Muhling, B. A., Franks, J., García, A., Tilley, J., Gerard, T., Ingram, Jr., W. and Lamkin, J. T. (2017) The first larval age and growth curve for bluefin tuna (*Thunnus thynnus*) from the Gulf of Mexico: comparisons to the Straits of Florida, and the Balearic Sea (Mediterranean). *Fish. Res.*, 190: 24–33.
- Malca, E., Shropshire, T.M., Landry M.R., Quintanilla, J.M., Laíz-Carrión, Shiroza, A., Stukel, M.R., Lamkin, J.T., Gerard, T.G., Swalethorp, R. (2022) Influence of food quality on larval growth of Atlantic bluefin tuna (*Thunnus thynnus*) in the Gulf of Mexico. *J. Plankton Res.*, 44(5): 747-762, doi.org/10.1093/plankt/fbac024.
- McDowell, J.R., Bravington, M., Grewe, P.M., Lauretta, M., Walter, J.F.III, Baylis, S.M., Gosselin, T., Malca, E., et al. (2022) Low levels of sibship encourage use of larvae in western Atlantic bluefin tuna close-kin mark-recapture. *Sci. Reports*, 12:18606.
- McGillicuddy, D.J., Jr, Robinson, A.R., Siegel, D.A., Jannasch, H.W., Johnson, R., Dickey, T.D., McNeil, J., Michaels, A.F., and Knap, A.H. (1998) Influence of mesoscale eddies on new production in the Sargasso Sea. *Nature* 394: 263-266.
- Millet, A., (2015) Southeast area monitoring and assessment program 2015 spring plankton survey. *Cruise Rep.* 1–33 (RS-15-02, OR312).
- Millet, A. (2016) Southeast area monitoring and assessment program 2016 spring plankton survey. *Cruise Rep.*, 1–32 (RS-16-02, OR317).
- Millet, A., (2017) Southeast area monitoring and assessment program 2017 spring plankton survey. *Cruise Rep.*, 1–29 (RS-17-02, OR322).
- Muhling, B. A., Lamkin, J. T. and Roffer, M. A. (2010) Predicting the occurrence of Atlantic bluefin tuna (*Thunnus thynnus*) larvae in the northern Gulf of Mexico: building a classification model from archival data. *Fish. Oceanogr.*, 19, 526–539.
- Muhling, B. A., Lamkin, J. T., Quattro, J. M., Smith, R. H., Roberts, M. A., Roffer, M. A., Ramirez, K. (2011) Collection of larval bluefin tuna (*Thunnus thynnus*) outside documented western Atlantic spawning grounds. *Bull. Mar. Sci.*, 87:687–694.
- Muhling, B.A., Reglero, P., Ciannelli, L., Alvarez-Berastegui, D., Alemany, F., Lamkin, J.T., Roffer, M.A. (2013) Comparison between environmental characteristics of larval bluefin

- tuna *Thunnus thynnus* habitat in the GOM and western Mediterranean Sea. Mar. Ecol. Prog. Ser., 486: 257–276.
- Ohshimo, S., Sato, T., Okochi, Y., Ishihara, Y., Tawa, A., Kawazu, M., Hiraoka, Y., et al. (2018) Long-term change in reproductive condition and evaluation of maternal effects in Pacific bluefin tuna, *Thunnus orientalis*, in the Sea of Japan. Fish. Res., 204: 390-401.
- Ortner, P.B., Wiebe, P.H., Haury, L., Boyd, S. (1978) Variability in zooplankton biomass distribution in the northern Sargasso Sea: the contribution of Gulf Stream cold core rings. Fish. Bull., 76: 323–334.
- Pepin, P., Robert, D., Bouchard, C., Dower, J.F., Falardeau, M., Fortier, L., Jenkins, G.P., et al. (2014) Once upon a larva: revisiting the relationship between feeding success and growth in fish larvae. ICES J. Mar. Sci., 72 (2): 359–373.
- Perez, K.O., and Munch, S.B. (2010) Extreme selection on size in the early lives of fish. Evolution, 64: 2450-2457
- R Core Team. (2022) R: A Language and Environment for Statistical Computing. R Foundation for Statistical Computing, Vienna, Austria. <https://www.R-project.org/>.
- Richards, W.J., Leming, T., McGowan, M.F., Lamkin, J.T., Kelley-Fraga, S. (1989) Distribution of fish larvae in relation to hydrographic features of the loop current boundary in the Gulf of Mexico. Rapp. Reun. Cons. Int. Explor. Mer., 191: 169–176.
- Richards, W.J., Leming, T., McGowan, M.F., Lamkin, J.T., and Kelley, S. (1993) Larval fish assemblages at the Loop Current boundary in the Gulf of Mexico. Bull. Mar. Sci. 53: 475–537.
- Richards, W. (2005) Early Stages of Atlantic Fishes: An Identification Guide for the Western Central North Atlantic. CRS Press, Boca Raton, FL, USA, 600 pp.
- Richardson, D.E., Marancik, K.E., Guyon, J.R., Lutcavage, M.E., Galuardi, B., Lam, C.H., Walsh, H.J., Wildes, S., Yates, D.A., Hare, J.A. (2016) Discovery of a spawning ground reveals diverse migration strategies in Atlantic bluefin tuna (*Thunnus thynnus*). PNAS, 113: 3299-3304.
- Rooker, J.R., Alvarado Bremer, J.R., Block, B.A., Dewar, H., De Metrio, G., Corriero, A., et al. (2007) Life history and stock structure of Atlantic bluefin tuna (*Thunnus thynnus*). Reviews in Fisheries Science 15: 265-310.
- Rooker, J. R., Secor, D. H., DeMetrio, G., Kaufman, A. J., Ríos, A.B., Ticina, V. (2008) Evidence of trans-Atlantic movement and natal homing of bluefin tuna from stable isotopes in otoliths. Mar. Ecol. Prog. Ser., 368: 231–239.
- Rowe, G.T. (2017) Offshore plankton and benthos of the Gulf of Mexico: In Habitats and Biota of the Gulf of Mexico: Before the Deepwater Horizon Oil Spill, C.H. Ward (ed.), 641-767, doi: 10.1007/978-1-4939-3447-8_7.
- Russo, S., Torri, M., Patti, B., Musco, M., Masullo, T., Di Natale, M.V., Sarà, G., Cuttitta, A. (2022) Environmental conditions along tuna larval dispersion: Insights on the spawning

- habitat and impact on their development stages. *Water*, 14, 1568:1-16, doi.org/10.3390/w14101568.
- Rypina, I.I., Dotzel, M.M., Pratt, L.J., Hernandez, C.M., Llopiz, J.K. (2021) Exploring Interannual variability in potential spawning habitat for Atlantic bluefin tuna in the Slope Sea. *Prog. Ocean.*, 192, 102514.
- Satoh, K., Tanaka, Y., Iwahashi, M. (2008) Variations in the instantaneous mortality rate between larval patches of Pacific bluefin tuna *Thunnus orientalis* in the northwestern Pacific Ocean. *Fish. Res.*, 89: 248-256.
- Satoh, K., Masujima, M., Tanaka, Y., Okazaki, M., Kato, Y., Shono, H. (2014) Transport, distribution and growth of larval patches of Pacific bluefin tuna (*Thunnus orientalis*) in the northwestern Pacific Ocean. *Bull. Fish. Res. Agency Jpn.* 38:81–86.
- Scott, G.P., Turner, S.C., Grimes, C.B., Richards, W.J., Brothers, E.B. (1993) Indices of larval bluefin tuna, *Thunnus thynnus*, abundance in the GOM: Modeling variability in growth, mortality, and gear selectivity: Ichthyoplankton methods for estimating fish biomass. *Bull. Mar. Sci.* 53: 912-929.
- Searcy, S.P. and Sponaugle, S. (2001) Selective mortality during the larval-juvenile transition in two coral reef fishes. *Ecology* 82: 2452-2470.
- Shiroza, A., Malca, E., Lamkin, J. T., Gerard, T., Landry, M. R., Stukel, M. R., Laiz-Carrión, R. and Swalethorp, R. (2021) Diet and prey selection of Atlantic bluefin tuna (*Thunnus thynnus*) larvae in spawning grounds of the Gulf of Mexico. *J. Plankton Res.*, 44(5), 728-746. Doi:10.1093/plankt/fbab020.
- Shropshire, T. A. (2020a) Modeling Pelagic Ecosystems and Larval Atlantic Bluefin Tuna Dynamics in the Gulf of Mexico under Current and Future Climate Conditions. FSU Ph.D. Thesis, 135 pp.
- Shropshire, T.A., Morey, S.L., Chassignet, E.P., Bozec, A., Coles, V.J., Landry, M.R., Swalethorp, R., Zapfe, G. et al., (2020b) Quantifying spatiotemporal variability in zooplankton dynamics in the Gulf of Mexico with a physical-biogeochemical model. *Biogeosci. Discuss.*, 17, 3385–3407.
- Shropshire, T. A., Morey, S. L., Chassignet, E.P., Karnauskas, Coles, V.J., Malca, E., Laiz-Carrión R., Fiksen, O., Reglero P., Shiroza, A., Quintanilla, J.M., Gerard T., Lamkin J.T., Stukel, M.R. (2021) Trade-offs between risks of predation and starvation in larvae make the shelf break an optimal spawning location for Atlantic bluefin tuna. *J. Plankton Res.*, 44(5): 782-798, doi.org/10.1093/plankt/fbab041.
- Shulzitski, K., Sponaugle, S., Hauff, M., Walter, K., Alessandro, E. K. and Cowen, R. K. (2015) Close encounters with eddies: oceanographic features increase growth of larval reef fishes during their journey to the reef. *Biol. Lett.*, 11, 20140746, doi:10.1098/rsbl.2014.0746.
- Sponaugle, S. (2010) Otolith microstructure reveals ecological and oceanographic processes important to ecosystem-based management. *Environ. Biol. Fish.*, 89:221-238. doi: 10.1007/s10641-010-9676-z.

- Tanaka, Y., Satoh, K., Iwahashi, M., Yamada, H. (2006) Growth-dependent recruitment of Pacific bluefin tuna *Thunnus orientalis* in the northwestern Pacific Ocean. *Mar. Ecol. Prog. Ser.* 319: 225–235.
- Tilley, J. D., Butler, C. M., Suárez-Morales, E., Franks, J. S., Hoffmayer, E. R., Gibson, D., Comyns, B. H., Ingram, Jr., G. W. et al., (2016) Feeding ecology of larval Atlantic bluefin tuna, *Thunnus thynnus*, from the central Gulf of Mexico. *Bull. Mar. Sci.*, 92: 321–334.
- Uriarte, A., Johnstone, C., Laiz-Carrión, R., García, A., Llopiz, J. K., Shiroza, A., Quintanilla, J.M., Lozano-Peral, D. et al. (2019) Evidence of density-dependent cannibalism in the diet of wild Atlantic bluefin tuna larvae (*Thunnus thynnus*) of the Balearic Sea (NW-Mediterranean). *Fish. Res.*, 212, 63–71.
- Varela, J.L., Cañavate, J.P., Medina, A., Mourente, G. (2019) Inter-regional variation in feeding patterns of skipjack tuna (*Katsuwonus pelamis*) inferred from stomach content, stable isotope and fatty acid analyses. *Mar. Env. Res.*, 152(104821), doi.org/10.1016/j.marenvres.2019.104821.
- Ward, C.H., Tunnell, J.W. Jr. (2017) Habitats and biota of the Gulf of Mexico: an overview. In *Habitats and Biota of the Gulf of Mexico: Before the Deepwater Horizon Oil Spill*, C.H. Ward (ed.), 1-54, doi 10.1007/978-1-4939-3447-8_1.
- Watai, M., Ishihara, T., Abe, O., Ohshimo, S., Strussmann, C. A. (2017) Evaluation of growth-dependent survival during early stages of Pacific bluefin tuna using otolith microstructure analysis. *Mar. Freshwater Res.*, 68: 2008-2017.
- Watai, M., Hiraoka, Y., Ishihara, T., Yamasaki, I., Ota, T., Ohsimo, S., Strüssmann, S. (2018) Comparative analysis of the early growth history of Pacific bluefin tuna *Thunnus orientalis* from different spawning grounds. *Mar. Ecol. Prog. Ser.*, 607: 207-220, doi.org/10.3354/meps12807.
- Yasuike, M., Kumon, K., Tanaka, Y., Saitoh, K., Sugaya, T. (2021) Linking Pedigree Information to the Gene Expression Phenotype to Understand Differential Family Survival Mechanisms in Highly Fecund Fish: A Case study in the larviculture of Pacific bluefin tuna. *Curr. Issues Mol. Biol.*, 2021, 43: 2098–2110. <https://doi.org/10.3390/cimb43030145>.
- Young, J. W. and Davis, T. L. (1990) Feeding ecology of larvae of southern bluefin, albacore and skipjack tunas (Pisces: Scombridae) in the eastern Indian Ocean. *Mar. Ecol. Prog. Ser.*, 61: 17–29.